Control of Wound Field Synchronous Machine Gensets for Operation in a CERTS Microgrid

Prepared For:

US Department of Energy

Final Report Task 5.
Value and Technology Assessment to Enhance the Business Case for the CERTS Microgrid

Prepared By:
Shashank Krishnamurthy
Robert Lasseter
University-of-Wisconsin

March 6, 2009
DE-FC02-06CH11350

Acknowledgments

The authors are grateful for the support of Merrill Smith, U S Department of Energy, Office of Electricity Reliability and Energy Delivery and Steve Waslo, U S Department of Energy, Chicago Program Office. This research was funded by the U S Department of Energy under contract DE-FC02-06CH11350

.

This work has resulted in a U.S. Patent Application No.: 11/681,014

Filing Date: 03/01/2007.

Title: Non-Inverter Based Distributed Energy for Use in a Dynamic Distribution System

Executive Summary

Distributed generation (DG) is any small-scale electrical power generation technology that provides electric power at or near the load site; it is either interconnected to the distribution system, directly to the consumer's facilities, or to both. Developments in small-scale power generation technologies, ranging from reciprocating engines to micro turbines to fuel cells, provide credibility for DG's central premise of electric-power generation at or near load centers. The effect of the penetration of DG's in the distribution system on system stability, their interconnection with the utility, coordination of protection schemes and their control needs to be understood. A multitude of different technologies such as PV, solar, fuel cell, batteries, wind, microturbines, IC engines etc which can be used as prime movers for DG make this issue a complex challenge.

The objective of this work is to determine how an internal combustion (IC) engine driven wound field synchronous genset can be used most effectively as a DG in a microgrid environment.The genset operates synchronously which implies that the speed of the engine needs to be regulated within a narrow range to ensure that the terminal voltages meet the desired power quality standards. The focus of this work is to study the modeling and control issues related to IC engine driven wound field synchronous generators for their operation in a distribution system that contains multiple DG's. A special challenge posed by the genset is the fact that its dynamic response is considerably slower than that of several other types of DG sources that have much faster power electronic interfaces to the microgrid. Conventional IC engine gensets utilize a voltage regulator that controls the terminal voltage to a fixed value. In a distribution system like the microgrid that has

multiple sources, the regulation of the voltage to a constant value results in large circulating VAR's in the system. These circulating VAR's decrease efficiency of the system and increase the rating of components.

To improve the performance of the genset for operation in a microgrid environment this work presents the design of a state variable controller based on a system observer. The state variable controller incorporates droop curves on real and reactive power that enable the IC engine genset to respond to load changes and interact with other sources in the absence of any form of communication system. The operation of the observer and controller are demonstrated using simulation and experimental tests. The results of the tests show that using the proposed controller the IC engine based genset is able to interact with other sources during load changes and maintain system frequency and voltage within prescribed limits and maintain power quality in the microgrid system. The genset is able to reduce the circulating reactive power in the system and share load more evenly with other sources. The proposed controller enhances the integration of the diesel genset into the microgrid environment.

The work also investigates the effects of line starting induction machines in a microgrid setup with diverse sources. Using machine scaling laws the required starting kVA for a large range of induction machines was calculated and guidelines are presented on sizing the induction machine that can be started in such a manner in microgrids.

The work also presents a stability analysis of the microgrid system based on Lyapunov's first method. The resulting analysis shows that for the operating conditions studied, the system is stable with all eigenvalues in the left half plane for variations in power frequency droop value as well as power reference.

Finally the work looks at the applicability of the control scheme for gensets of different ratings. The work quantifies the change in frequency during the engine delay for a step load change for machines with higher power ratings. A discussion on the tuning of the controller gains for higher rating gensets is also presented

Table of Contents

Executive Summary i
Table of Contents iv
List of Figures vi
List of Tables xvi
CHAPTER 1. Introduction 1
1.1 Discussion of research need 1
1.2 Research objectives 3
1.3 Summary 4
CHAPTER 2. State of the art review 6
2.1 Distributed generation 7
2.2 IC engine based genset as a distributed generator 9
2.3 Microgrid state of the art 12
2.4 Review of IC engine systems 20
2.5 Summary 25
CHAPTER 3. Modeling of IC engine based genset 27
3.1 Model of IC engine using mean effective pressure 27
3.1.1 Model of mechanical governor 32
3.2 Model of synchronous machine 35
3.2.1 Flux voltage model of synchronous machine 37
3.2.2 Interfacing machine model with network equations 38
3.3 Model of brushless exciter 42
CHAPTER 4. Diesel genset test setup and modeling of conventional gensets 44
4.1 Hardware components and system configuration 45
4.2 Test results for step load and voltage changes 49
4.3 EMTP model of IC engine based genset model 53
4.4 Comparison of simulation and experimental results for isolated diesel genset operation 58
4.5 Summary 59
CHAPTER 5. Test results for operation of conventional gensets in a microgrid environment 60
5.1 Model of UW-Microgrid 60
5.2 Simulation and experimental results for operation of conventional diesel genset in a Microgrid 62
5.3 Simulation and experimental results for operation of diesel genset with grid and microsource 68
5.4 Summary 75
CHAPTER 6. Design of diesel genset controller 76
6.1 Operating point model of diesel genset 77
6.2 Real and reactive power droop controllers 78
6.3 Observer design and analysis 80
6.3.1 Rotor angle observer 81
6.3.2 Synchronous machine electrical states observer 84

6.4 Controller design and analysis 87
6.5 Experimental setup for genset controller 91
6.6 Test results for operation of modified genset controller in a microgrid 95
6.6.1 Test results for genset power reference variation while connected to grid ... 96
6.6.2 Test results for operation of modified diesel genset in a Microgrid 98
6.6.3 Test results for modified genset controller in microgrid environment with inverter based microsource 102
6.6.4 Test results for operation of multiple gensets in microgrid environment ... 108
6.7 Summary 111
CHAPTER 7. Induction machine starting in a microgrid environment 113
7.1 Starting kVA requirements for line start induction machines 113
7.2 EMTP based simulation results for induction machine starting 117
7.2.1 Induction machine starting in microgrid system with conventional genset 118
7.2.2 Induction machine starting in a microgrid system with inverter 121
7.2.3 Induction machine starting in microgrid system with modified genset controller 124
7.2.4 Induction machine starting in microgrid system with conventional gensets and inverter 127
7.2.5 Induction machine starting in microgrid system with modified gensets and inverters 131
7.3 Summary 134
CHAPTER 8. Stability analysis of UW-Microgrid system using Lyapunov's first method 136
8.1 Introduction 136
8.2 Modeling of system components 137
8.2.1 Modeling of inverter based source 137
8.2.2 Modeling of network 138
8.3 Eigenvalues of microgrid system 140
8.3.1 Eigenvalues of grid connected microgrid system 141
8.3.2 Eigenvalues of islanded microgrid system 145
8.4 Summary 147
CHAPTER 9. Scaling of controller scheme 149
9.1 Time delay associated with power stroke for larger machines 149
9.2 Inertia and friction losses for large machines 151
9.3 Electronic governors for large engines 155
9.4 Voltage regulator and exciter machines for large generators 156
9.5 Summary 157
References 159

List of Figures

Fig. 1: Typical structure of the traditional electric power system [5] 6

Fig. 2 : Typical structure of microsource 8

Fig. 3: Microgrid system controller implemented in [13] using communication system . 14

Fig. 4: Typical structure of a Microgrid [20] 16

Fig. 5 : Real power droop curve for power sharing between microsources 17

Fig. 6: Distribution system with synchronous machine and inverter based source analyzed in [60] 19

Fig. 7 : Illustration of the four strokes in diesel engine [Maritime.org] 22

Fig. 8: Diesel engine model accounting for individual cylinder pressure and clutch, road and cylinder friction [39] 23

Fig. 9: Simplified model of IC engine for operation in a power system from[40] 24

Fig. 10: Simplified model of IC engine for operation in a power system from[42] 25

Fig. 11 : Typical configuration of IC engine based genset system 27

Fig. 12 : Output power versus fuel input at rated speed for Yanmar engine 31

Fig. 13 : Schematic of mechanical governor [51] 32

Fig. 14 : Salient pole synchronous machine structure 36

Fig. 15 : DQ equivalent circuit for wound field synchronous machine 37

Fig. 16 : Schematic of two pole three phase brushless exciter 43

Fig. 17 : Configuration of Kohler 10kW diesel genset system 44

Fig. 18 : Diesel genset test setup at the University of Wisconsin-Madison 46

Fig. 19: Test setup for Kohler 10kW genset located outside engineering hall 47

Fig. 20: Picture of Yanmar diesel engine used in 10kW Kohler genset 47

Fig. 21 : Experimental results for 4kW load switching..... 50

Fig. 22 : Experimental results for 4kW load switching waveform depicting change in frequency 51

Fig. 23 : Experimental results for 4kW load increase followed by 2kW decrease and increase in load..... 52

Fig. 24 : Experimental results for 4kW load increase followed by 2kW decrease and increase in load with speed output in Hz..... 53

Fig. 25 : Lab setup modeled in EMTP 54

Fig. 26 : Internal model of diesel genset in EMTP 54

Fig. 27: Model of exciter and voltage regulator in EMTP 57

Fig. 28 : Governor and IC engine model in EMTP..... 58

Fig. 29 : Comparison of simulated and experimental values of speed for step 4kW load change 59

Fig. 30 : Layout of UW-Microgrid 62

Fig. 31 : EMTP model of diesel genset connected to grid through static switch 63

Fig. 32 : Simulated genset output real power, reactive power, frequency and voltage waveforms for load increase (@t=1s) and islanding (@t=6s) scenario 64

Fig. 33 : Simulated load voltage waveform load increase (@t=1s) and islanding (@t=6s) test with genset in a microgrid environment..... 65

Fig. 34 : Experimental genset real power, reactive power, frequency and terminal voltage waveforms for load increase (@t=3s) and islanding (@t=10.2s) test..... 66

Fig. 35 : Experimental waveforms of grid real and reactive power for load increase (@t=3s) and islanding (@t=10.2s) test..... 67

Fig. 36 : Power frequency droop curves for diesel genset and inverter based microsource illustrating diesel genset controlling system frequency..... 68

Fig. 37 : EMTP model of diesel genset operating in a microgrid environment with inverter based microsource..... 69

Fig. 38 : Simulated genset real power, reactive power, frequency and voltage waveforms for (@ 2s) and load increase (@6s) scenario in microgrid with inverter based microsource at power limit..... 70

Fig. 39 : Simulated inverter real power, reactive power and voltage waveforms for islanding (@ 2s) and load increase (@6s) scenario in microgrid with inverter based microsource at power limit..... 71

Fig. 40 : Simulated load voltage for islanding (@ 2s) and load increase (@6s) scenario in microgrid with genset and inverter based microsource..... 72

Fig. 41 : Experimental waveforms for inverter real power, reactive power, frequency and voltage for islanding scenario in microgrid with inverter based microsource (Power base and time scale different)..... 72

Fig. 42 : Experimental waveforms for genset real power, reactive power, frequency and voltage for islanding (@ 1.5s) and load increase (@8s) scenario in microgrid with inverter based microsource..... 73

Fig. 43 : Experimental waveforms for grid real and reactive power output for islanding (@ 1.5s) and load increase (@8s) scenario in microgrid with inverter based microsource..... 74

Fig. 44: Operating point model of kohler genset 78

Fig. 45 : Reactive power droop curve for microsource control 79

Fig. 46 : Real power droop curve for power sharing between microsources 80

Fig. 47: Overall block diagram of genset observer 81

Fig. 48: Closed loop observer for rotor position and rotor speed 82

Fig. 49 : Speed estimation magnitude as a function of frequency for speed observer 83

Fig. 50: Speed estimation phase as a function of frequency for speed observer 84

Fig. 51: Schematic of closed loop observer for ‘d’ axis mutual flux voltage 85

Fig. 52: Magnitude of $\frac{\hat{\psi}_{md}(s)}{\psi_{md}(s)}$ as a function of frequency 86

Fig. 53: Phase of $\frac{\hat{\psi}_{md}(s)}{\psi_{md}(s)}$ as a function of frequency 87

Fig. 54: Overall block diagram of proposed voltage regulator 88

Fig. 55: Magnitude of $\frac{v_{qsr}}{v_{qsr}^{*}}$ as a function of frequency 89

Fig. 56: Overall block diagram of proposed electronic governor 90

Fig. 57: Magnitude of $\frac{\omega_r}{\omega_r^{*}}$ as a function of frequency 90

Fig. 58: Microgrid setup at University of Wisconsin Madison 91

Fig. 59: Test setup for characterizing solenoid for diesel genset electronic governor 92

Fig. 60: Solenoid voltage and current waveforms for test involving sudden removal of supply voltage at fixed solenoid position 92

Fig. 61: Solenoid flux linkage variation as a function of solenoid current 93

Fig. 62: Schematic of power stage board used to drive exciter and governor solenoid.... 94

Fig. 63 : EMTP model of diesel genset connected to grid through static switch 96

Fig. 64: Experimental waveforms for genset real , reactive power and grid real, reactive power during power reference variation of genset with modified controller 97

Fig. 65: Experimental waveforms for system frequency and genset voltage during power reference variation of genset with modified controller 98

Fig. 66: Simulated genset output real power, reactive power, frequency and voltage waveforms with modified controller for load increase and islanding test..... 99

Fig. 67: Simulated load voltage waveform with modified controller for islanding and load decrease scenario 100

Fig. 68: Experimental waveforms for genset real power, reactive power and frequency with modified controller for load increase and islanding test..... 101

Fig. 69: Experimental waveforms for grid real and reactive power during islanding operation of modified genset in a microgrid..... 101

Fig. 70: EMTP model of diesel genset with modified controller in UW-microgrid system 102

Fig. 71: Power frequency droop curves for microsource and genset with modified controller..... 103

Fig. 72: Simulated genset real power, reactive power, voltage and frequency waveformd in a microgrid system with modified genset and inverter based source..... 103

Fig. 73: Simulated load voltage waveform in a microgrid system with modified genset controller and inverter based source..... 104

Fig. 74: Simulated real power, reactive power and voltage waveforms for inverter based source in a microgrid system with modified genset controller 105

Fig. 75: Experimental waveforms for genset real power, reactive power, frequency and voltage during islanding operation of modified genset in a microgrid with inverter based sources..... 106

Fig. 76: Experimental waveforms for inverter real power, reactive power, frequency and voltage during islanding operation of modified genset in a microgrid with inverter based source 107

Fig. 77: Experimental waveforms for grid real and reactive power during islanding operation of modified genset in a microgrid..... 107

Fig. 78: EMTP model of UW-Microgrid containing multiple gensets each equipped with modified controller 108

Fig. 79: Simulation waveforms for Genset 1 real power, reactive power, frequency and voltage for operation in a microgrid system with two gensets operating with modified controller 109

Fig. 80: Simulation waveforms for Genset 2 real power, reactive power, frequency and voltage for operation in a microgrid system with two gensets operating with modified controller 110

Fig. 78: Starting kVA required by induction machine for line start at rated voltage 115

Fig. 79: Starting kW and kVAr required by induction machine for line start at rated voltage..... 116

Fig. 80: EMTP model for testing line start of induction machine in Microgrid with conventional genset 119

Fig. 81: Simulated genset output real and reactive power waveforms for induction machine line start with conventional controller 119

Fig. 82: Simulated genset output voltage and genset per unit speed waveforms for line start with conventional controller 120

Fig. 83: Simulated load voltage and induction machine phase current waveforms for induction machine line start with conventional controller 120

Fig. 84: EMTP model for testing line start of induction machine in Microgrid with inverter 121

Fig. 85: Simulated inverter output real and reactive power waveforms for induction machine line start 122

Fig. 86: Simulated inverter output voltage and inverter frequency waveforms for line start of induction machine 123

Fig. 87: Simulated load voltage and induction machine phase current waveforms for induction machine line start with inverter based source 123

Fig. 88: EMTP model for testing line start of induction machine in Microgrid with genset with modified controller 124

Fig. 89: Simulated genset output real and reactive power waveforms for induction machine line start with modified controller 125

Fig. 90: Simulated genset output voltage and genset per unit speed waveforms for line start with modified controller 125

Fig. 91: Simulated load voltage and induction machine phase current waveforms for induction machine line start with modified controller 126

Fig. 92: EMTP model for testing line start of induction machine in Microgrid with inverter and genset with conventional controller 127

Fig. 93: Simulated genset output real and reactive power waveforms for induction machine line start with inverter based source and genset with conventional controller 128

Fig. 94: Simulated genset output voltage and genset per unit speed waveforms for line start with inverter based source and genset with conventional controller 128

Fig. 95: Simulated inverter output real and reactive power waveforms for induction machine line start with inverter based source and genset with conventional controller 129

Fig. 96: Simulated load voltage and induction machine phase current waveforms for induction machine line start with inverter based source and genset with conventional controller 130

Fig. 97: : EMTP model for testing line start of induction machine in Microgrid with inverter and genset with modified controller 131

Fig. 98: Simulated genset output real and reactive power waveforms for induction machine line start with inverter based source and genset with modified controller 132

Fig. 99: Simulated genset output voltage and genset per unit speed waveforms for line start with inverter based source and genset with modified controller 132

Fig. 100: Simulated inverter output real and reactive power waveforms for induction machine line start with inverter based source and genset with modified controller 133

Fig. 101: Simulated load voltage and induction machine phase current waveforms for induction machine line start with inverter based source and genset with modified controller 134

Fig. 102: UW-Microgrid schematic with two inverter based sources and a diesel genset source 139

Fig. 103: UW-Microgrid schematic with two inverter based sources and a diesel genset source 140

Fig. 104: Eigenvalues for microgrid system with two inverter based sources and a IC engine based source with mp of 1% and mq of 5% 142

Fig. 105: Eigenvalues for microgrid system with grid, two inverter based sources and a IC engine based source with mp of 1% and mq of 5% 143

Fig. 106: Critical eigenvalues for microgrid system with grid, two inverter based sources and a IC engine based source with mp of 1% and mq of 5% 143

Fig. 107: Critical eigenvalue migration for genset mp variation from 1% to 5% for microgrid system with grid, two inverter based sources and a IC engine based source 144

Fig. 108: Critical eigenvalue migration for genset mq variation from 1% to 5% for microgrid system with grid, two inverter based sources and a IC engine based source 145

Fig. 109: Critical eigenvalue migration for genset mp variation from 1% to 5% for microgrid system with two inverter based sources and a IC engine based source 146

Fig. 110: Critical eigenvalue migration for genset mq variation from 1% to 5% for microgrid system with two inverter based sources and a IC engine based source 147

Fig. 111: Inertia of 480V (LV) and 6.3kV (HV) synchronous generators manufactured by Uljanik Inc [85]. 152

Fig. 112: Model for 100HP to 1000HP Diesel Genset [84] 153

Fig. 113: Model for 100HP to 1000HP Diesel Genset [84] 154

List of Tables

Table 1 : Comparison of DG Technologies [3]……..…9

Table 2: Parameters for synchronous machine in Kohler 10ROZ Genset …….……48

Table 3 : Parameters of various components in UW-Microgrid system…….……61

Table 4: Inertia constant in seconds for various generators……..…..151

CHAPTER 1. Introduction

Deregulation at the federal, state, and local levels is creating significant changes in the electric power industry. The goal of deregulation is to create a competitive market where businesses succeed by meeting customer demands such as lower electricity prices, and increased energy efficiency. Amid these major industry changes, technology advancements have positioned distributed generation (DG) as a potentially major transformational force. Developments in small-scale power generation technologies, ranging from reciprocating engines to micro turbines to fuel cells, provide credibility for DG's central premise of electric-power generation at or near load centers. The DG approach to power generation and delivery represents a viable complementary or alternative paradigm to the conventional central power generation model.

1.1 Discussion of research need

With growing consumer demand the current electric power grid infrastructure is been utilized to its maximum capacity. Growing environmental concerns as well as constraints of right of way have prevented the generation and transmission networks from keeping pace with increased demand [1]. This has resulted in congestion of the transmission system and operation of the power grid near its stability limit. To relieve the congestion and to reduce the stress on the power grid system planners have been favoring the use of distributed generators located near the loads [2].

According to the Distributed Energy Program office of the DOE, "*The United States will have the cleanest and most efficient and reliable energy system in the world by maximizing the use of affordable distributed energy resources."* The program estimates that distributed power has the potential to capture up to 20% of all new generating capacity, or 35 Gigawatts (GW), over the next two decades [2]. The Electric Power Research Institute estimates that the DG market could amount to 2.5 to 5 GW/year by 2010. The effect of the high penetration of DG's in the distribution system on system stability, their interconnection with the utility, coordination of protection schemes and control needs to be understood. The aggregation of DG's in a local distribution system has been the subject of intense research over the last five years. A multitude of different technologies such as PV, solar, fuel cell, batteries, wind microturbines, IC engines etc which can be used as prime movers for DG make this issue a complex challenge.

Gensets consist of a diesel-based IC engine and a synchronous generator coupled on the same shaft. Such systems are widely used as backup or emergency power in commercial as well as industrial installations. Standby generators historically have used wound field synchronous machines connected to either diesel or gas engines. No inverter is needed as the machine provides the AC voltage of the desired frequency as long as the speed of the shaft is kept at a fixed value. One of the primary drawbacks of this system is that without the inverter front end the dynamics of the prime mover cannot be decoupled from the output of the generator. The reduced cost of the system due to the absence of the power electronic front end is one of the major advantages. The feasibility of using IC engine

based gensets in a microgrid environment and the necessary modifications to the engine governor and the generator voltage regulator is the focus of this research effort.

1.2 Research objectives

The focus of this work is to study the modeling and control issues related to IC engine driven wound field synchronous generators for their operation in a microgrid. The interaction and integration of such distributed resources with sources that have a power electronic front end will be studied. The use of real power – frequency droop and reactive power – terminal voltage droop curves in the genset to maintain power quality and stability in the microgrid during islanded and grid connection without the need for an external communication system will be demonstrated. A state variable controller that utilizes local measurements and an observer to estimate the state of system has been developed. This controller enables the genset to share load with other sources in the system and keep circulating reactive power in check without the need for an external communication network in the system. The response of the genset controller scheme to load changes and islanding events has been shown using simulation studies and is also validated experimentally. The scaling of the controller scheme with power level and the issues related to modeling gensets of different power levels is also discussed. This work also examines the effects of starting induction machines in microgrids and provides estimates for the starting kVA requirements using machine scaling laws. Finally an operating point analysis of the microgrid system with inverter and genset based sources is carried out and a discussion on the stability of the system based on Lyapunov's first method is also presented.

1.3 Summary

The report is organized as follows:

Chapter 2 contains a detailed literature review of the various aspects covered in this research work. The state of the art in distributed resources, microgrids and IC engine modeling and control is examined and the motivation for the use of IC engine driven wound field synchronous generators as a distributed resource is presented.

Chapter 3 describes the modeling of the individual components of the IC engine genset. The procedure is used to develop a physical model for a Kohler diesel genset that has been installed in the UW-Microgrid test setup. The genset will be used to experimentally verify the key control concepts presented in this work.

Chapter 4 describes the various components in the UW-Microgrid test setup. Test results used to characterize the machine based on the models in Chapter 3 are also included here.

Chapter 5 explains the simulation model developed for the genset in the EMTP simulation environment. Simulation and experimental results for the genset operating in an isolated system as well as in a microgrid system with other sources are contained in this chapter. Based on these results the motivation for improving the voltage regulator and governor is presented.

Chapter 6 describes the modified controller that has been designed for the genset. It presents the design of the observer for the genset system and the design of the state variable controller in the continuous time domain. The improved performance of the genset using the modified controller is also demonstrated in this chapter using simulation and validated using experimental results.

Chapter 7 discusses the issues related to staring induction machines in a microgrid environment and presents analysis based on scaling laws on the starting kVA required. The chapter also presents some general guidelines on the size of induction machines that can be line started in a microgrid.

Chapter 8 contains a detailed operating point analysis of the microgrid system containing inverter based sources as well as IC engine based gensets. The eigenvalues of the system at steady state are calculated for various operating points and the stability of the system is analyzed by examining their real part.

Chapter 9 discusses the issues related to scaling of the controller with genset power rating. This report presents detailed analysis and design of the controller for a specific rating genset and this chapter looks at the various issues related to using this scheme for other genset ratings.

CHAPTER 2. State of the art review

Conventionally power generation has been provided by large (100's of MW) coal fired or nuclear power plants that are located at a considerable distance from the load centers. The power plants feed the power that they produce into a network of lines known as the transmission network (Fig. 1). The transmission network is an integral part of the power system and its need arises due to the geographical separation between the generating stations and the consumer load. The transmission lines carry the power at high voltage to reduce losses. The distribution system refers to the lines and equipment that supply electric power to the consumer. The distribution system is connected to the transmission system at substations that step down the voltage and also have metering and protection equipment.

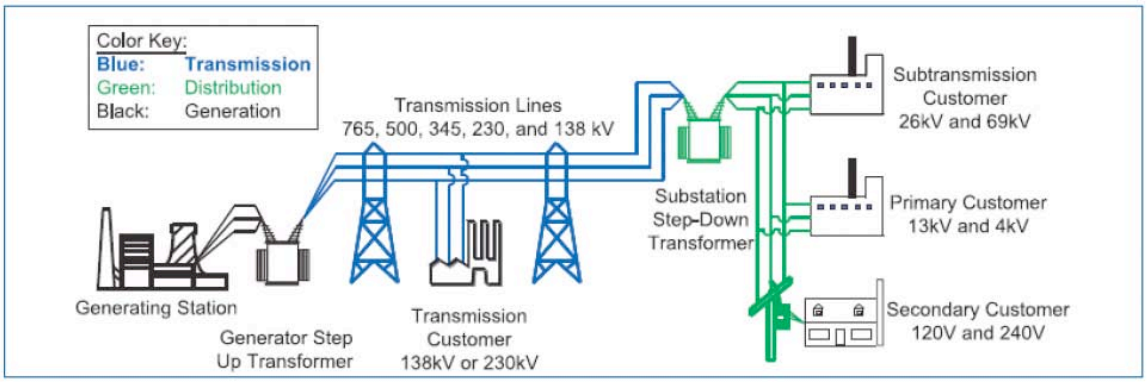

Fig. 1: Typical structure of the traditional electric power system [5]

With growing consumer demand the current generation, transmission and distribution facilities are being utilized to their maximum capacity. Growing environmental concerns

as well as constraints of right of way have prevented the generation and transmission networks from keeping pace with increased demand [1]. This has resulted in congestion of the transmission system and operation of the power grid near its stability limit. To relieve the congestion and to reduce the stress on the power grid system planners have been favoring the use of distributed generators located near the loads [2].

2.1 Distributed generation

Distributed Generation (DG) refers to the use of small electric generators located near consumer loads to supply their power demand. The concept of using local generators is not new and has been traditionally used in backup and standby applications for providing emergency power. These sources are activated when the utility fails and provide power to the critical systems in the consumer's installation. The utilization of local generators to supplement grid power during its availability to improve power and quality and reliability is new and forms the basis for the DG concept. The difference between conventional generators and distributed generators can be attributed to their power levels. The exact range of output power that defines a DG varies and depends primarily on the organization defining it [16]. Typically distributed generators have an output that ranges from several kW to few MW's.

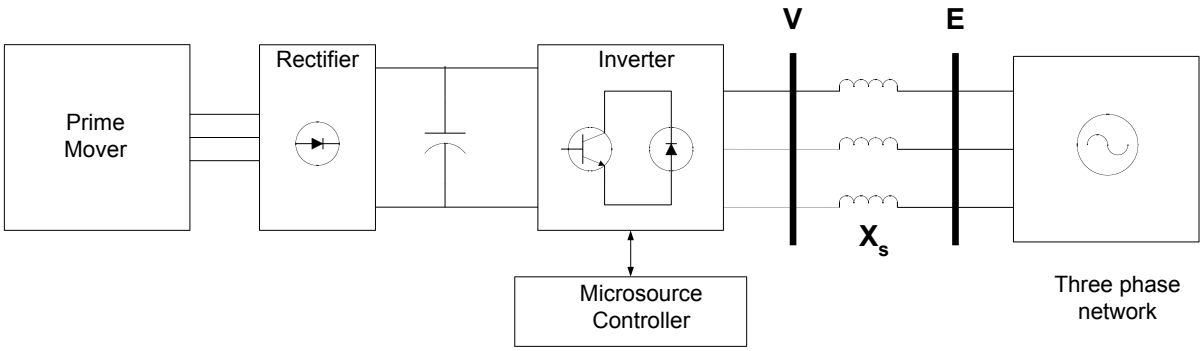

Fig. 2 : Typical structure of microsource

Prime movers for distributed generators are varied and can either use renewable or no-renewable energy sources. Sources such as natural gas based microturbines, fuel cells, PV panels, wind turbines use a power electronic interface on the front end to provide the necessary AC voltage at the utility frequency which is either 50Hz or 60Hz. The generic structure of microsource that uses power electronic inverter is shown in Fig. 2.For sources with AC output such as high speed microturbines [6] the voltages are first rectified to produce a DC output and inverted to produce the desired AC voltage and frequency. The inverter is typically a voltage source converter and provides the necessary controls over the phase and magnitude of the bus voltage. Storage can be added at the DC bus to decouple the dynamics of the prime mover from the output [23]. Sources such as fuel cells and PV panels produce DC directly and only an inverter is needed to produce AC output at desired voltage and frequency.

From Table 1 we can see that conventional diesel/gas gensets have the lowest capital cost among the various DG technologies. The O&M costs shown in Table 1 do not account for the cost of fuel and would have to be considered for an overall economic evaluation.

The lower capital costs for IC engine based gensets and their high energy density have been the chief driving forces for their investigation as DG sources.

	Diesel/Gas genset	Microturbine	Photovoltaic	Wind turbine	Fuel cell
Efficiency	35%	29-42%	6-19%	25%	40-57%
Energy density kW/m^2	50	59	0.02	0.01	1-3
Capital cost $/kW	200-350	450-870	6600	1000	3750
O&M Cost * $/kW	0.01	0.005-0.0065	0.001-0.004	0.01	0.0017

Table 1 : Comparison of DG Technologies [3]

* O&M cost does not include fuel cost

2.2 IC engine based genset as a distributed generator

Gensets consist of a diesel or gas based IC engine and a synchronous generator coupled together on the same shaft. Such systems are widely used as backup or emergency power in commercial as well as industrial installations. Gensets are typically classified based on the output rating and annual hours of operation as [7]:

- Standby: Output available with varying load for the duration of the interruption of the normal source power. Maximum expected usage equals 500 hours a year. Standby power in accordance with ISO8528.

- Prime: Output available with varying load for an unlimited time. Prime power in accordance with ISO8528. 10% overload power in accordance with ISO3046, AS2789 and BS5514 is available for emergency use for a maximum of 1 hour in 12, but for no more than 25 hours per year
- Continuous: Output available without varying load for an unlimited time.

Gensets used in prime and continuous applications are typically designed to operate at a higher efficiency as in the long run the fuel costs will dominate the initial capital costs. Such systems are heavily used in remote locations where it is economically expensive to have power from a utility connected to a large grid.

The generator in the genset can in principle either be a permanent magnet or a wound field synchronous machine. In the case of a permanent magnet generator the front end consists of a rectifier and a voltage source converter to provide the necessary AC voltage at the desired frequency [8-11]. The presence of a power electronic front end does increase the overall cost of the system and decreases its fault tolerance. However the presence of the inverter enables non-synchronous operation of the engine which has the potential of increased power density and higher efficiency [8-11]. Machines with wound field generators have an exciter and a voltage regulator to control the AC voltage produced by the machine. No inverter is needed as the machine provides the AC voltage of the desired frequency as long as the speed of the shaft is kept around a fixed value. However one of the primary drawbacks of this system is that without the inverter front end the dynamics of the prime mover cannot be decoupled from the output of the

generator. The reduced cost of the system due to the absence of the power electronic front end is one of the major advantages.

Wound field synchronous generators are the most prevalent type of generator used in the electric power system. Most large power plants have these generators connected to either steam or hydraulic turbines and form the backbone of the electric power grid. In the power grid several of these generators are connected via the transmission network to form a synchronous connection which improves the reliability of the network. Interconnecting various generators increases the overall inertia of the system and improves dynamic stability. The effect of the loss of one generator or load on the whole system is negligible. When the demand on the grid changes, the effect on individual generators and especially on their speed is small. For such small changes the prime mover output gradually changes to meet the new demand and restore the frequency to its nominal value. Time constants for steam and hydraulic prime movers are quite long and typically are several minutes [68]. Hence in dynamic studies it is acceptable to assume that the output of the prime mover is constant during various events. For large interruptions where the frequency change is more dramatic [1] the generators are configured to trip themselves out of the network. Machines with wound field generators have an exciter and a voltage regulator to control the AC voltage produced by the machine and a governor to regulate the speed of the shaft. The design of the voltage regulator and the governor and their effect on power system stability has been studied in detail in the past [72-74].

The operation of a wound field synchronous generator driven by an IC engine based genset in a distribution system is quite different in comparison to the operation of those driven by large steam or hydraulic turbines. In a distribution system as the rating of each generator is comparable to the size of individual loads in the system the loss of even a single load causes significant changes in the system frequency. The response of the IC engine prime mover is much faster than the large steam and hydraulic turbines and its output cannot be considered to be constant during load changes. The effect of the response of the governor and prime mover must be accounted for in the analysis of distribution systems with such resources. The DG's present in the system must respond to load changes and meet the demand instead of tripping and disconnecting from the system which would defeat the purpose of having them in the first place. The addition of a power electronic converter with storage on the DC bus provides a convenient method to decouple the dynamics of the IC engine prime mover [23] from the output terminals but results in a significant cost increment.

2.3 Microgrid state of the art

According to the Distributed Power Coalition of America (DPCA), research indicates that distributed power has the potential to capture up to 20% of all new generating capacity, or 35 Gigawatts (GW), over the next two decades [2]. The Electric Power Research Institute estimates that the DG market could amount to 2.5 to 5 GW/year by 2010. The effect of the high penetration of DG's in the distribution system on system stability, their interconnection with the utility, coordination of protection schemes and control needs to be understood. One of the chief concerns of regulators and policy makers is whether the

inclusion of DG would necessitate the complete overhaul of the existing distribution system. This dramatic and expensive change would hinder the development of DG technology and prevent its benefits from being fully realized. For example in traditional systems the flow of power is from the utility to the load. With the presence of local generation the direction of power flow is not fixed and could vary depending on the output of local generators and load. In such a scenario the operation of conventional protection schemes would be compromised as they are designed using a fixed direction of power flow in radial systems. Hence to fully utilize the benefits of DG the design of distribution systems needs to be revisited and a method to incorporate them in the least disruptive fashion needs to be devised.

The connection of DG to the utility systems must conform to specific regulations and SCC21 is the committee within IEEE which has been assigned the task of defining these requirements. The IEEE 1547 standard being developed by the committee focuses on establishing criteria and requirements for connecting local generators to the area electric power systems (EPS). As per the Energy Policy Act of 2005 [12], Section 1254, *"Interconnection services shall be offered based upon the standards developed by the Institute of Electrical and Electronics Engineers: IEEE Standard 1547 for Interconnecting Distributed Resources With Electric Power Systems, as they may be amended from time to time."* Some of the guidelines presented in the standard specific to the interconnection are:

- *The interconnection system paralleling-device shall be capable of withstanding 220% of the interconnection system rated voltage.*

- *The distributed resource (DR) unit shall cease to energize the Area electric power system (EPS) for faults on the Area EPS circuit to which it is connected.*
- For a given range of abnormal voltages and frequencies in area EPS the interconnection system must disconnect within a specified clearing time.
- *export of real or reactive power by the DR to the Area EPS is not permitted*

The guidelines presented above need to be implemented on the interconnection of each DG to the grid and represent a significant expense and barrier to the high penetration of local generation in the distribution system. The aggregation of DG's in a local distribution system has been the subject of intense research over the last five years [13 - 15]. A multitude of different technologies such as PV, solar, fuel cell, batteries, wind microturbines, diesel engines, gas engines etc make this issue a complex challenge.

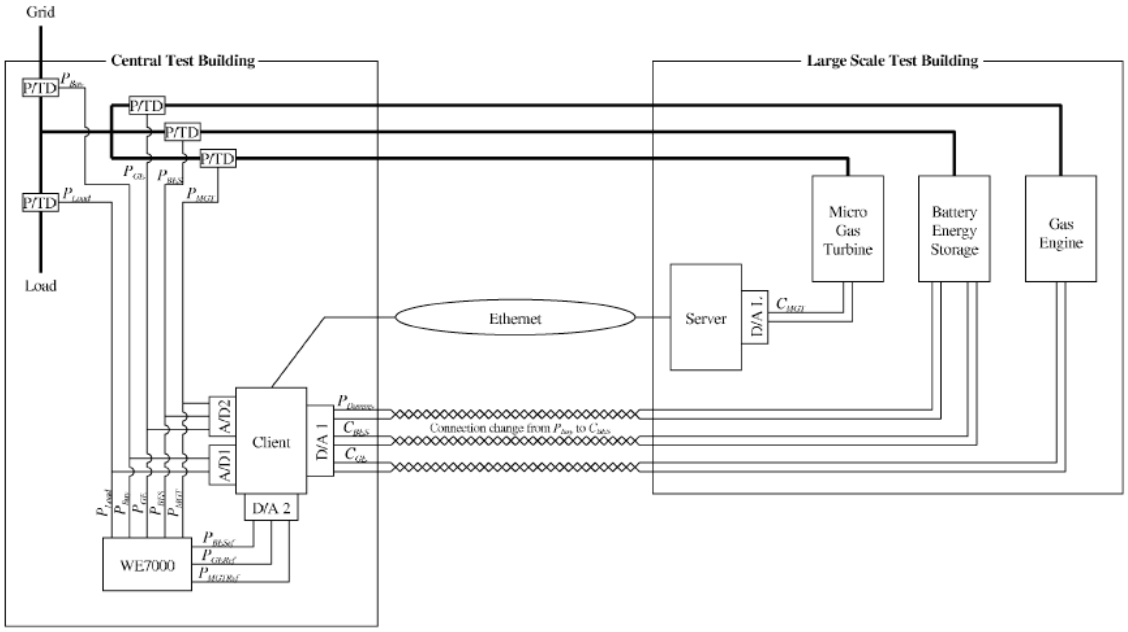

Fig. 3: Microgrid system controller implemented in [13] using communication system

In [13] the operation of a distribution system with micro-turbine, gas engine and battery energy storage system has been studied and is shown in Fig. 3. The control of the system is through a master controller which communicates with each source using dedicated communication lines. A high bandwidth communication interface is used for implementing the real time control algorithm. The power dispatch of each unit is handled by the controller which factors in the load demand and the capability and dynamic response of each distributed resource. The presence of a communication interface significantly increases the cost of deploying DG's in the system. Each time a new source is added a new line needs to be installed and the capability of the master controller needs to be updated. Loss of the master controller due to internal faults will severely impair the operation of the system. A centralized controller with communication channel has also been used in [14]. In this approach knowledge of the system real and reactive load from a load forecast is required for the proper dispatch of the distributed resources.

The Microgrid concept presented by CERTS [19] is an advanced approach for enabling integration of, in principle, an unlimited quantity of distributed resources into the electricity grid in a cost-effective fashion. The CERTS Microgrid [18-19] (henceforth referred to simply as the microgrid) refers to a collection of sensitive loads and sources connected to the utility via a static switch as shown in Fig. 4. The sources in the microgrid are distributed generators that can be locally dispatched and controlled. The aim of the microgrid is to improve the quality of power seen by the load and to improve the reliability of the supply. To the utility the microgrid appears as a single controllable supply that responds dynamically to changes in the transmission and distribution system.

The major features of the CERTS Microgrid are:

1. Peer to peer environment
2. No explicit communication system
3. Plug and play
4. Scalable system
5. CHP to improve efficiency
6. Smooth transfer between island and grid connected operation

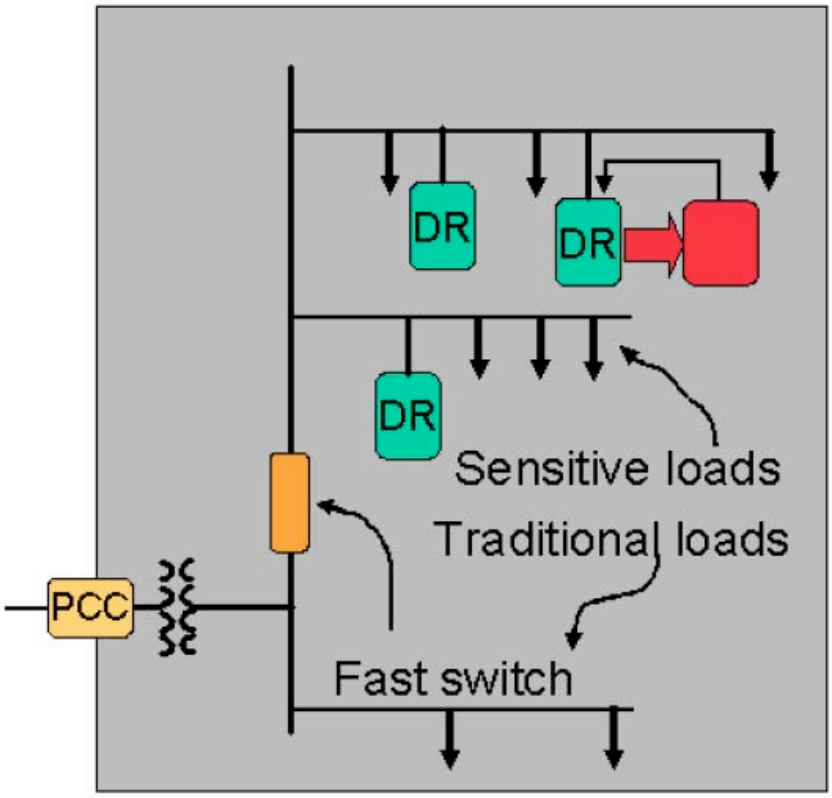

Fig. 4: Typical structure of a Microgrid [20]

The Microgrid has two main components, the static switch and the microsource. The static switch has the ability to autonomously island the microgrid from disturbances such

as faults, IEEE 1547 events or power quality events. After islanding, the reconnection of the microgrid is achieved autonomously after the tripping event is no longer present. This synchronization is achieved by using the frequency difference between the islanded microgrid and the utility grid. Each microsource can seamlessly balance the power on the islanded microgrid using a power vs. frequency droop controller (Fig. 5).

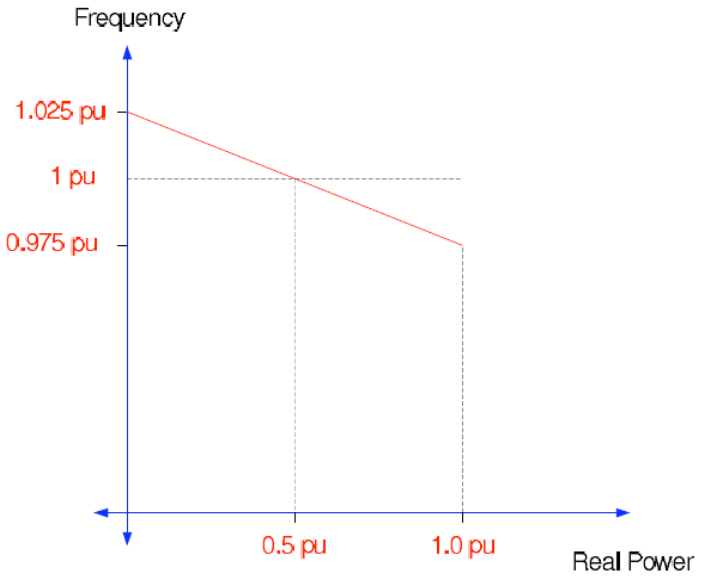

Fig. 5 : Real power droop curve for power sharing between microsources

In a microgrid there is no "master" controller or source. Each of the sources are connected in a peer to peer fashion and a decentralized control scheme is implemented. This arrangement increases the reliability of the system in comparison to having a master-slave or centralized control scheme. In the case of master-slave controller architecture [13] the failure of the master controller would compromise the operation of the whole system. The decentralized control in the microgrid is achieved without an explicit communication system using real and reactive power droop based local controllers. A communication system can be setup to vary DG set points to improve

efficiency or decrease the overall cost of operation. However this communication network is not needed for the dynamic stability of the system. As the presence of a communication network is not critical the introduction of new resources into the microgrid can be achieved quite easily. This plug and play approach allows us to expand the microgrid and scale it to meet the requirements of the customer.

The control of inverter based DG's for operation in a microgrid environment using real and reactive power droop controllers has been demonstrated in [20-22]. Standby generators historically have used wound field synchronous machines connected to either diesel or gas engines. No inverter is needed as the machine provides the AC voltage of the desired frequency as long as the speed of the shaft is kept around a fixed value. One of the primary drawbacks of this system is that without the inverter front end the dynamics of the prime mover cannot be decoupled from the output of the generator. The reduced cost of the system due to the absence of the power electronic front end is one of the major advantages. The interaction between power electronic based sources and traditional sources like steam and hydraulic turbine driven units was studied in [15] in the context of optimal dispatch under market conditions. It was shown that unstable operation could result due to the connection of "slow" prime movers with power electronic sources. The chief cause for the instability is the absence of the reactive power droop curves for the various sources. During disturbances the lack of these droop curves cause large circulating currents which can cause the system to lose synchronism. In the microgrid each source uses the power frequency as well as reactive power – terminal voltage droop to maintain power quality and system stability.

In [60] and [61] the use of engine driven synchronous machine based distributed resources in a microgrid environment has been studied. The interaction of these sources with power electronic sources in [60] has been simulated using the PSCAD/EMTDC platform and the block diagram of the system studied is shown in Fig. 6. The engine based system has been modeled using standard models described in IEEE standards [25] which are applicable to large (MVA range) synchronous machines. Smaller gensets have different governor and regulator schemes as shown in [55-58] and need a different control strategy. Furthermore the approach did not modify the controller of the synchronous machine voltage regulator to incorporate reactive power droop and incorporated the droop only in the inverter based sources. In the case of microgrids that have only synchronous machine based sources this would leave to significant circulating VAR's in the system.

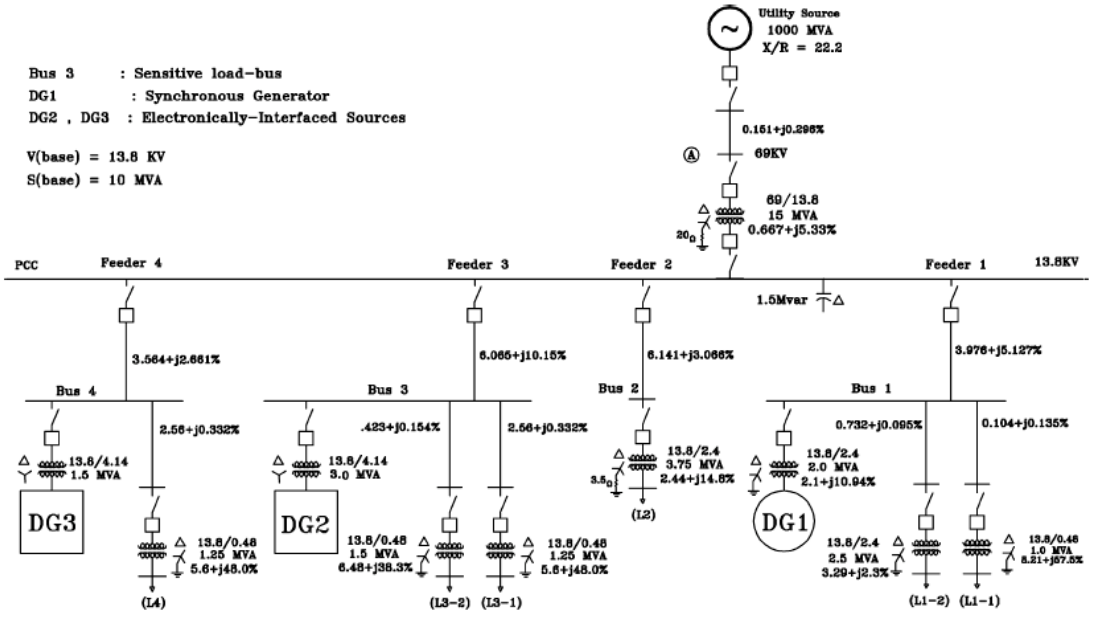

Fig. 6: Distribution system with synchronous machine and inverter based source analyzed in [60]

The feasibility of using such small IC engine driven wound field synchronous generators in a microgrid environment and the necessary modifications to the engine governor and the generator voltage regulator is the focus of this research effort. An integrated genset controller that utilizes an observer to estimate the various states has been developed. The various modifications proposed in this work will also be verified experimentally in the UW-Microgrid test bed [20 - 21].

2.4 Review of IC engine systems

The internal combustion (IC) engine is a type of prime mover in which the thermal energy produced during the combustion of fuel is converted to mechanical energy. The IC engine is used almost exclusively for mobile propulsion in vehicles, aircrafts and ships. The high energy density of the fuel (typically hydrocarbon based) provide the engine with an excellent power to weight ratio. IC engines can be broadly classified into spark ignition (SI) or compression ignition based systems. In SI engines the compressed air fuel mixture is ignited using a spark produced electrically whereas in a CI engine the heat produced during compression self ingites the air fuel mixture. The SI engine is also referred to as the petrol/gas engine or as the Otto engine after its inventor. The CI engine is referred to as the diesel or oil engine; where the fuel is also named after its inventor. Each engine can operate in either four stroke cycle or a two stroke cycle depending on the number of piston strokes completed to achieve a power stroke. The principles of operation of a four stroke cycle are explained using the diesel cycle.

The operation of the four stroke diesel engine is illustrated in Fig. 7. The entire cycle can be broken down into four principal phases:

- Intake stroke
- Compression stroke
- Expansion stroke
- Exhaust stroke

During the intake (or induction) stroke the intake valve is open and fresh air occupies the cylinder volume as the piston moves downward from top dead center to bottom dead center. Resistance to airflow in the intake valve results in the pressure being slightly less than atmospheric pressure. During the initial part of this stroke the exhaust valve is open for some time to improve the scavenging of the cylinder.

In the second stroke the air in the cylinder is compressed by the piston moving upwards. During this period both the intake and exhaust valves are closed. During this compression process the temperature inside the cylinder rises and when its high enough to self ignite the fuel the injection of fuel oil into the cylinder begins. After an ignition delay the fuel oil self ignites. Typically the fuel oil is injected before the piston reaches top dead center position.

Once the fuel ignites it releases heat which expands the gases inside the chamber. The rise in pressure forces the piston to move to bottom dead center and provides the power for operating the engine. During this stroke the pressure in the cylinder rises to a peak and then starts falling as the piston moves downwards.

The final stroke in the four cycle operation is the exhaust stroke. During this time the upward motion of the piston forces the exhaust gases out of the cylinder via the exhaust valve which is opened. To aid in scavenging the exhaust valve remains open for a fraction of time in the intake stroke as well.

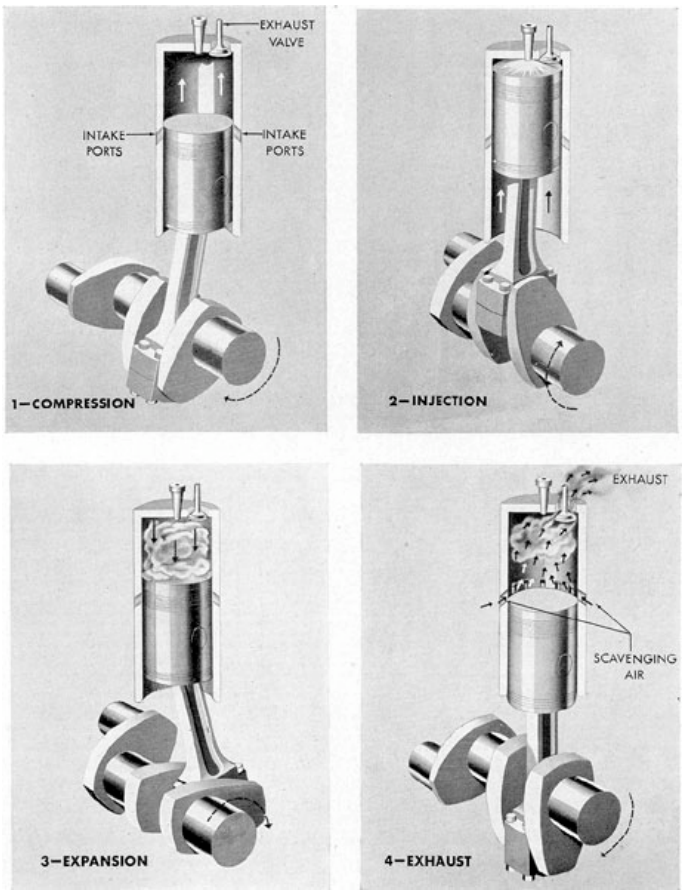

Fig. 7 : Illustration of the four strokes in diesel engine [Maritime.org]

In the two stroke cycle the power and exhaust stroke are combined into one to form one stroke and the compression and intake are combined to form the next stroke. This is accomplished by utilizing the space beneath the piston and by carefully placing the intake and exhaust ports. The intake and compression phases take place in the space beneath the piston and the power and exhaust take place in the space above the piston. Two-stroke cycle based IC engines have a higher power to weight ratio in comparison to the four stroke engine but they generally have higher emission and are less efficient.

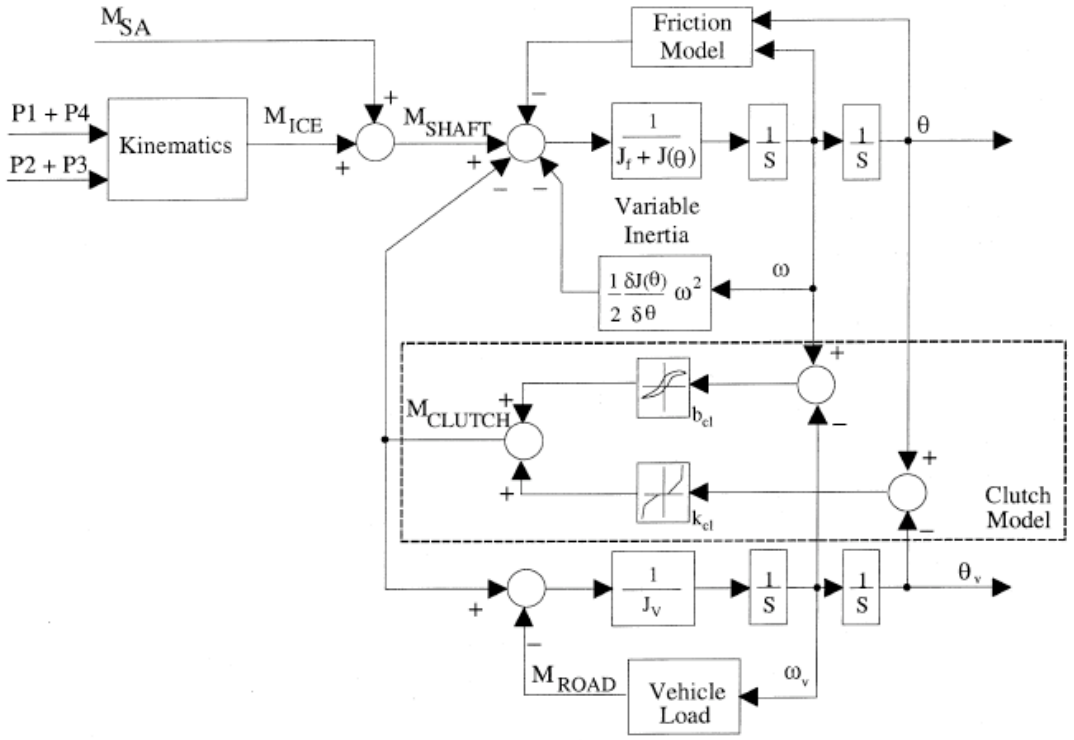

Fig. 8: Diesel engine model accounting for individual cylinder pressure and clutch, road and cylinder friction [39]

The instantaneous torque produced by an IC engine depends on the various thermodynamic processes taking place within the cylinder as well as the mechanical linkages that connect the cylinder to the crankshaft. A detailed model of the engine would account for all these dynamic processes [29, 33-39, 43-49]. For example in [39, 7] the individual cylinder pressures for a diesel engine are coupled with the crank dynamics and clutch friction to generate the indicated torque produced by the engine as shown in Fig. 8. The model requires the detailed characterization of the pressure inside the cylinder during each stroke including the effect of varying fuel level. The desire to decrease emissions and improve the response of the engine has led to the need for modeling the exact physical processes using computational fluid dynamics (CFD) that take place inside the cylinder during the various strokes [34]. However for operation of the IC engine based

genset in a distribution system it is not necessary to model the engine in such detail. Our focus in this area is to use the engine to provide the input mechanical torque to the generator to meet the desired load.

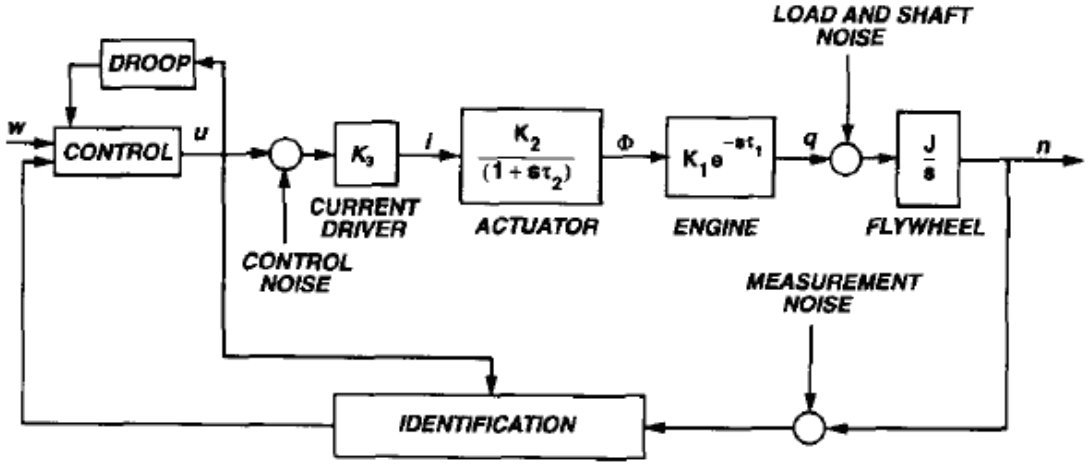

Fig. 9: Simplified model of IC engine for operation in a power system from[40]

In a distribution system that contains different sources the response of the engine will be slower in comparison to those sources that have power electronic inverters. Hence we need to utilize an engine model that quantifies the major delays and relates the input fuel command to the average torque produced on the shaft. Furthermore as we operate the generator at a very narrow range of speeds to produce 60Hz output the friction losses in the engine can be considered relatively constant. The simplified modeling of IC engine gensets for simulation in power system applications has been carried out in [31, 40, 41, 42] and is shown in Fig. 9 and Fig. 10. Detailed modeling of the mechanical governor used in small engine systems has been carried out in [51] and is used in conjuction with the engine models described in [31, 40, 41, 42]. The key feature of the engine model is the use of a pure time delay to represent the time it takes for a fuel command to translate as torque on the shaft.

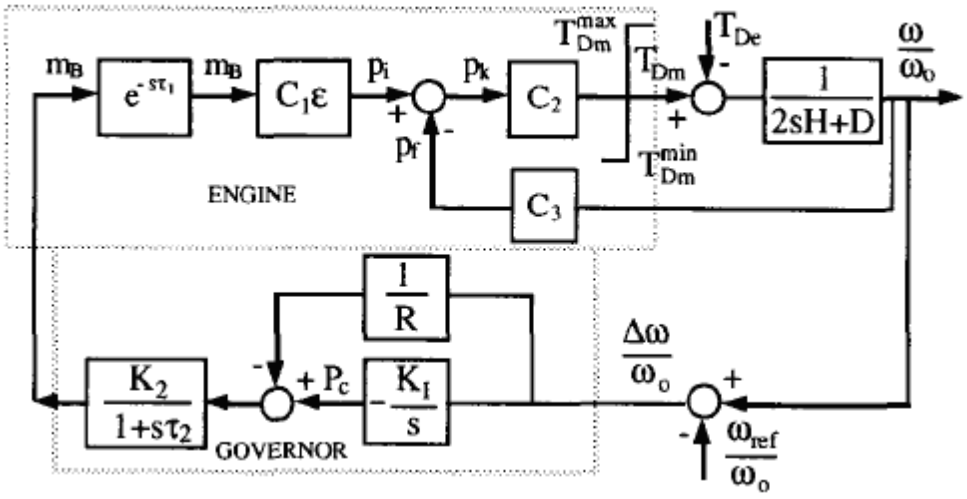

Fig. 10: Simplified model of IC engine for operation in a power system from[42]

The value of this time delay depends on the speed at which the shaft is rotating and the number of active cylinders in the engine. The value of the time delay is essentially the time it takes for a power stroke to repeat. The governor model in [40, 41, 42] assume that load restoration takes place and that the reference frequency is always 50 or 60Hz. In the case of a microgrid however the frequency during island operation can vary and depends on the load in the system. The model used utilizes the governor model from [51] and uses curve fitting to estimate the various constants.

2.5 Summary

The chapter contains a detailed literature review of the various aspects covered in this research work. The state of the art in distributed resources, microgrids and IC engine modeling and control is examined and the motivation for the use of IC engine driven wound field synchronous generators as a distributed resource is presented. The

operational differences between the large wound field synchronous generators used in power generation and the smaller generators used in gensets is discussed. The reduced capital cost for IC engine based gensets is one of the main driving forces for their consideration as a DG. This chapter has presented the state of the art for the use of such gensets in DG applications. It has discussed the need for the modifications of their controls for their operation in a microgrid environment and presented the sources for the models used in this research work.

CHAPTER 3. Modeling of IC engine based genset

Typical IC engine based gensets have an IC engine connected to a wound field synchronous machine connected together on the same shaft (Fig. 11). To provide the field excitation for the main generator a brushless exciter arrangement is typically used. The brushless exciter is controlled using the voltage regulator to maintain the desired terminal voltage. The IC engine has a governor that controls the torque on the shaft to maintain the desired output frequency. The frequency of the voltage produced by the generator depends on the shaft speed. Hence the speed has to be regulated within a narrow range to generate the desired 50/60 Hz output. The modeling of the various individual components is discussed and sample calculations pertaining to a 10kW Kohler genset are presented.

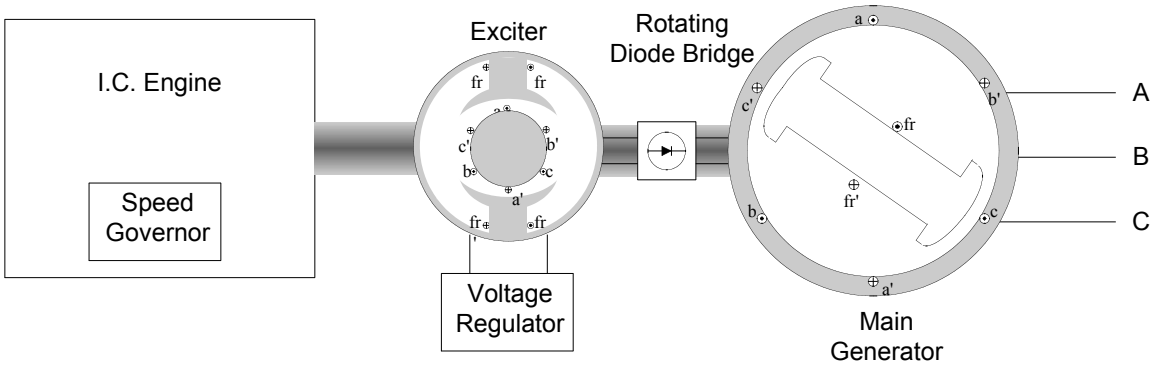

Fig. 11 : Typical configuration of IC engine based genset system

3.1 Model of IC engine using mean effective pressure

The detailed modeling of the engine involves modeling the pressure in the various cylinders as a function of the crank angle. Using the pressure in the cylinder we can

integrate over the volume as a function of the crank angle and obtain the torque produced by the engine as a function of time. However to accurately calculate this we need various parameters which are not easily obtainable. We will instead develop a simplified model using the mean effective pressure of the engine. The test engine used for the calculations is a Yanmar diesel engine used in a Kohler genset that will be used for experimental verification of all the control algorithms proposed.

Mean effective pressure

The mean indicated pressure is equivalent to a constant pressure acting on the cylinder that would produce work during one stroke of the piston equal to the work of the actual variable pressure of the cylinder charge during one working cycle. The output of the engine using the mean effective pressure value is given by equation 1 from [37]:

$$52.3\ D^2\ c_m p_e k z \tag{1}$$

The various quantities in the equation are defined as follows:

- 52.3 comes about as part of unit conversion
- D = Bore diameter
- c_m = Mean piston speed
- p_e = Mean effective pressure
- k = 0.5 for four stroke engines
- z = Number of cylinders

On a steady state basis the mean effective pressure inside the cylinder depends on the rate of fuel flow in the engine. For a given speed of operation mean effective pressure increases linearly with fuel rate.

The relevant parameters of the Yanmar engine used in the Kohler genset are:

- Nominal operating speed (1800 rpm)
- Mean piston speed (5.4 m/sec)
- Counterclockwise rotation (viewed from flywheel)
- No 2 fuel oil
- Mean effective pressure for 13.8kW output = 6.12kg/cm^2
- Fuel rate at rated speed and 13.8kW output = 238g/kWhr

Modeling the fuel input for a given speed

Using the manufacturer specified values for mean effective pressure and piston speed the rated continuous output of the engine is calculated to be equal to 18.3 kW. The mechanical output from the data sheet for the given mean pressure is 13.8 kW. We can assume that the difference arises due to the mechanical losses in the system. Due to this the net output power would be less than the power developed in the cylinders .The calorific value of number 2 fuel oil is approximately 18300 BTU/lb or 11.82 kWhr/kg. The rated fuel consumption of the Yanmar engine is 238g/kWhr for a continuous output of 13.8 kW. The input power for the specified fuel consumption is 38.83 kW which translates into an overall efficiency of approximately 35% . To calculate the fuel required for part load we need to divide the losses in the system into mechanical and thermodynamic losses. We will assume that the mechanical losses remain constant and thermodynamic losses vary with loading. This can be represented as:

$$
\begin{aligned}
P_{out} &= P_{fuel} - P_{mech} - P_{thermal} \\
P_{thermal} &= 20.5kW \\
P_{mech} &\approx 4.5kW \\
\eta_{thermal} &= 18.3/38.8 = 0.47
\end{aligned}
$$

We will further assume that the thermodynamic efficiency does not vary with loading. The speed command from the machine is converted into an equivalent fuel command for a 5% droop using the following steady state relationships:

- Fuel needed to produce 13.8 kWhr = 3.284kg (0.238×13.8)
- Fuel wasted to provide for mechanical losses 4.5 kWhr = 0.808 kg
- Fuel wasted to provide for mechanical losses 4.5 kW = 0.2244g/sec
- Fuel needed to produce 6.25kW output (power at which frequency is 60Hz) = 0.5362 g/sec
- Fuel needed to produce 12.5kW output (power at which frequency is 58.5Hz) = 0.8486 g/sec
- Fuel command(g/sec) for 5% droop = $(1-\omega_{pu}) \times 2 \times \left[\frac{0.8486 - 0.5362}{0.05}\right]$ + 0.5362
- Fuel command(g/sec) for 5% droop = $(1-\omega_{pu})12.47 + 0.5362$

Hence the fuel input command determines the resulting power frequency droop. The fuel input command depends on the rotor speed and hence if the machine slows down the fuel would increase proportionately to achieve a desired droop. In the Kohler genset the power frequency droop is implemented using the mechanical governor. The governor implements the droop and also imparts some dynamics to the whole process. The above equation represents the steady state power frequency droop. The dynamic equations for

the mechanical governor are presented in another section. The resulting power produced in the engine as a function of fuel rate is shown in Fig. 12

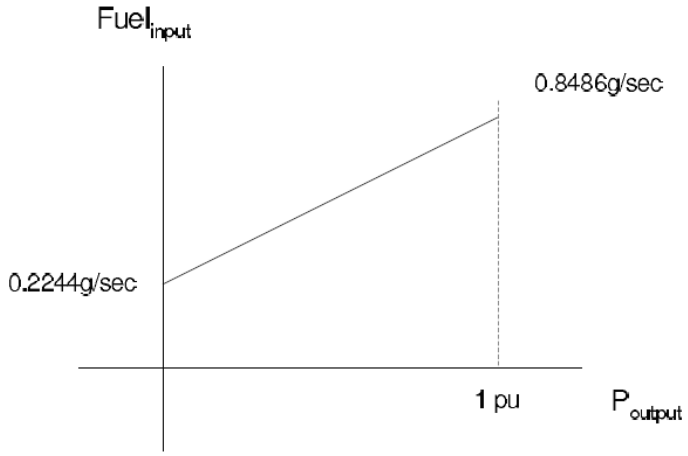

Fig. 12 : Output power versus fuel input at rated speed for Yanmar engine

Modeling combustion dynamics

The actual combustion process is modeled as a time delay. The value of the time delay can be estimated by assuming the change in power occurs after completing a power strok following the updating of the fuel command. For a four stroke three cylinder engine operating at 1800 rpm the time delay can be calculated to be Td = $\frac{240}{360}\frac{1}{30}$ = 22ms. This full power stroke delay actually represents the upper limit on the amount of time before the engine responds to a command change. If the command change occurs at a point in the cycle just before the fuel is injected into the cylinder the delay would be much smaller. Hence on an average the time delay will be less than one power stroke. However if we include the fuel actuator time constant and the intake manifold dynamics the net time delay can be reasonably modeled as one full power stroke.

3.1.1 Model of mechanical governor

A typical mechanical governor is shown in Fig. 13. The governor can be modeled analyzing the forces that act on the various components. The governor is connected to the shaft of the engine either directly or using a gear arrangement. The shaft rotation causes the flyweights to move outward or inward depending on the speed. The centrifugal force caused due to the rotation of the flyweights is balanced by a spring force. The spring is connected to the fuel lever whose position is affected by the rotating flyweights.

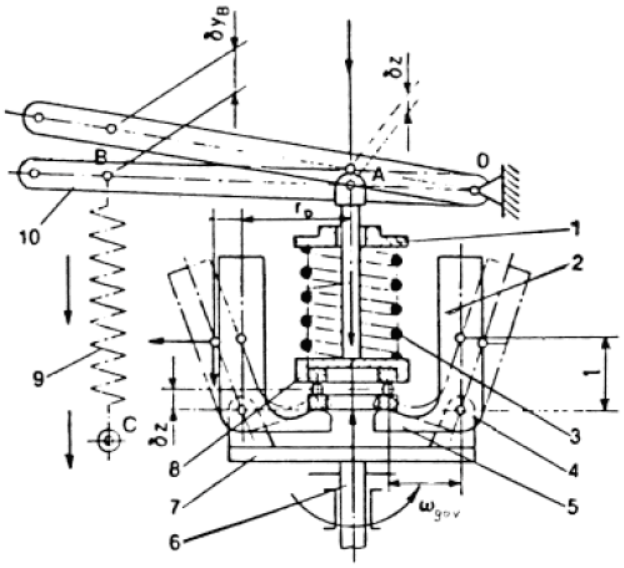

Fig. 13 : Schematic of mechanical governor [51]

In steady state the centrifugal force balances the spring restoring force. The steady state fuel lever position can be related to the speed using the following relationships obtained from [].

$$F_{cf} = (a_{se} + b_{se} z) i_{gov}^2 \omega^2 \quad (2)$$

$$F_{sp} = k\, i_{tr}\, (y + i_{tr} z) \quad (3)$$

$$z = \frac{a_{se} i_{gov}^2 \omega^2 - k\, i_{tr} y}{k\, i_{tr}^2 - b_{se} i_{gov}^2 \omega^2} \quad (4)$$

- F_{cf} = Centrifugal force
- F_{sp} = Spring force
- $a_{se} = nm_{fw}\frac{d}{r_o}l$
- n = Number of flyweights
- m_{fw} = Mass of flyweight
- d = Ball arm finger length
- r_o = Initial radius of gyration of flyweights
- l = Ball arm length
- $b_{se} = nm_{fw}\left(\frac{l}{d}\right)^2$
- i_{gov} = Transmission ratio from rotor shaft to governor rotation
- m_{gov} = Mass of clutch element
- ω = Rotor speed
- k = Spring constant
- i_{tr} = Transmission ratio of the clutch to the spring
- y = Constant spring strain (initial setting)
- z = Fuel lever position

We can see that the fuel lever position is a function of the square of the shaft speed.

However the governor operates in a region where the function is linear to impart a predesigned droop to the genset. During transient operation we can use Newton's Laws to determine the rack position.

$$m_{gov}\frac{d^2z}{dt^2} + f\frac{dz}{dt} + \left(k\, i_{tr}^2 - b_{se} i_{gov}^2 \omega^2\right) z = a_{se} i_{gov}^2 \omega^2 - k\, i_{tr} y \qquad [5]$$

If the above parameters were available it would be possible to accurately predict the response of the governor. However in the absence of the exact parameters the mechanical governor response needs to be modeled using a transfer function. The governor transfer function used in the system has the following form.

$$G_2(s) = \frac{T_2 s^2 + T_1 s + 1}{T_4 s^2 + T_3 s + 1} \qquad [6]$$

The various time constants need to be tuned to achieve a suitable match with experimental results.

The diesel engine can now be modeled using the fuel to torque conversion ratio, mechanical losses and the engine time delay. We know that the mean effective pressure in the cylinder is directly proportional to the fuel input. Increasing the fuel input increases the pressure increasing the mechanical torque applied by the prime mover on the shaft. Using the fuel consumption rate and the combustion dynamics we will calculate the relationship between fuel input and output mechanical power.

• Mechanical losses assuming speed deviation is small : 4.5kW or 0.36pu (12.5 kVA base) at base speed The frictional loss at other speeds can be linearized around this point.

• Power produced by input fuel : $\eta_{thermal} \times$ Calorific Value $\times$ Fuel Rate -

Mechanical Losses

- Power produced by input fuel at rated speed: $0.47 \times \frac{11.8238 \times 3600}{12500} m_f - 0.36$
- Power produced by input fuel at rated speed : $1.6 m_f - 0.36$

The power produced by the combustion of the fuel appears at the shaft after the combustion delay. When we replace the mechanical governor with the electronic governor we will use the following equation to model the diesel engine dynamics:

$$T_{mech}(t) = 1.6\, m_f(t - T_d) - 0.36\, \omega_r(t) \quad (7)$$

In this equation the fuel input rate is m_f and the combustion delay is T_d.

3.2 Model of synchronous machine

In wound field synchronous machines there are two sources of input power, namely the DC field and the mechanical shaft power. The power factor of the machine can be varied by changing the magnitude of the DC field excitation. The wound field rotor can be constructed in two major variations:

- Salient or projecting pole construction
- Smooth or round rotor

The round rotor is typically used for high speed applications and is either a two pole or four pole machine whereas salient pole machines are typically used for slower speed generators.

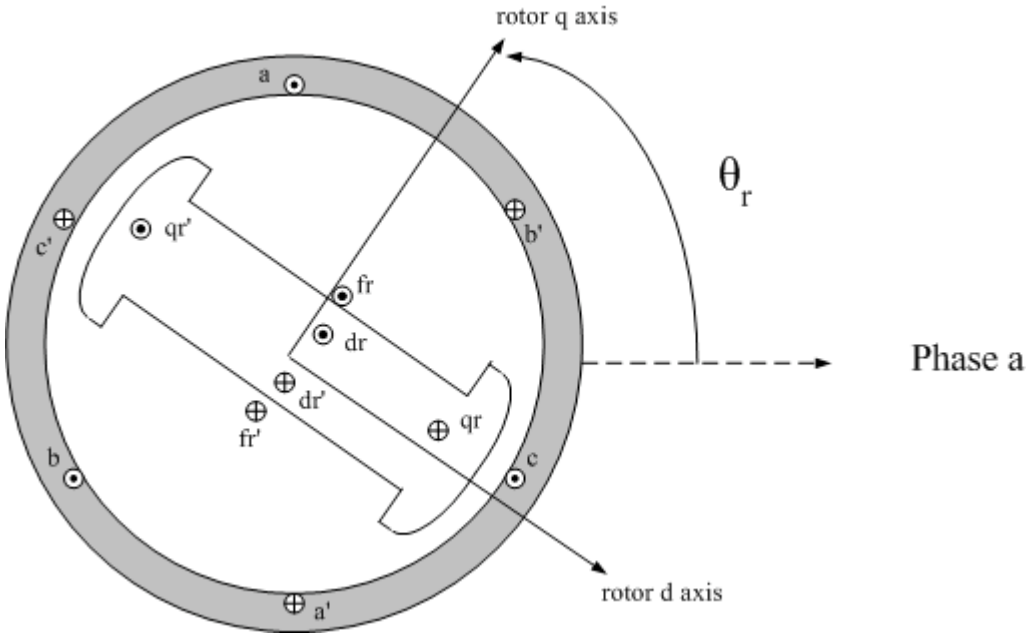

Fig. 14 : Salient pole synchronous machine structure

The field winding in a salient pole machine (Fig. 14) consists of concentrated windings mounted on projecting rotor poles. Additional rotor windings (amortisseur) are often used in salient pole machine for providing damping torque during transient conditions. They consist of bars inserted along periphery of poles that are shorted by end rings. A number of models for synchronous machines exist depending on the level of complexity that needs to be modeled. Typical models of synchronous machines as shown in Fig. 15 account for one damper in the d-axis and one damper in the q-axis.

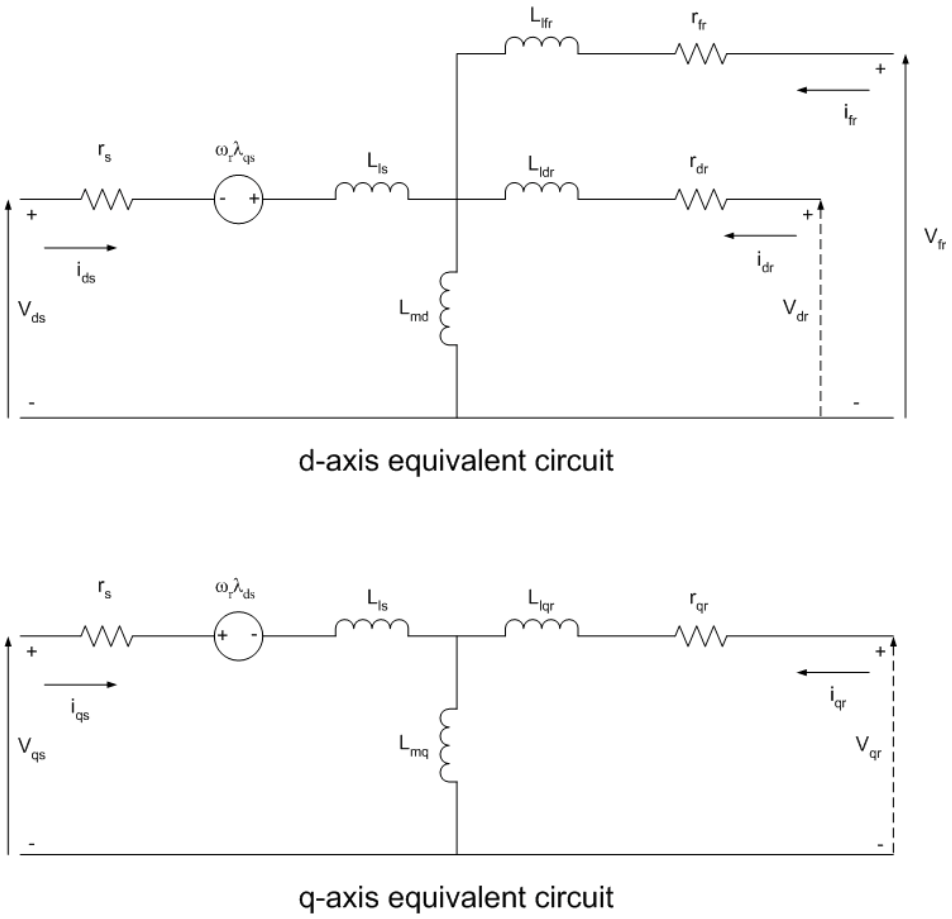

Fig. 15 : DQ equivalent circuit for wound field synchronous machine

3.2.1 Flux voltage model of synchronous machine

The machine state equations in terms of flux voltages for a model that consists of one damper in the d axis and one damper in the q axis (Fig. 15) is given below [69, 70].

$$p\psi_{ds}^{r} = \omega_b \left[v_{ds}^{r} + \omega_r \psi_{qs}^{r} + r_s \left(\frac{\psi_{md}^{r} - \psi_{ds}^{r}}{x_{ls}} \right) \right] \tag{8}$$

$$p\psi_{kd}^{r} = \omega_b r_{kd} \left(\frac{\psi_{md}^{r} - \psi_{kd}^{r}}{x_{lkd}} \right) \tag{9}$$

$$p\psi_{fd}^{r} = \omega_b \left[E_f \frac{r_{fd}}{x_{md}} + r_{fd}\left(\frac{\psi_{md}^{r} - \psi_{fd}^{r}}{x_{lfd}} \right) \right] \tag{10}$$

$$p\psi_{qs}^{r} = \omega_b \left[v_{qs}^{r} - \omega_r \psi_{ds}^{r} + r_s\left(\frac{\psi_{mq}^{r} - \psi_{qs}^{r}}{x_{ls}} \right) \right] \tag{11}$$

$$p\psi_{kq}^{r} = \omega_b \, r_{kq}\left(\frac{\psi_{mq}^{r} - \psi_{kq}^{r}}{x_{lkq}} \right) \tag{12}$$

$$p\omega_t = \frac{T_e + T_{mech}}{2H} \tag{13}$$

3.2.2 Interfacing machine model with network equations

The conventional flux voltage model presented above presents a challenge while interfacing with the network equations. Conventionally the network constraints are modeled as algebraic equations (power flow equations). The machine equations are differential equations that need to be interfaced with the power flow equations. This is done by starting of at an initial point that is solved for using load flow technique. For this initial point the machine states are calculated. If a change in input or change in network occurs the instantaneous values of currents flowing through the network are solved using load flow. These currents with field and mechanical input are then fed to the machine model and the machine states are calculated. Stator transients are neglected which allows us to calculate the terminal voltages of the machine from the states which are used in the power flow equations. This process is repeated until steady state is reached.

The flux voltage formulation however uses the terminal voltage in the state equations. Hence this model cannot be directly interfaced into the network equations. To utilize the

flux voltage model presented earlier we need to modify the model to accept the stator currents as inputs. Using the stator currents transformed into the rotor reference frame we can calculate each of the states using just the currents, mechanical input, field voltage and initial conditions for the states. However we must realize that once we use the stator currents as inputs the stator flux voltages "ψ_{ds}" and "ψ_{qs}" are no longer states but become dependent variables. Hence the stator dynamics are now captured in the network differential equation that models the stator "*dq*" currents. This procedure enables to use as detailed a model as we wish with the network during the simulation of the microgrid. The modifications of the state equations to incorporate currents as inputs are shown below:

$$\dot{i}^{s}_{qs} = \left[\frac{2i_{as} - i_{bs} - i_{cs}}{3}\right] \tag{14}$$

$$\dot{i}^{s}_{ds} = \left[\frac{-i_{bs} + i_{cs}}{\sqrt{3}}\right] \tag{15}$$

$$\dot{i}^{r}_{qs} = \left[\dot{i}^{s}_{qs}\cos\theta_r - \dot{i}^{s}_{ds}\sin\theta_r\right] \tag{16}$$

$$\dot{i}^{r}_{ds} = \left[\dot{i}^{s}_{qs}\sin\theta_r + \dot{i}^{s}_{ds}\cos\theta_r\right] \tag{17}$$

$$\psi^{r}_{qs} = x_{ls}\dot{i}^{r}_{qs} + x_{MQ}\left[\frac{\psi^{r}_{qs}}{x_{ls}} + \frac{\psi^{r}_{kq}}{x_{lkq}}\right] \tag{18}$$

$$\psi^{r}_{qs} = \frac{x_{ls}\,\dot{i}^{r}_{qs} + x_{MQ}\left(\frac{\psi^{r}_{kq}}{x_{lkq}}\right)}{1 - \frac{x_{MQ}}{x_{ls}}} \tag{19}$$

$$\psi^{r}_{mq} = \frac{\frac{\psi^{r}_{kq}}{x_{lkq}} + i_{qs}}{\frac{1}{x_{mq}} + \frac{1}{x_{lkq}}} \tag{20}$$

$$\psi^{r}_{ds} = x_{ls} i^{r}_{ds} + x_{MD}\left[\frac{\psi^{r}_{ds}}{x_{ls}} + \frac{\psi^{r}_{kd}}{x_{lkd}} + \frac{\psi^{r}_{fd}}{x_{lfd}}\right] \tag{21}$$

$$\psi^{r}_{ds} = \frac{x_{ls} i^{r}_{ds} + x_{MD}\left(\frac{\psi^{r}_{kd}}{x_{lkd}} + \frac{\psi^{r}_{fd}}{x_{lfd}}\right)}{1 - \frac{x_{MD}}{x_{ls}}} \tag{22}$$

$$\psi^{r}_{md} = \frac{\frac{\psi^{r}_{kd}}{x_{lkd}} + \frac{\psi^{r}_{fd}}{x_{lfd}} + i_{ds}}{\frac{1}{x_{md}} + \frac{1}{x_{lkd}} + \frac{1}{x_{lfd}}} \tag{23}$$

In steady state the terminal dq voltages are

$$V^{r}_{qs} = r_s i^{r}_{qs} + \omega_r \psi^{r}_{ds} \tag{24}$$

$$V^{r}_{ds} = r_s i^{r}_{ds} - \omega_r \psi^{r}_{qs} \tag{25}$$

Hence the state equations of the machine are

$$p\psi^{r}_{kq} = \omega_b r_{kq}\left(\frac{\psi^{r}_{mq} - \psi^{r}_{kq}}{x_{lkq}}\right) \tag{26}$$

$$p\psi^{r}_{kd} = \omega_b r_{kd}\left(\frac{\psi^{r}_{md} - \psi^{r}_{kd}}{x_{lkd}}\right) \tag{27}$$

$$p\psi_{fd}^{r} = \omega_b \left[E_f \frac{r_{fd}}{x_{md}} + r_{fd} \left(\frac{\psi_{md}^{r} - \psi_{fd}^{r}}{x_{lfd}} \right) \right] \quad (28)$$

$$p\omega_r = \frac{T_e + T_{mech}}{2H} \quad (29)$$

$$p\theta_r = \omega_b \omega_r + \theta_{r0} \quad (30)$$

In conventional power system models the torque angle of the machine "δ" is used to convert the stator voltages into the rotor reference frame. The angle "δ" is calculated using the swing equation and the assumption that the reference frequency in the system is always a constant (either 50Hz or 60Hz). This assumption enables us to calculate the slip speed and hence the value of the torque angle as a function of time. Hence the conversion of the stator voltage and current quantities to the rotor reference frame involves a two step process:

1. Conversion of the stator "abc" quantities into synchronous frame "dq" values using base frequency angle variation
2. Conversion of the synchronous frame "dq" values into rotor reference frame using torque angle

In a microgrid application however the reference frequency is not fixed and hence we cannot convert the stator quentities into rotor reference frame quantities using the above procedure. Instead as shown in Eq. 30 the rotor speed is integrated to calculate the position of the rotor and this angle is directly used in Eq. 16, 17 and similarily for voltage to calculate the rotor reference frame "dq" quantities.

3.3 Model of brushless exciter

The brushless exciter is an inverted synchronous machine with a DC stator winding and AC windings on the rotor (Fig. 16). In larger generators the rotor windings are typically three phase [54]. In smaller machines (typically less than 50kW rating) the windings are generally single phase. The AC voltage is rectified into DC using a diode bridge that sits on the rotor. Hence depending on the input voltage to the brushless exciter the main field voltage can be controlled. The exact dynamic equations of the brushless exciter depend on the exciter machine parameters and the behavior of the diode bridge under dynamic loading.

In gensets the rating of the brushless exciter is typically 10% the rating of the main generator. These machines typically operate unsaturated. The entire exciter with diode bridge can be modeled as a first order transfer function for such small machines [31, 55]. The input current to the brushless exciter controls the flux and hence the voltage output of the machine. The variation in input current with voltage is a first order system with the time constant representing the ratio of inductance to resistance of the machine. Hence the input to the exciter is a voltage command (V_c) and the output is the main field voltage E_f and the dynamics can be represented using the following equations:

$$L_e p I_e = -I_e R_e + V_c \tag{31}$$

$$E_f = I_e K_e \tag{32}$$

In the above equations L_e and R_e represents the inductance and resistance of the exciter

respectively and I_e is the brushless exciter current. K_e is a constant and is the voltage produced by one ampere of brushless exciter current .

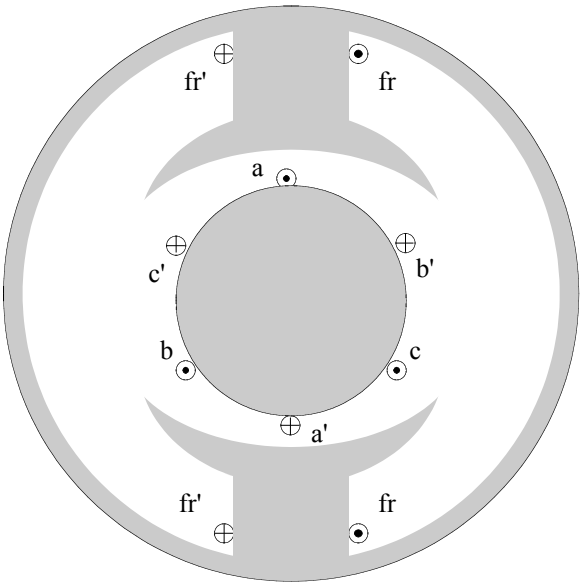

Fig. 16 : Schematic of two pole three phase brushless exciter

CHAPTER 4. Diesel genset test setup and modeling of conventional gensets

The architecture of a typical diesel genset with a wound field synchronous machine is shown in Fig. 17. The engine governor could either be mechanical or electronic in nature. Small gensets (rating less than 25kW) typically have mechanical governors to minimize the cost of the system. The synchronous generator is coupled to the engine and its field winding is powered by a separate exciter machine. There are various exciter configurations possible and the most common structure consists of a brushless exciter. As described in the preceding chapter a brushless exciter is essentially an inverted synchronous machine with the DC input winding on the stator and AC output windings on the rotor. The output of the brushless exciter is rectified using a diode bridge that is placed on the shaft and is commonly known as a flying rectifier arrangement. The output of the rectifier bridge is connected to the field winding of the main synchronous machine.

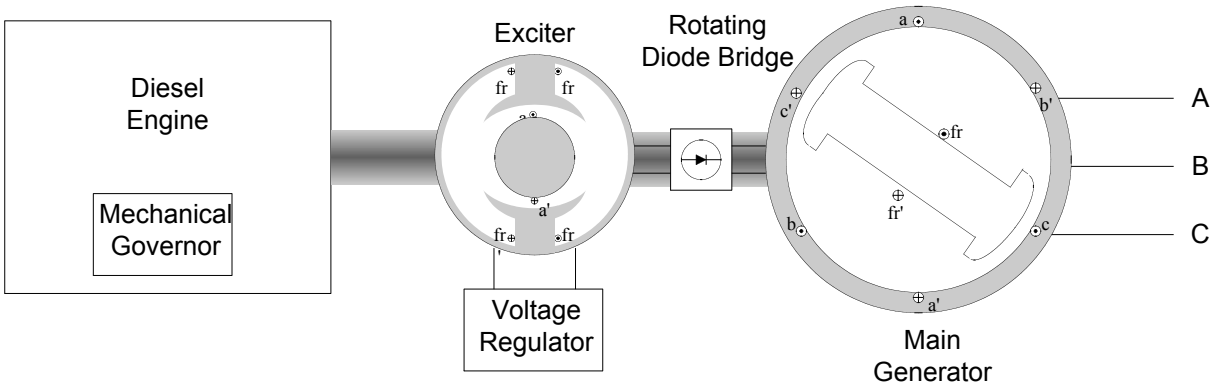

Fig. 17 : Configuration of Kohler 10kW diesel genset system

The field voltage of the main synchronous machine is controlled by varying the input DC voltage of the brushless exciter. Typically the input DC voltage is controlled using PWM switching allowing the controller to vary the field winding voltage as desired. Gensets operating in an islanded mode are setup to operate at a fixed voltage that can be modified by the user. To predict the behavior of the diesel genset in a microgrid environment it is necessary to develop a model that captures the required dynamics. The model for the diesel genset was developed by studying its behavior in an islanded environment. To develop this model a 10kW diesel genset manufactured by Kohler was installed at the University of Wisconsin-Madison. The next section describes the test setup and the hardware test results used in developing the genset model.

4.1 Hardware components and system configuration

The Kohler genset (Model no. 10ROZ) consists of a 10kW diesel engine coupled to a wound field synchronous machine. The speed regulator in the genset is a mechanical governor and the exciter is of the brushless type having a single phase output. A voltage regulator provides the input to the brushless exciter using a standard 12V battery supply. The connection diagram for the Kohler genset is shown in Fig. 18. The Kohler genset is mounted outdoors on a grating adjacent to the main WEMPEC lab as shown in Fig. 19 and Fig. 20. The windings of the generator have been connected to provide 480V line to line rms voltage. This was done using the winding diagram provided in the operations manual of the genset. The output of the generator is brought into the lab using gauge 12 wires into a disconnect switch. Number # 4 wires then carry the power to a 45 kVA ΔY

transformer. The transformer steps the voltage down from 480V to 208V line to line. Resistor banks are connected at the secondary of the transformer to load the machine.

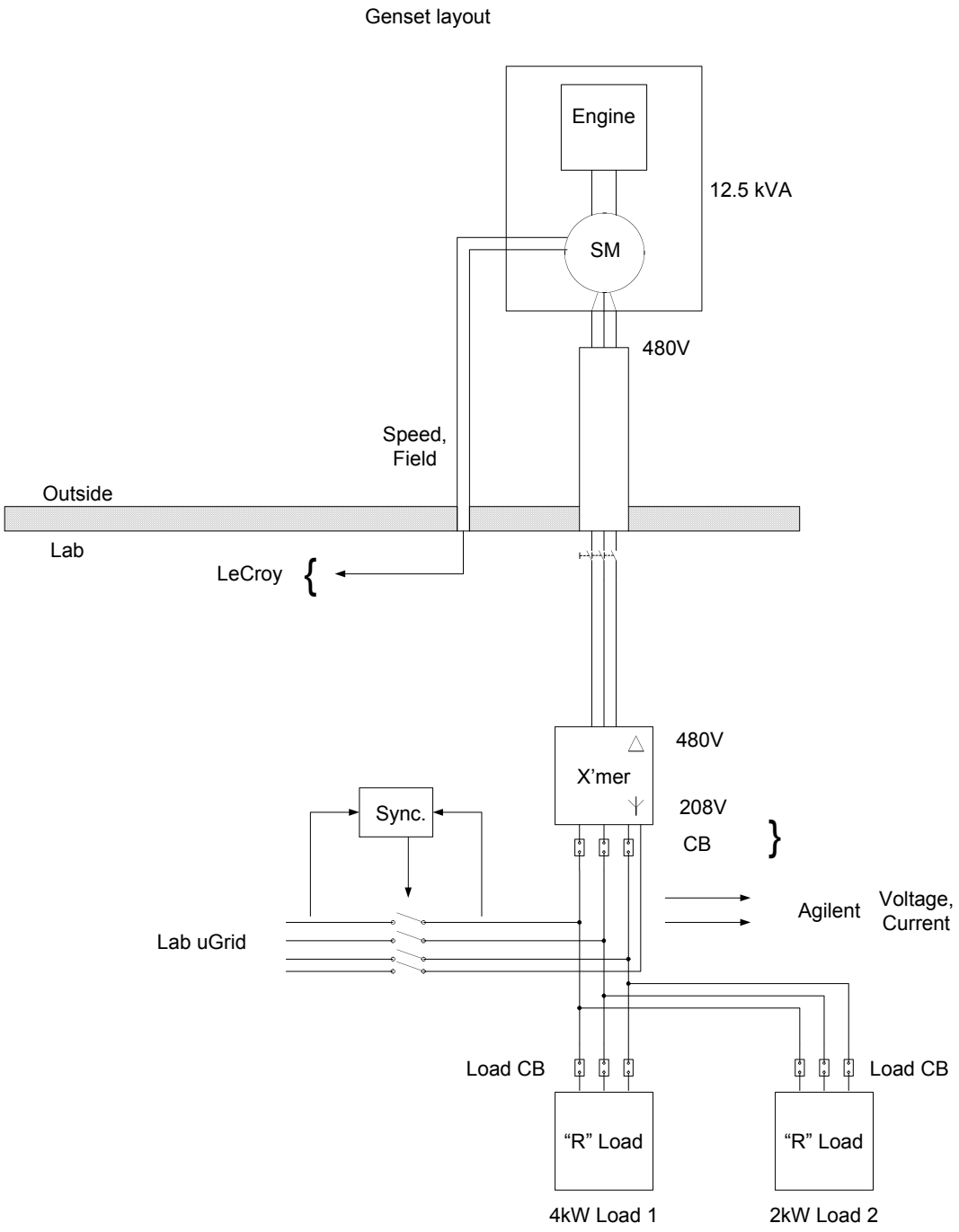

Fig. 18 : Diesel genset test setup at the University of Wisconsin-Madison

Fig. 19: Test setup for Kohler 10kW genset located outside engineering hall

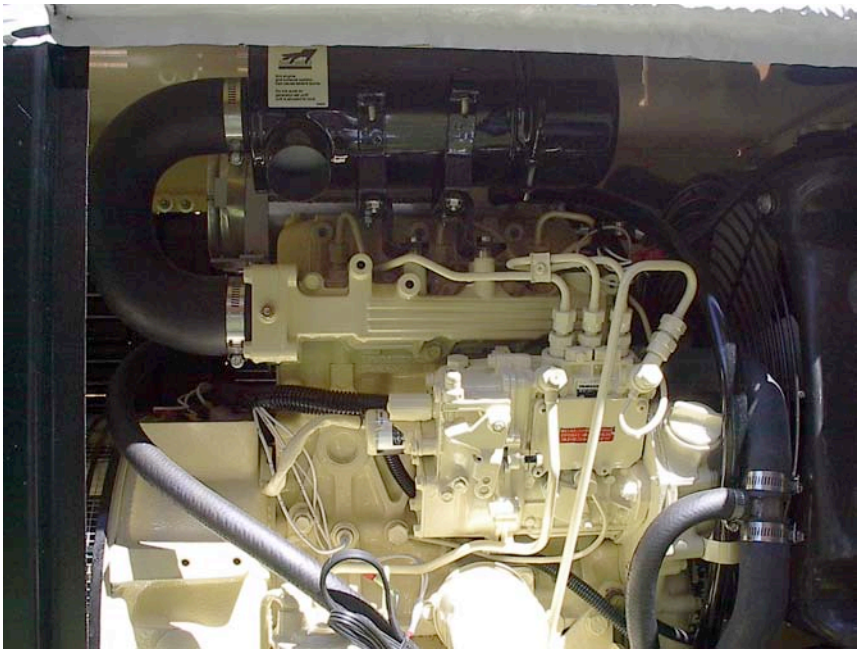

Fig. 20: Picture of Yanmar diesel engine used in 10kW Kohler genset

The parameters for the synchronous machine were obtained from Kohler and are given in Table 2.

Parameter	Value
V_{base}	240V
P_{base}	12.5kVA
x_d	1.204pu
x_q	0.533pu
$x_d^{'}$	0.125pu
$x_d^{''}$	0.056pu
$x_q^{''}$	0.051pu
x_l	0.037pu
$T_{d0}^{'}$	0.355s
$T_{d0}^{''}$	0.00015s
$T_{q0}^{''}$	1.235s
J	$0.4344 kg - m^2$

Table 2: Parameters for synchronous machine in Kohler 10ROZ Genset

4.2 Test results for step load and voltage changes

A series of step load tests were performed to determine the characteristics of the diesel genset. The load connected to the machine was changed by 4kW and the shaft speed, terminal voltage, current and brushless exciter input voltage were measured using an Agilent scope and they are plotted in Fig. 21. The pulsed output of the speed sensor was converted to a speed signal via post processing and the resulting waveforms are plotted in Fig. 22. From the waveforms we can clearly see that there is a change in the steady state frequency with loading. The change in frequency is consistent with the manufacturer specified droop value of 5%. We can also see the second order dynamics of the mechanical governor in the speed waveform. We can also see that during the transient the load voltage waveform regains its steady state value within a few cycles. The voltage regulator provided by the manufacturer has a V/Hz component that changes the terminal voltage based on the shaft speed. The V/Hz component is required to improve the motor starting capability of the genset. Hence in steady state at lower speed (for the higher load) the terminal voltage is slightly lower that at higher speed. The contribution of the per unit speed to the per unit terminal voltage was calculated to be close to 1%. These conclusions were confirmed by performing another load test with a 2kW step change and the waveforms obtained are plotted in Fig. 23 and Fig. 24.

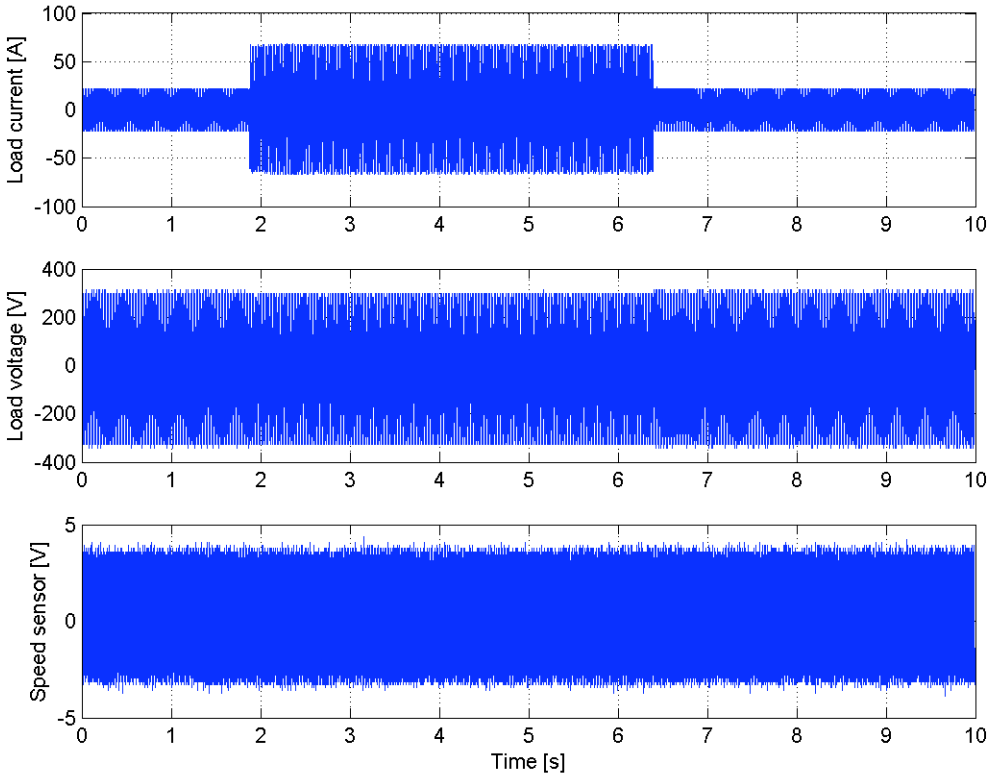

Fig. 21 : Experimental results for 4kW load switching

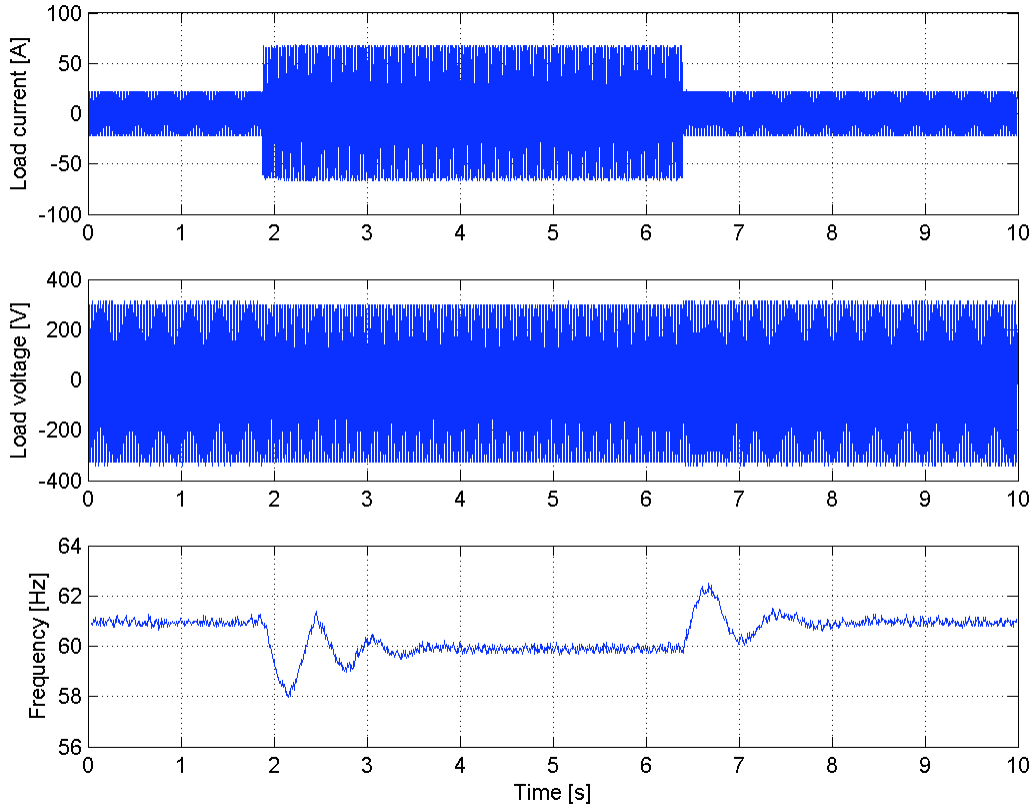

Fig. 22 : Experimental results for 4kW load switching waveform depicting change in frequency

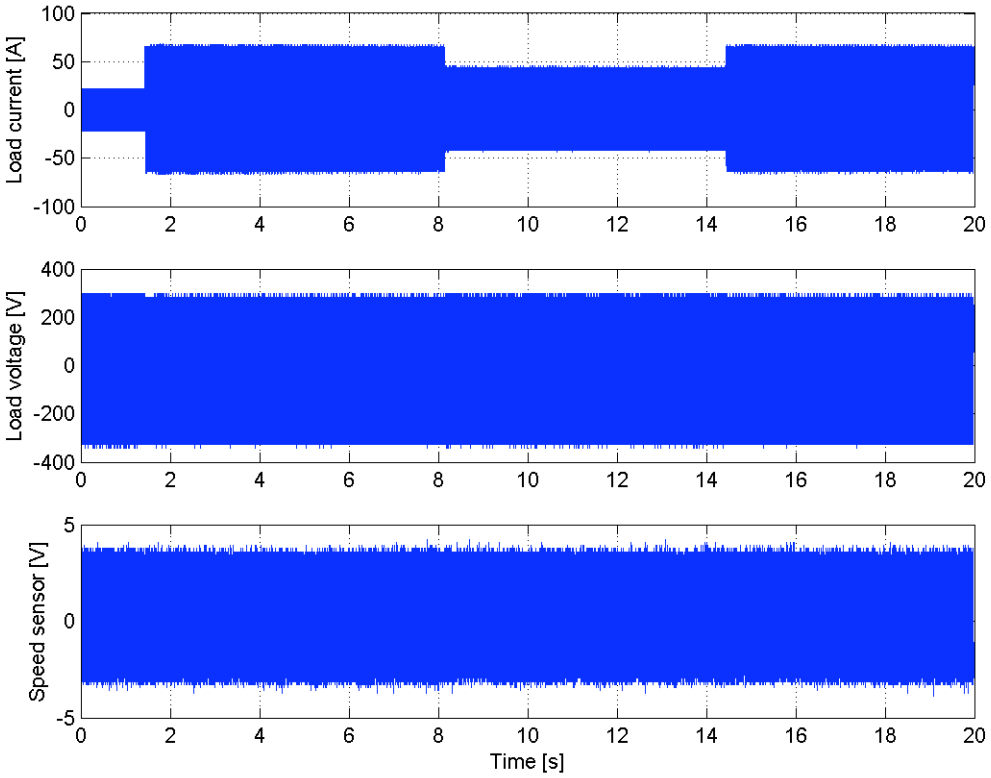

Fig. 23 : Experimental results for 4kW load increase followed by 2kW decrease and increase in load

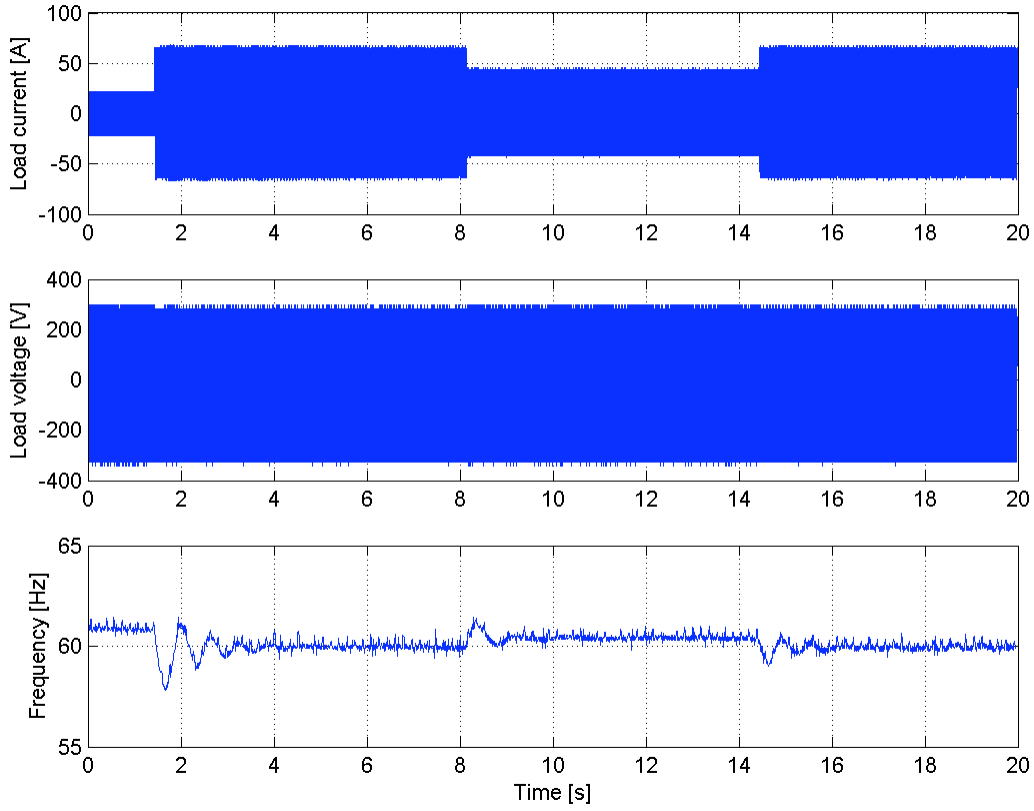

Fig. 24 : Experimental results for 4kW load increase followed by 2kW decrease and increase in load with

.

4.3 EMTP model of IC engine based genset model

Using the models for each component a model of the genset system was developed in the EMTP [75] simulation platform. EMTP is a sophisticated computer program for the simulation of electromagnetic, electromechanical and control systems transients in multiphase electric power systems. It features a wide variety of modeling capabilities encompassing electromagnetic and electromechanical oscillations ranging in duration from microseconds to seconds. This enables the simulation of the genset in a microgrid

environment. The lab setup shown previously in Fig. 18 is represented in EMTP as shown in Fig. 25.

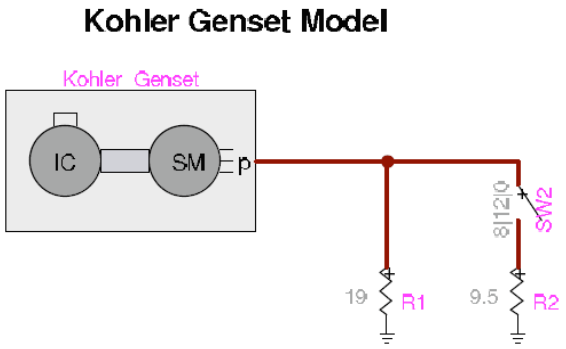

Fig. 25 : Lab setup modeled in EMTP

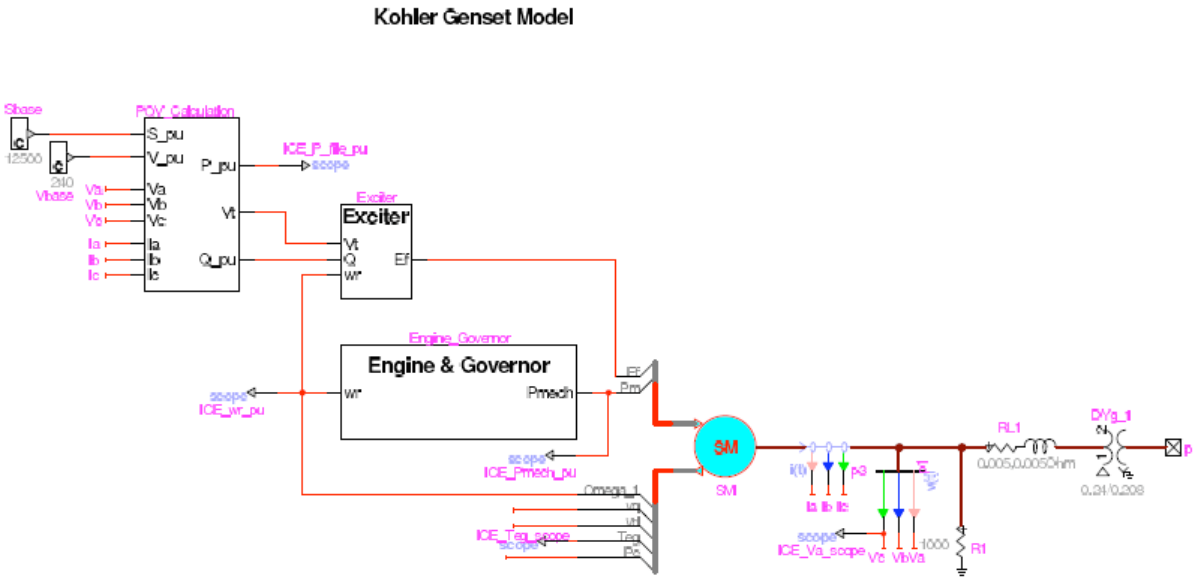

Fig. 26 : Internal model of diesel genset in EMTP

If we examine the model of the genset (Fig. 26) more clsoely we can see that it consists of four sub-blocks.

- Synchronous machine

- P,Q and V calculation block
- Exciter block
- Governor and Prime Mover Block

The output terminals of the synchronous machine are connected to a 45kVA transformer using a line impedance. A parallel resistive load of negligible value is connected at the synchronous machine terminals to alleviate numerical problems associated with disconnecting the synchronous machine from the rest of the system.

The synchronous machine model used is from the machines library of EMTP. While setting up the model we need to specify one damper in field axis circuit and one damper in the q axis circuit. To obtain a salient pole machine we set $x_q = x_{q'}$ and $T_{q0}' = 0$. We use maximum precision in the precision tab of the machine model and increase the number of maximum rotor speed iterations to 1000 to overcome numerical problems. The inertia of the machine is 0.19s and is calculated from the value specified by Kohler and is given in Table 1. The remaining electrical parameters are fed in the various tabs using the values given in Table 1. Also for simulation purposes the machine base voltage was specified as 240V and the transformer was modeled as a 240V/208V DYg transformer.

Kohler also specified the exciter machine to have a time constant of 1ms and that the voltage regulator was a PI controller. The voltage regulator has the following three control potentiometers:

- Volts/Hz setting
- Δ V setting
- Controller gain setting

For the exciter the reference voltage set point has two components:

- Speed dependent term

- Fixed reference point with ΔV control.

The three phase terminal voltages of the machine are rectified and filtered and passed to the exciter as the measured voltage. The difference between reference voltage and measured voltage is fed to a PI controller as shown Fig. 27 . The gain values Kp and Ki for the controller were set to mimic the dynamic performance observed in the hardware. During a transient change the variation in voltage was fairly negligible and this can be attributed to a high gain setting.

The desired field voltage obtained from the PI controller is passed through a time constant which describes the exciter machine. The exciter machine is configured with a DC field in the stator and a single phase winding on the rotor. The output of the exciter machine is rectified and fed to the main field of the machine. The rectifier arrangement is not modeled and instead the time constant represents the whole exciter and brush arrangement. The exciter provides the field voltage required for the main field of the synchronous machine.

The voltage regulator utilizes the terminal voltage and reactive power values calculated from the PQV calculation block and the per unit rotor speed. The reactive power is needed only for modifying the reference voltage command to incorporate QV droop. The Kohler genset does not incorporate QV droop and hence the value of droop is set to zero. The initial value of the PI controller output is set to minimize the startup transient. The per unit rotor speed deviation also contributes to the reference voltage calculation. From experimental tests the contribution was calculated to be equal to 0.01.

The exciter machine is represented as a first order system with a time constant of 1ms

(specified by Kohler). Typically machines with ratings less than 100 kW can be represented using either first order or second order systems instead of the more complex standard IEEE exciter definitions.

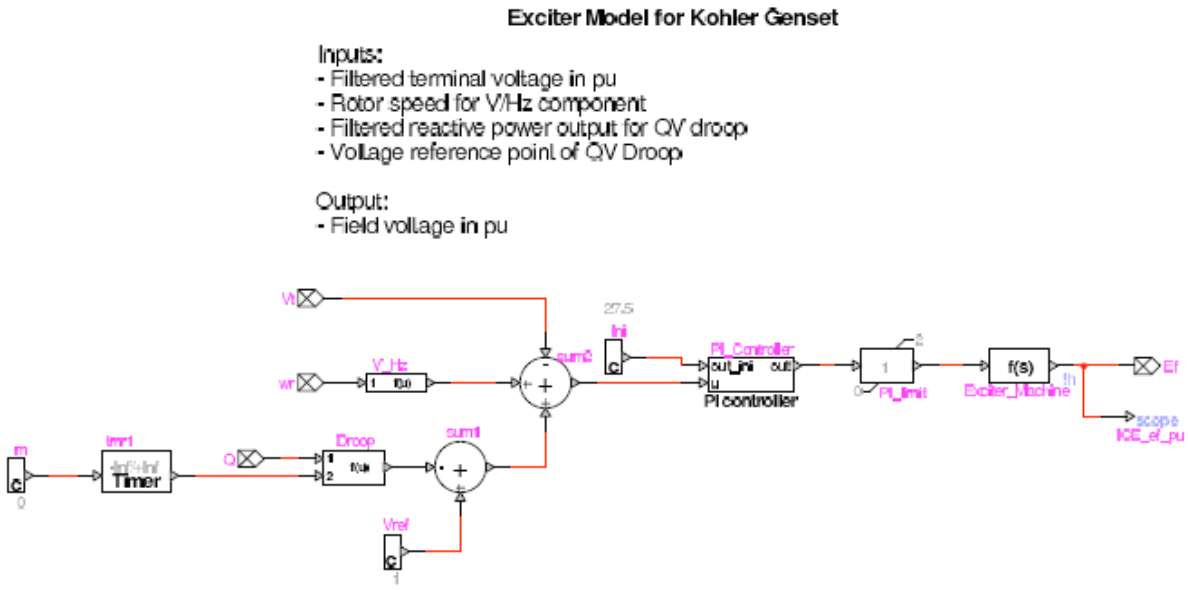

Fig. 27: Model of exciter and voltage regulator in EMTP

The mechanical governor utilizes the speed of the shaft to determine the opening and closing of a fuel valve. The combined dynamics of the governor, fuel actuator and combustion dynamics are represented by a second order lead-lag transfer function. A time delay further represents the engine dynamics. The governor used in the genset is mechanical in nature and provides for a 5% droop from no load to full load. The governor provides the mechanical power required by the synchronous machine. Thegovernor and engine model uses the rotor speed as its input. The rotor speed is used with the 5% droop to determine the required engine torque. This torque command is passed through a lead-lag transfer function and then through the combustion time delay. The torque value is

then multiplied by the rotor speed to calculate the mechanical input power.

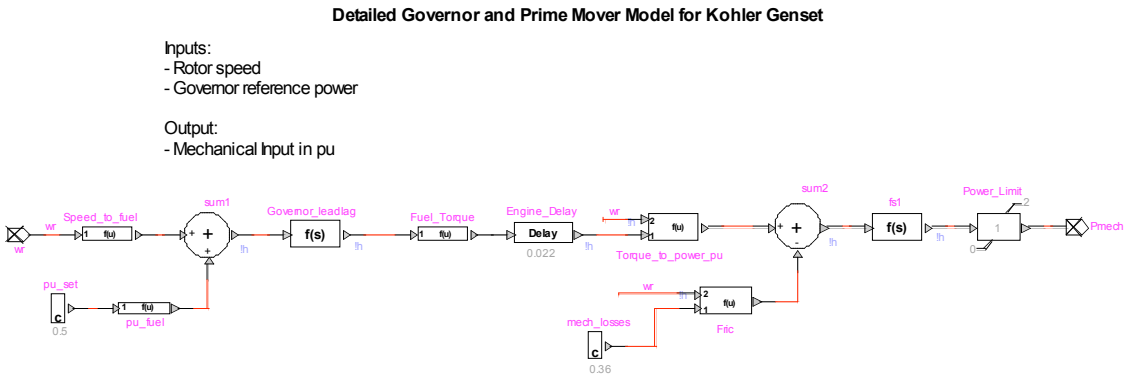

Fig. 28 : Governor and IC engine model in EMTP

4.4 Comparison of simulation and experimental results for isolated diesel genset operation

The developed model with its tuned gains was verified by simulating a step load change and comparing the results with the experiemental results obtained in the hardware run. Fig. 29 shows the simulated speed waveforms for a 4kW step load change and compares it with the measured hardware response for the same change. From Fig. 29 we can see that we have a good match between the waveforms. Similar results were obtained for the 2kW step load change as well.

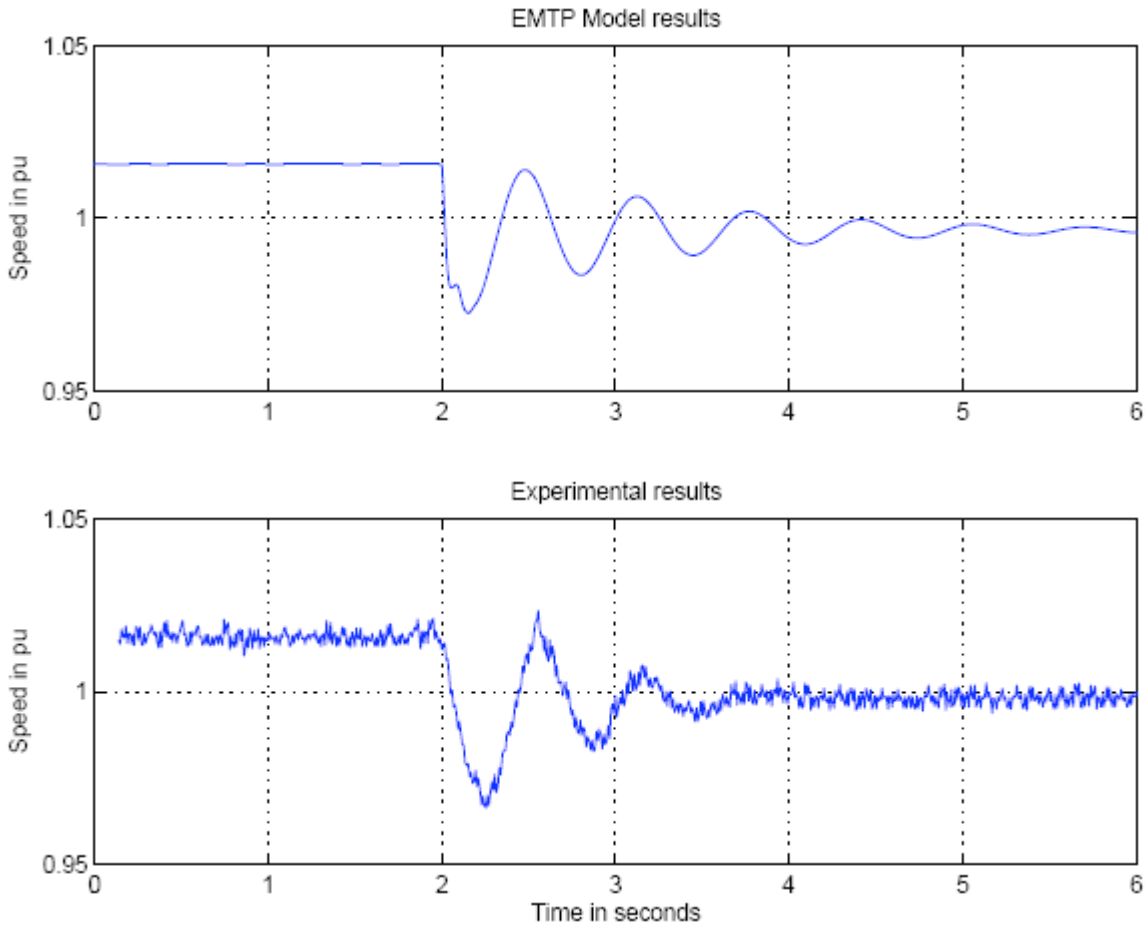

Fig. 29 : Comparison of simulated and experimental values of speed for step 4kW load change

4.5 Summary

The chapter describes the test setup for an IC engine based genset at the University of Wisconsin-Madison. The setup will be used to validate the controller scheme that will be proposed in this research work. Test results for step load changes are presented in this chapter that allows us to characterize the mechanical governor of the machine. The exciter and voltage regulator parameters were obtained from the manufacturer.

CHAPTER 5. Test results for operation of conventional gensets in a microgrid environment

In Chapter 4 we used the test setup to develop physical models for the IC engine based genset. We will now use the model for the genset to study the interactions of this source with other inverter based sources in the Microgrid environment. The EMTP [75] software platform will be used to simulate the operation of the microgrid.

5.1 Model of UW-Microgrid

The operation of the diesel genset can be predicted by simulating its behavior when included as part of a microgrid model. The model of the microgrid in the EMTP simulation platform has already been developed [20]. The description of the UW-Microgrid setup and each of its components is given below.

The microgrid test setup shown in Fig. 30 incorporates the typical components that can be found in a distribution system. The setup connects to the local 480V utility supply via a 75 kVA three phase transformer. The UW-Microgrid is a radial system with loads and distributed resources (microsources). The microsources generate power at the voltage level of 480 V and is then transformed to the network voltage by a 45kVA transformer. Each microsource is a voltage source inverter powered by a battery that provides the DC bus voltage. To smooth the output waveform a LC filter is placed at the output terminals of the inverter. The microgrid network is a three phase four wire system and hence we have the ability to connect single phase as well as three phase loads to the system. The

inverter of the microsource implements the reactive power-voltage droop as well as the real power-frequency droop characteristics.

The overall single phase equivalent circuit diagram of the microgrid is shown in Fig. 30. The building utility supply is assumed to be the stiff electric source for the system. The utility supply is connected to the microgrid network via a variac. A static switch is placed in series to intentionally island as well as to synchronize the microgrid with the utility. From the static switch terminals we have a three wire cable (Z1) that connects to a 75kVA transformer T1. The parameters of the variac and the transformer are given in Table 2. We have a short 4 wire cable (Z2) that connects to the first microsource (MS1) and the first load center (L1). From there we have a 75 yard, 4 wire cable (Z3) to reach an intermediate load center (L2). The last 25 yard of cable (Z4) connects the second microsource (MS2) and the last load center (L3). The impedances of the lines and transformers in the system are sumamrized in Table 3.

	V	S	Length	$R_p(\Omega)$	$X_p(\Omega)$
T1	480/208	75kVA		0.153@480V	0.153@480V
T2,T3	480/208	45kVA		0.256@480V	0.256@480V
Z1	480	216kVA	180ft	0.0225	0.0055
Z2	208	62.4kVA	20ft	0.00535	0.00068
Z3	208	62.4kVA	225ft	0.0194	0.0026
Z4	208	62.4kVA	75ft	0.0065	0.00085

Table 3 : Parameters of various components in UW-Microgrid system

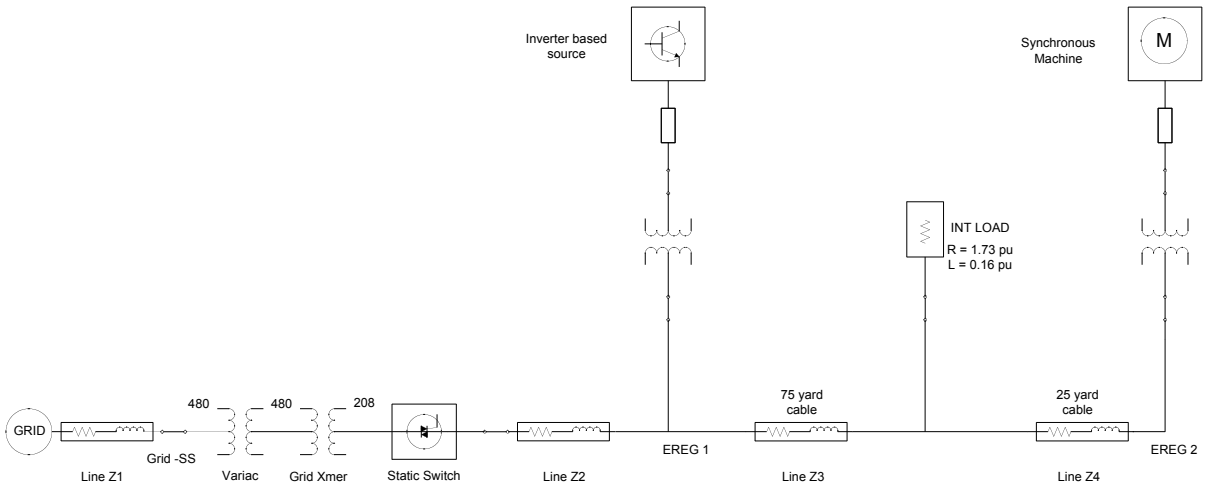

Fig. 30 : Layout of UW-Microgrid

5.2 Simulation and experimental results for operation of conventional diesel genset in a Microgrid

The EMTP model for the diesel genset in a microgrid environment with grid is shown in Fig. 31. In this test no inverter based source is present and the behavior of the genset in grid connected as well as islanded model of operation is studied

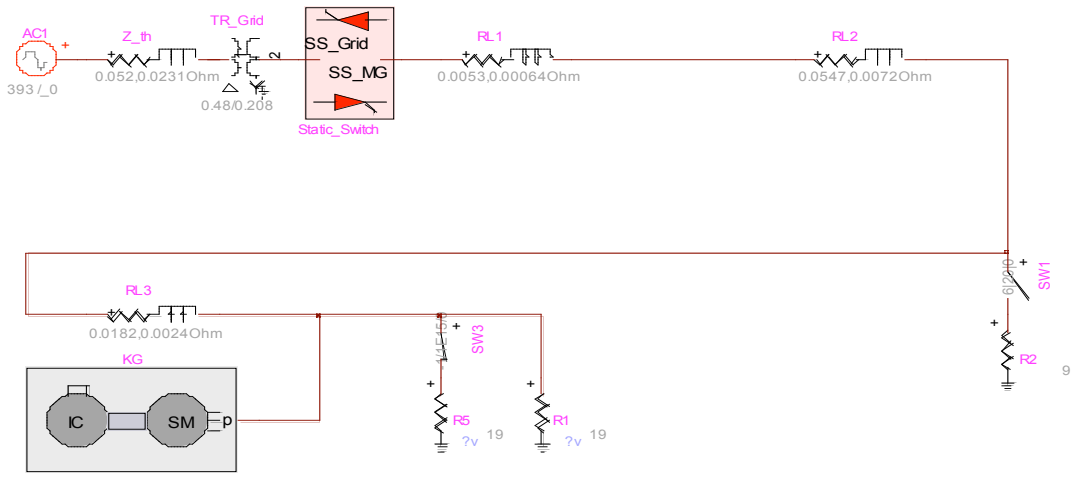

Fig. 31 : EMTP model of diesel genset connected to grid through static switch

Initially the diesel genset is connected to the grid and the genset delivers its reference power. The various events that take place in the simulation as well as the conducted experiment are listed below:

* Load is increased by 4.3kW, 1s simulation , 3s experiment
* Microgrid is islanded from utility grid, 6s simulation, 10.2s experiment

The objective of the experiment was to evaluate the performance of the diesel genset in a microgrid system without modifying its controls. The stability of the system during islanding and subsequent load changes has been observed and also the power quality in the system was monitored.

The simulation results for the test without modifying the controls of the genset are shown in Fig. 32 and Fig. 33 and the experimental results are shown in Fig. 34 and Fig. 35 (base power 10kW). Initially the genset is connected to the grid. Hence when the load is increased the genset does not pick up any of the load in steady state as seen in Fig. 32 and Fig. 34. The reactive power output of the genset changes due to the change in system

node voltages due to the load increase.

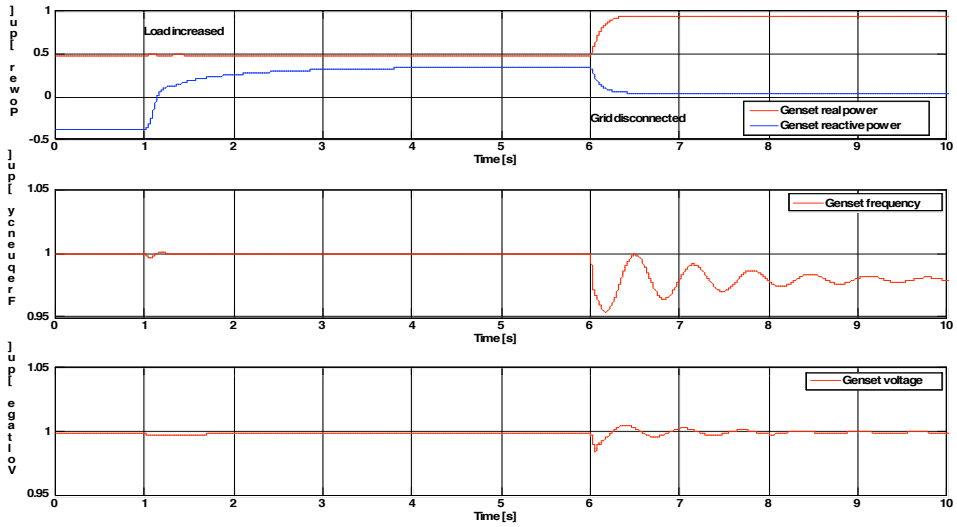

Fig. 32 : Simulated genset output real power, reactive power, frequency and voltage waveforms for load increase (@t=1s) and islanding (@t=6s) scenario

When the grid disconnects the genset has to pick up the additional load and the second order dynamics of the mechancial governor are reflected in the simulated frequency waveforms shown in Fig. 32 and the experimental waveforms shown in Fig. 34. The drop in frequency depends on the initial setpoint of the genset, the final load on genset and the frequency droop characteristics. After islanding the governor takes upto 5s to stabilize the speed of the machine. Furthermore depending on the load change the 5% droop of the governor can lead to a change in frequency beyond the limits of microgrid operation. Fig. 35 shows the output real and reactive power of the grid during the experimental tests. We can see that the grid almost exclusively picks up the initial load increase that causes node voltages and hence the reactive power circulation within the system to change. Due to the absence of QV droop there is a large amount of circulating VAR's within the microgrid

due to the incorrect genset voltage setpoint.

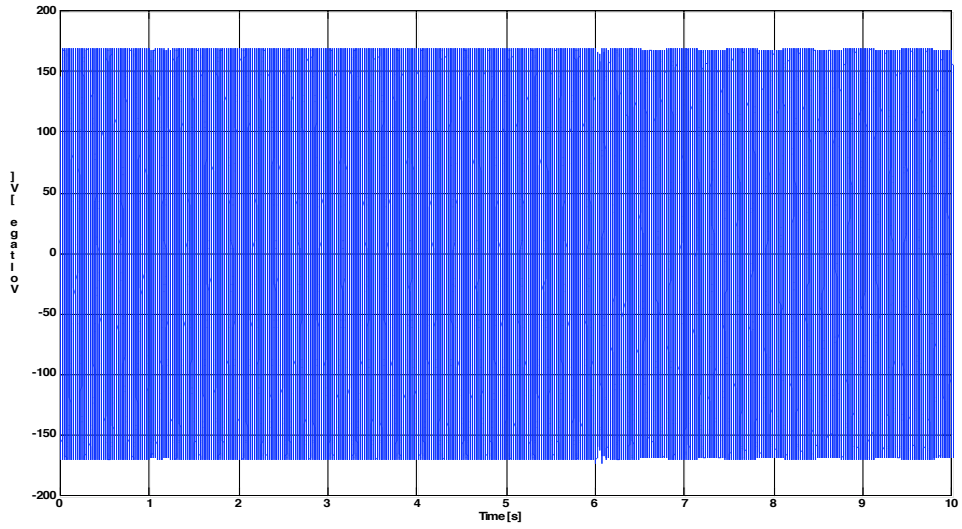

Fig. 33 : Simulated load voltage waveform load increase (@t=1s) and islanding (@t=6s) test with genset in a microgrid environment

In a distributed generation environment a QV droop curve is essential in determining the voltage setpoints for the system in the absence of a communication system. Fig. 32 and Fig. 34 show that the genset is trying to hold a fixed voltage which is the cause of the circulating VAR's. Fig. 33 shows the voltage seen by the load during the simulation and the transient in the machine voltage is reflected in the load voltage.

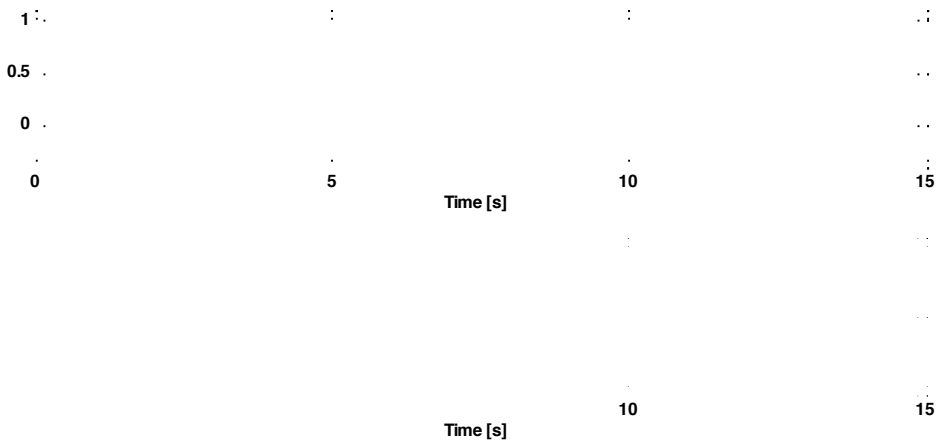

Fig. 34 : Experimental genset real power, reactive power, frequency and terminal voltage waveforms for load increase (@t=3s) and islanding (@t=10.2s) test

There are slight differences between the simualtion and experimental results. This is due to the fact that the setting of the genset voltage differs from the setpoint in the simulation by less than a volt. Also the simulation does not fully capture second order effects such as transformer saturation, static switch on-state drop, heating of components on load, signal conditioning and measurement noise. These slight differences and incomplete modeling causes the steady state reactive power value to differ between the simualtion and experiemnental tests. However the trends and dynamics do not change and we can clearly see that there is siginificant amount of reactive power circulation in the absence of droop control.

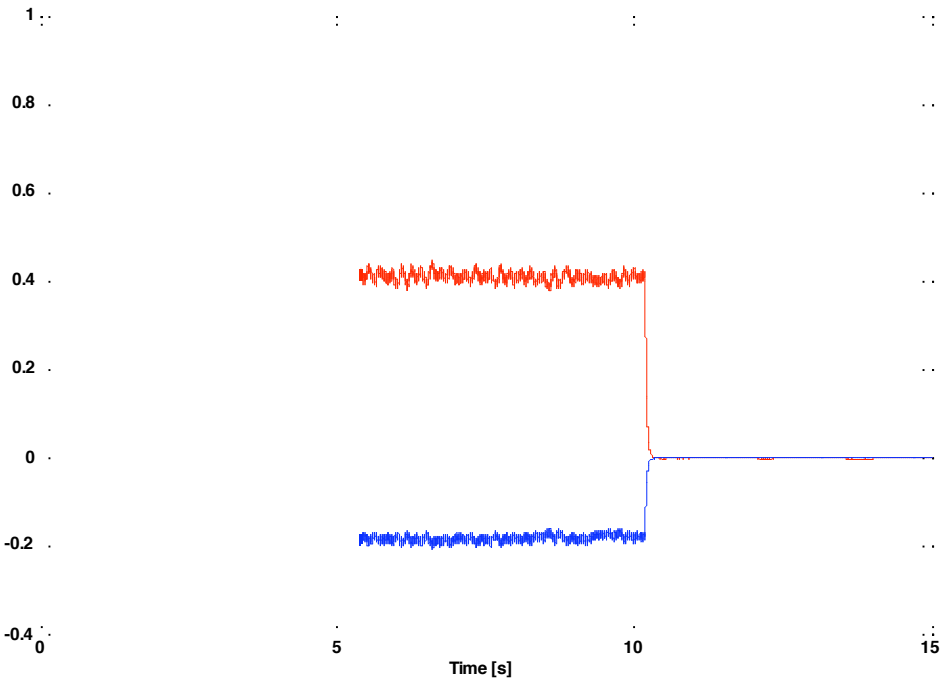

Fig. 35 : Experimental waveforms of grid real and reactive power for load increase (@t=3s) and islanding (@t=10.2s) test

From the simulation of the diesel genset in the microgrid network we can see that the system is stable during both grid connected and islanded mode. The steady state frequency of the system during islanded mode is governed by the genset frequency droop of 5%. This droop can cause the system to operate at frequencies which may be undesirable from the power quality standpoint. The droop must be decreased to meet the desired norms. Furthermore the mechanical governor introduces frequency dynamics which are undesirable and hence an electronic governor is required. It is clear that without QV droop there will be significant circulating VAR's in the system. Hence a modified voltage regulator which implements the QV droop is also required.

5.3 Simulation and experimental results for operation of diesel genset with grid and microsource

The power frequency droop curves of both types of microgrid sources are shown in Fig. 36. We can see that the inverter based microsource has a smaller power frequency droop in comparison to the diesel genset. Hence in island mode the inverter based source will dictate the frequency in the system. The diesel genset will follow the frequency set by the inverter and produce the desired output and the sum of the power produced by the two sources will be equal to the load power plus losses.

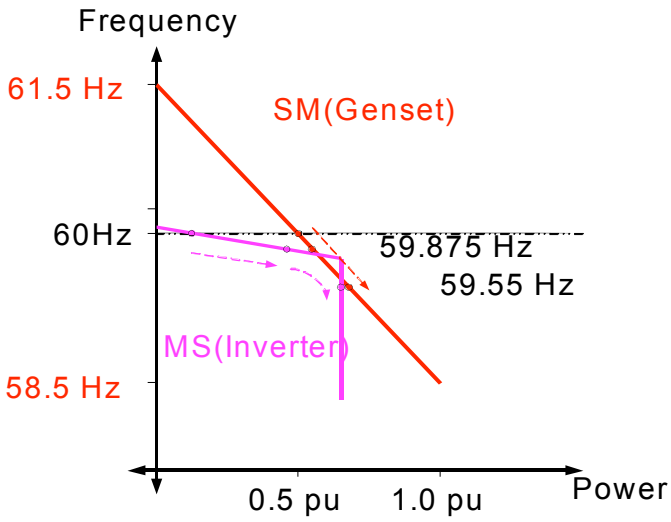

Fig. 36 : Power frequency droop curves for diesel genset and inverter based microsource illustrating diesel genset controlling system frequency

The EMTP model of the system under simulation is shown in Fig. 37. As mentioned earlier the inverter based source has a QV droop implemented in its control loop. The initial power set point of the diesel genset is 0.5 pu and 0.1 pu for the inverter based microsource. Hence in the initial phase of the simulation when the system is connected to the grid both of the sources in the microgrid will be delievring power equal to their

setpoints. When the system islands the sources will pickup the remaining load and share it based on their power frequency droop curves. The various events taking place in the test are:

1. Intially the grid, inverter based source(setpoint 0.1 pu), genset (setpoint 0.5 pu) and 8.6kW of resistive load are all connected
2. Grid is disconnected at 2s simulation and 1.5s experimental
3. Load is increased by 4.3kW at 6s simulation and 8s experimental

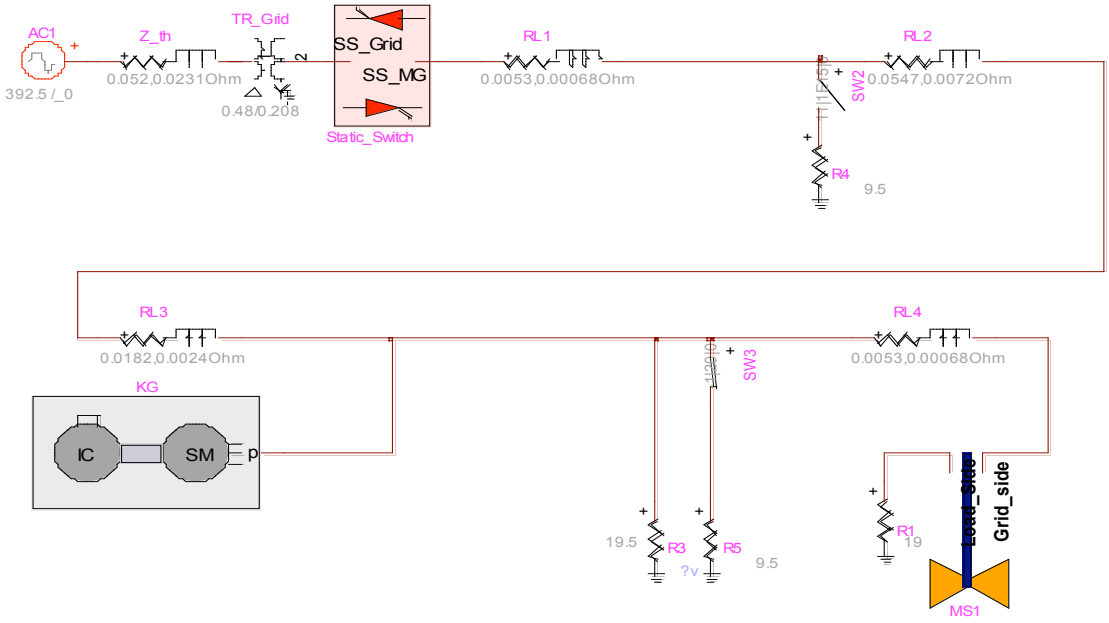

Fig. 37 : EMTP model of diesel genset operating in a microgrid environment with inverter based microsource

Fig. 38 to Fig. 40 show the simulation results and Fig. 41 to Fig. 43 show the experimental results obtained for a very similar test. We can see from Fig. 38 and Fig. 42 that prior to islanding the real power output of the genset is close to its setpoint of 0.5 pu

(base power 10kW). The slight difference is due to the fact that the droop is implemented for input power (i.e. mechanical power) and the experimental waveform displays output power. During islanding we can see that the inverter based microsource picks up most of the additional load and is operating close to its maximum power limit set artificially at 0.64pu. For the inverter results shown in Fig. 41 the power base (16kW) is different from that shown in theother figures (10kW). This is due to the fact that the data was captured using PCMaster as a picture file and the image cannot be modified to use the same power base as the other figures.

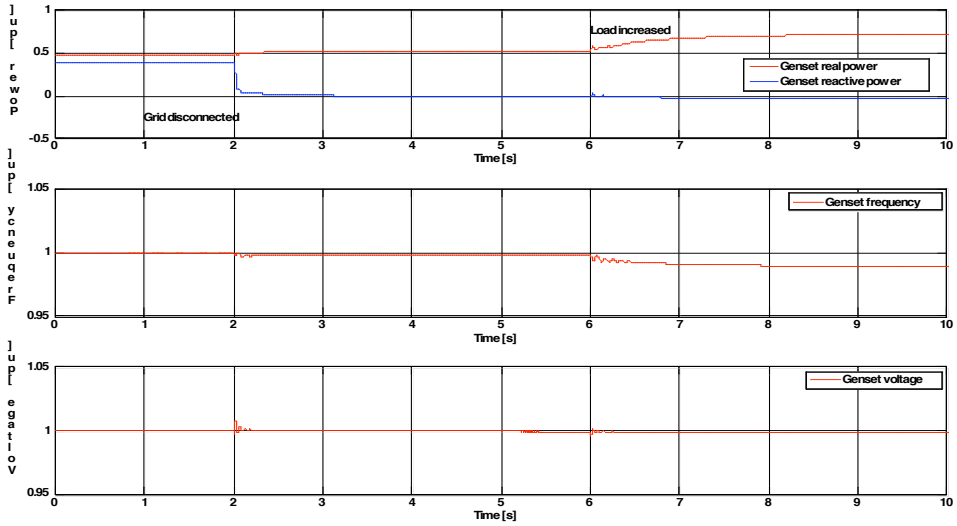

Fig. 38 : Simulated genset real power, reactive power, frequency and voltage waveforms for (@ 2s) and load increase (@6s) scenario in microgrid with inverter based microsource at power limit

During the subsequent load change the inverter utilizes some of its reserve capacity and overshoots its maximum to supply the load temporarily. This provides sufficient time for the diesel genset to pick up its output and supply the load. Due to the action of the inverter to provide for some of the load power during the transient event the dynamic

response of the genset is relatively benign.

In steady state the diesel genset uses a 5% droop curve and hence the frequency falls quite significantly causing the power quality to worsen. The transient for the mechanical governor of the diesel genset takes between 3s-5s to settle forcing the inverter based source to operate under overload conditions durign this time. Furthermore the dynamics of the mechanical governor cause oscillations in the speed waveform which can be supressed by employing an electronic governor. Since the diesel genset does not employ any QV droop there is a possibility for large significant circulating VAR's (5kW) prior to islanding as shown in Fig. 38 and Fig. 42 .

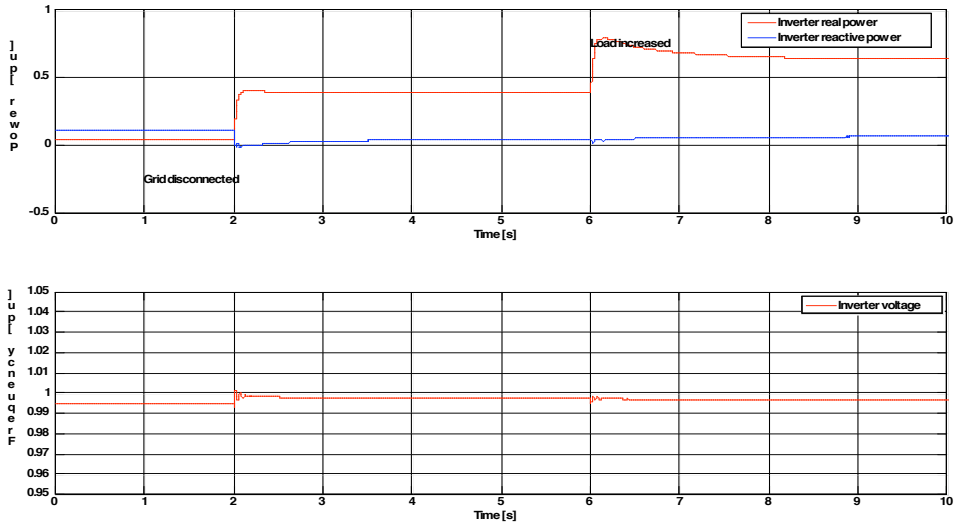

Fig. 39 : Simulated inverter real power, reactive power and voltage waveforms for islanding (@ 2s) and load increase (@6s) scenario in microgrid with inverter based microsource at power limit

The experimental results also confirm that once the inverter hits its power limit the genset controls the system frequency.

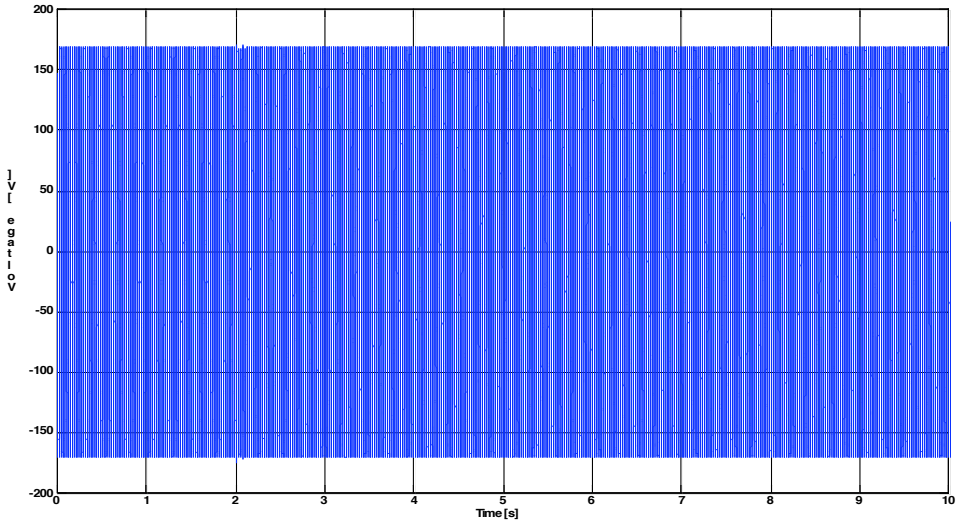

Fig. 40 : Simulated load voltage for islanding (@ 2s) and load increase (@6s) scenario in microgrid with genset and inverter based microsource

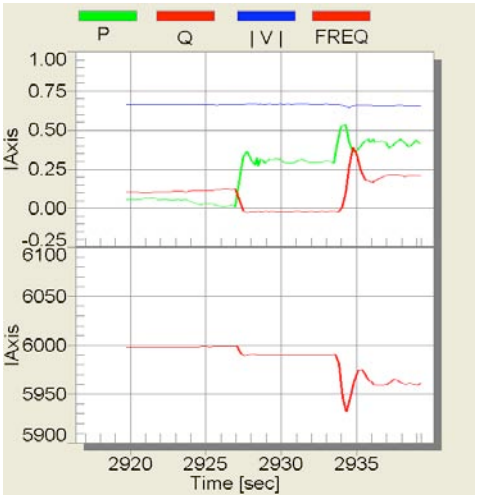

Fig. 41 : Experimental waveforms for inverter real power, reactive power, frequency and voltage for islanding scenario in microgrid with inverter based microsource (Power base and time scale different)

One key difference between the experimental results and the simulation results is the

absence of the governor dynamics after load increase in the simulation results. In the simulation results we can see a damped response to the load increase and there are no second order dynamics present. Closer examination reveals that in the simulation the inverter picks up the load increase much faster than in the experiment resulting in the genset seeing a smaller power difference, leading to a milder governor dynamic response.

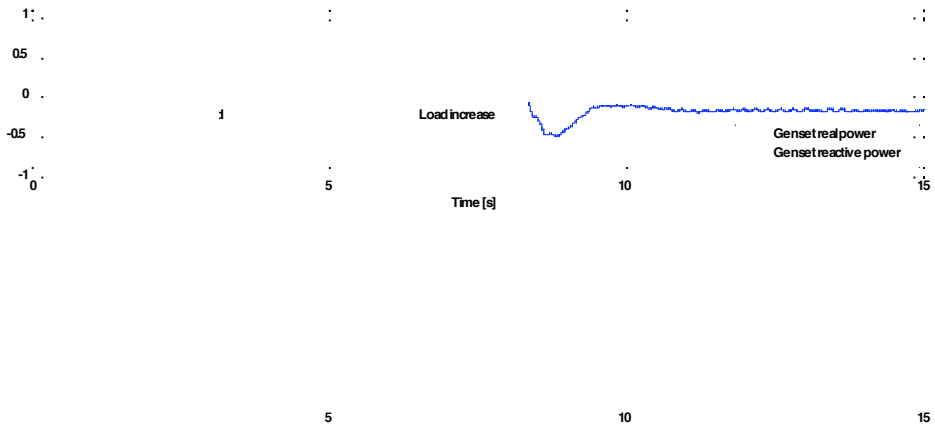

Fig. 42 : Experimental waveforms for genset real power, reactive power, frequency and voltage for islanding (@ 1.5s) and load increase (@8s) scenario in microgrid with inverter based microsource

The inverter model in EMTP is an averaged model that does not account for the capacitance of the DC bus, the dynamics of the power supply or the output LCL filter. As a result the simulated the inverter is able to respond to load changes faster than that observed in the experimental tests. The faster load pick up causes the genset to see less of a power difference. As the inverter slowly changes its power the genset output gradually

increases with minimal second order effects. Due to slight differences in reference voltages and the inability to model a physical system completely the experimental results do nto exactly match the simulation results. In order to get a better match the model of the inverter must be improved and should incorporate a detailed model of the power supply.

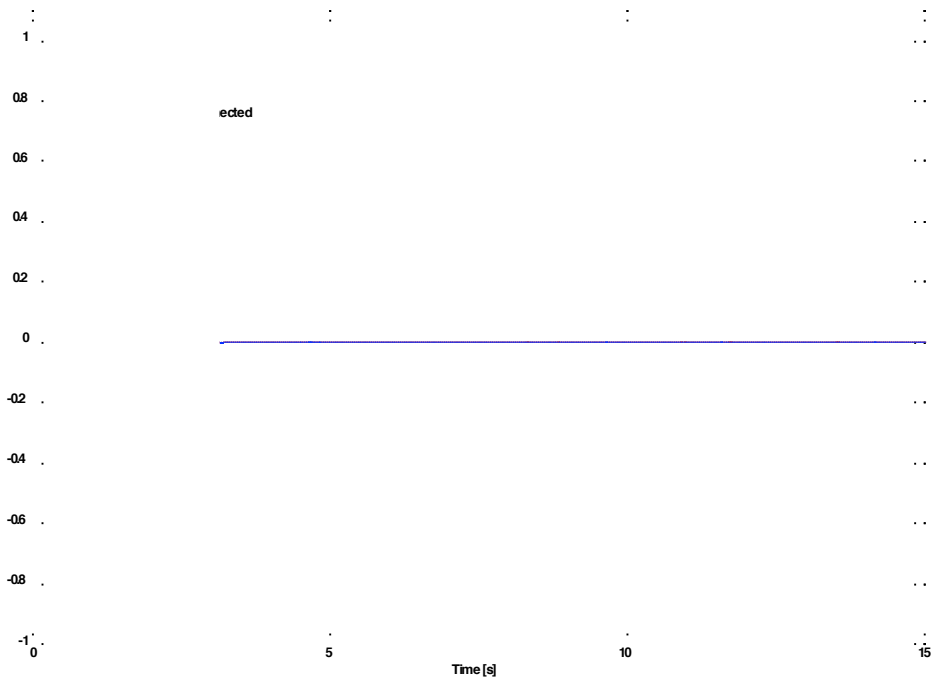

Fig. 43 : Experimental waveforms for grid real and reactive power output for islanding (@ 1.5s) and load increase (@8s) scenario in microgrid with inverter based microsource

The trends observed in the simulation compliment the experimental results very well. Due to the lack of a QV droop in the genset it is possible to have large circulating VAr's in the system. Furthemore the presence of a 5% droop on the genset governor causes it to pick up only a small percentage of a load change untill the other sources hit their power limits. Once the other sources reach their power limits the slower genset dynamics dominate the transient response of any event.

5.4 Summary

From the various simulations and experimental tests performed with the genset, inverter based microsource and grid we have seen that the system is stable during islanding events. After islanding the two units share power according to their power frequency droop curves. Most of the power will be picked up by the inverter based source as it has a much smaller droop. Once the inverter based sources hit their power limit the response of the system will be dominated by the slower second order dynamics of the mechanical governor. This will result in undesired oscillations of the speed of the genset, the voltage and hence the real power and reactive power. This issue can only be eliminated by employing an electronic governor and designing new control schemes for it. Furthermore once the inverter based microsource hits its maximum power limit the genset will determine the frequency of the system. Due to the 5% droop on the genset the frequency can sag beyond desired operating values and cause poor power quality. This problem can again be alleviated by using an electronic governor with smaller droop. In addition, the absence of QV droop in the genset voltage controls can cause large circulating VAR's to flow in the system which are undesirable but avoidable with proper design of the voltage regulator. These key problems with conventional gensets are addressed in the following chapter by designing a new genset controller.

The simulation results achieve a good match with the experimental results, validating the genset model proposed in this chapter. The discrepancies between the experimental and simulation results are explained in the chapter and can be attributed to slight differences in voltage setpoints, system impedances, transformer saturation and simplified models for the inverter and genset.

CHAPTER 6. Design of diesel genset controller

To operate the diesel genset in microgrid environment modifications in the governor control and voltage regulator control need to be made. The modified controller for the genset has been designed using state variable techniques. The first step in this process is to design an observer that would estimate the state of the system. An operating model for the genset has been developed from the state equations of the system. The machine model developed for the synchronous machine depends on the knowledge of the rotor position for achieving the rotor reference frame transformation. A rotor angle observer has been developed from the measured rotor position which enables us to estimate the speed accurately and convert the stator terminal quantities into the synchronous reference frame located on the rotor of the machine. In the wound field machine the d-axis field voltage is the only control handle that we have to change the terminal voltage. This field voltage controls the mutual d-axis flux linkage that governs the output q-axis terminal voltage. Hence to control the output voltage we need to accurately estimate the d-axis flux linkages. A closed loop observer for the machine state equations has been developed for this purpose.

The reference commands for the speed and terminal voltage for the genset are obtained from the real power –frequency droop and reactive power-terminal voltage droop curves. The design of a state variable controller that integrates the reference commands with the observer outputs is presented. Simulation and experimental results for the genset performance in the microgrid environment with the modified controller is also presented.

6.1 Operating point model of diesel genset

The various equations that describe the systems are:

$$\psi_{md}^{r} = \frac{\frac{\psi_{kd}^{r}}{x_{lkd}} + \frac{\psi_{fd}^{r}}{x_{lfd}} + i_{ds}}{\frac{1}{x_{md}} + \frac{1}{x_{lkd}} + \frac{1}{x_{lfd}}} \tag{33}$$

$$p\psi_{kd}^{r} = \omega_b r_{kd}\left(\frac{\psi_{md}^{r} - \psi_{kd}^{r}}{x_{lkd}}\right) \tag{34}$$

$$pE_f = \frac{-E_f + V_v}{\tau_e} \tag{35}$$

$$p\psi_{fd}^{r} = \omega_b \left[E_f \frac{r_{fd}}{x_{md}} + r_{fd}\left(\frac{\psi_{md}^{r} - \psi_{fd}^{r}}{x_{lfd}}\right)\right] \tag{36}$$

$$\psi_{mq}^{r} = \frac{\frac{\psi_{kq}^{r}}{x_{lkq}} + i_{qs}}{\frac{1}{x_{mq}} + \frac{1}{x_{lkq}}} \tag{37}$$

$$p\psi_{kq}^{r} = \omega_b r_{kq}\left(\frac{\psi_{mq}^{r} - \psi_{kq}^{r}}{x_{lkq}}\right) \tag{38}$$

$$T_{mech}(t) = 1.6m_f(t-T_d) - 0.36\omega_r(t) \tag{39}$$

$$p\omega_r = \frac{T_e + T_{mech}}{2H} \tag{40}$$

$$p\theta_r = \omega_b\omega_r \tag{41}$$

The nonlinear element in the equation set is the engine time delay in the genset model. In

the design of the observer this delay will be modeled using the Pade approximation. The entire model of the system is shown in Fig. 44.

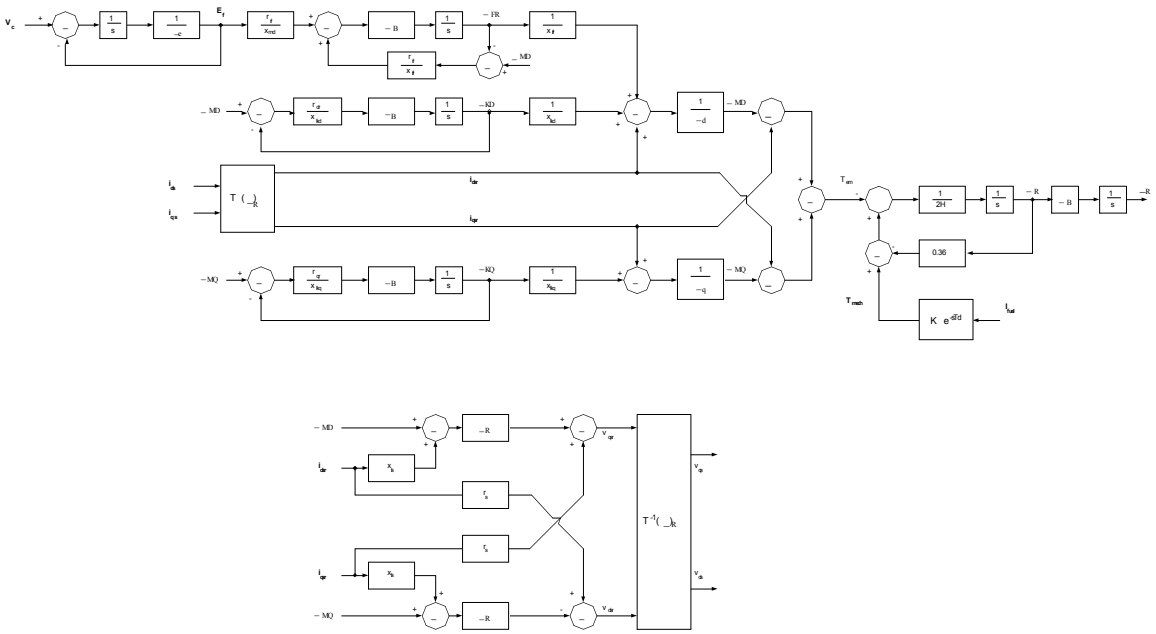

Fig. 44: Operating point model of kohler genset

6.2 Real and reactive power droop controllers

The DG controller must use only local information to control the source during all events. The main inputs to this controller are the desired steady state output power and bus voltage. For the DG to operate in a multi-source environment the controller must control the output voltage and power to ensure stable operation. In the absence of an explicit communication system this is achieved using real and reactive power droop curves.

Voltage regulation plays an important role in the operation of a microgrid. Without local voltage control distributed sources could face large voltage and/or reactive power

oscillations. During steady state incorrect voltage set points could lead to large circulating VAR's between the sources which could greatly diminish the real power capabilities of the sources. To alleviate these issues a reactive power versus voltage droop shown in Fig. 45 is necessary.

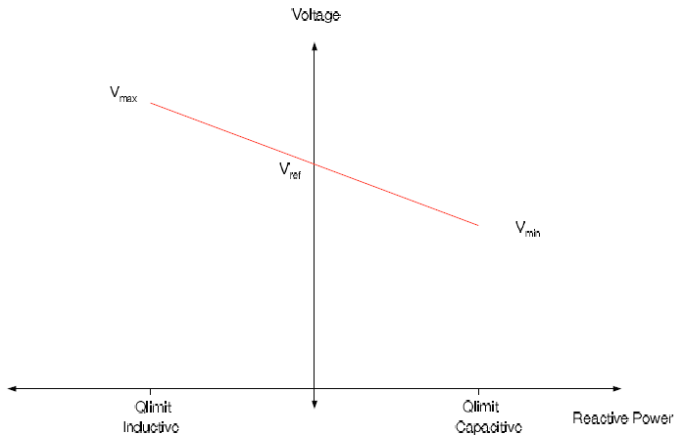

Fig. 45 : Reactive power droop curve for microsource control

In a microgrid several distributed resources coexist and its vital to regulate the power each units outputs. Each distributed resource implements a power versus frequency droop as shown in Fig. 46 that controls the power output of the source. When the microgrid is connected to the utility system each source puts out its reference power value. This value can be set based on an economic dispatch algorithm or a heating load requirement. In the event of an islanding scenario the sources share power based on the droop curve and the total local load. In the event one of the sources hits its maximum output the frequency will be determined by the other sources in the system. Hence in an islanded scenario the frequency of the microgrid can vary from the rated 60Hz within limits specified by the user. The user sets these limits based on the desired power quality.

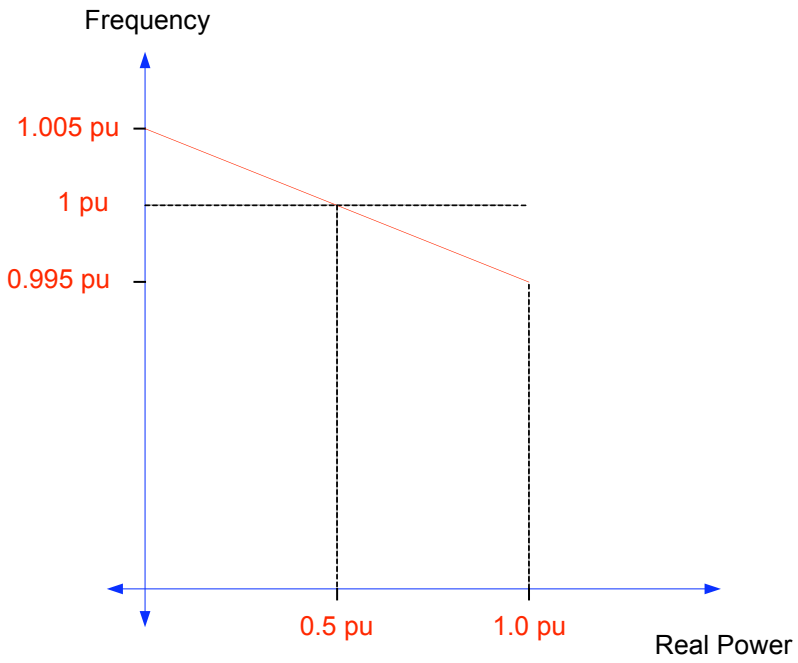

Fig. 46 : Real power droop curve for power sharing between microsources

6.3 Observer design and analysis

The design of the observer shown in Fig. 47 is performed in two stages. The first step is to design the rotor angle observer. For the rotor angle observer the inputs are the fuel command, electric torque on shaft, and sampled rotor position. The analysis for the observer is performed in continuous time and as part of future work a discrete-time observer will be developed. The second step is to design an observer for the electrical states of the system. For this the inputs are the field command, stator ‘d’ and ‘q’ axis voltages and currents in the rotor reference frame. The design of the observer is presented in the following sections.

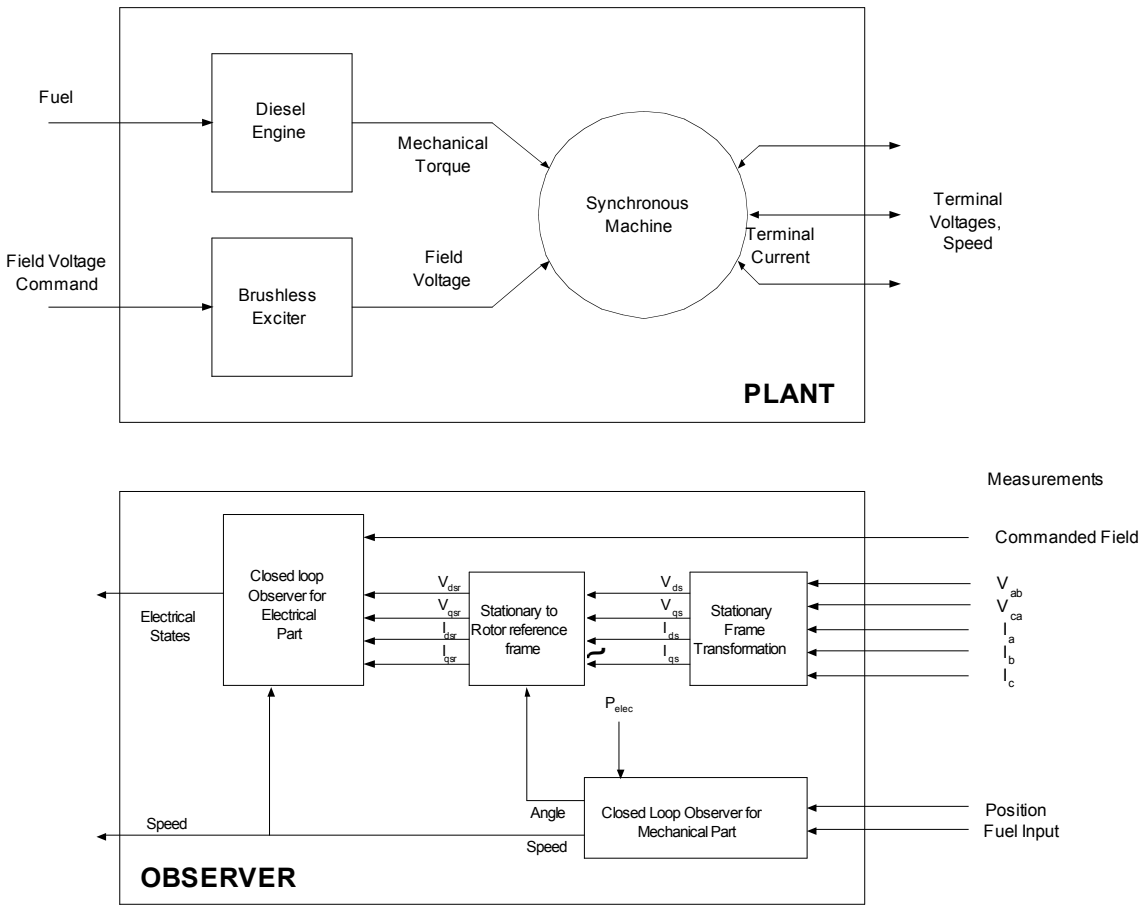

Fig. 47: Overall block diagram of genset observer

6.3.1 Rotor angle observer

The measurement of the rotor angle of the machine enables us to convert the stator 'abc' quantities into the rotor reference frame. A resolver output is used in this analysis to provide for the measured rotor position. To convert the resolver output into the position of the rotor 'q' axis we need to determine the angle offset between the two. This is obtained by realizing that during no load the terminal voltage is equal to the back emf of the machine. Hence at no load the rotor angle is simply the arc tangent of $\frac{-v_{ds_s}}{v_{qs_s}}$. The

output of the resolver is processed to obtain the rotor position. The resolver output is correlated with the rotor angle obtained from the back emf at no-load. Once the angle offset between the two measurements is calculated the machine can be loaded and the resolver output can be used to determine rotor position based on the angle offset calculated.

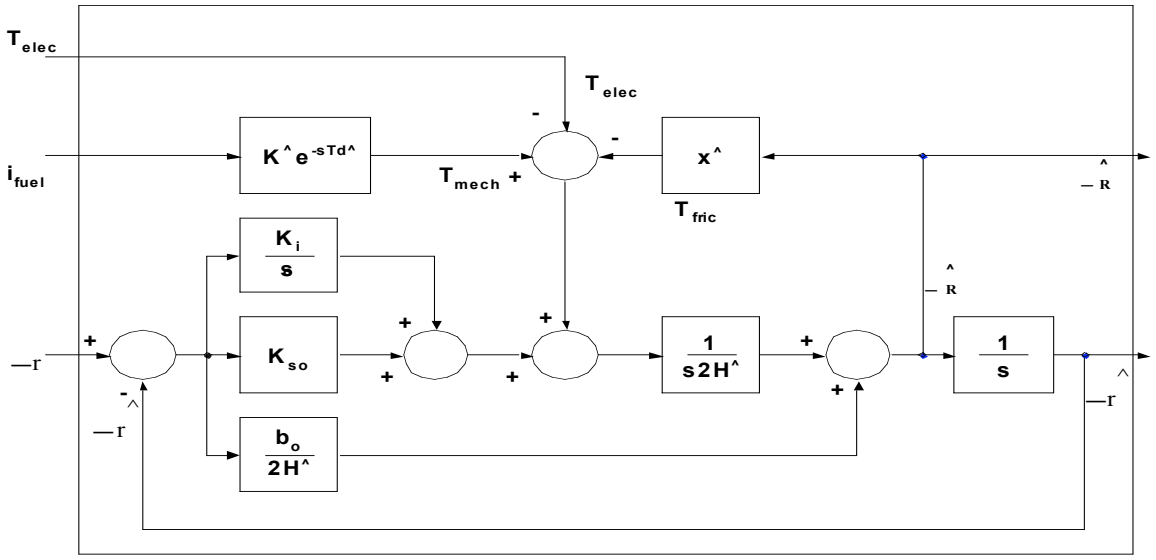

Fig. 48: Closed loop observer for rotor position and rotor speed

Now that we have the position information we can design a closed loop observer for the speed. The structure of the observer is shown in and is an enhanced luenberger style implementation [71]. The inputs to the observer are the measured rotor position from the resolver, fuel command from the fuel solenoid and electrical torque estimate. The estimation transfer function for the rotor speed is:

$$\frac{\hat{\omega}_r}{\omega_r} = \frac{K_i + sK_p + s^2 b_o + s^2(x\hat{} + s2H\hat{})}{K_i + sK_p + s^2 b_o + s^2(x\hat{} + s2H)\left[\frac{K\hat{}e^{-sT_d\hat{}}}{Ke^{-sT_d}}\right]} \quad (42)$$

The bode plots for the magnitude and phase of the estimation transfer function with a ± 15% and 5% error in friction, engine time delay, and fuel solenoid gain are shown in Fig. 49 and Fig. 50.

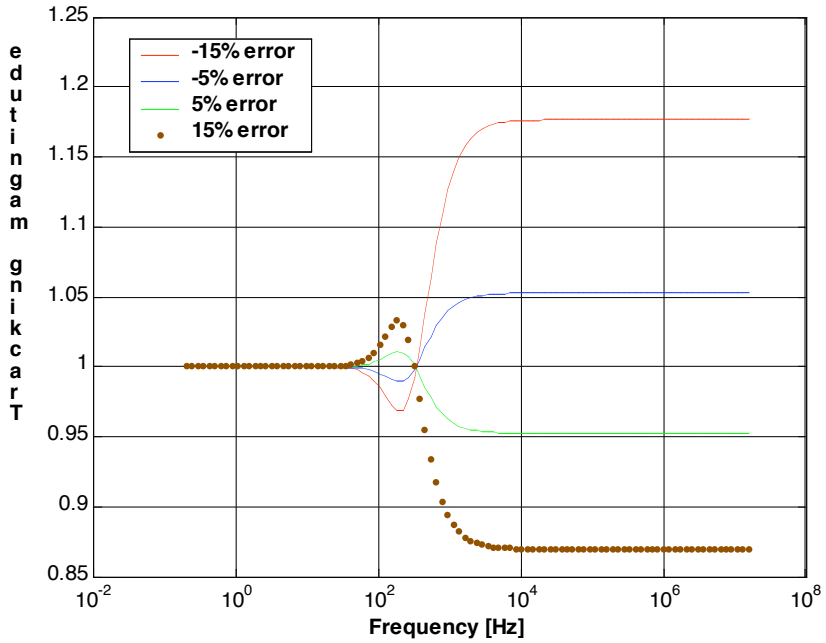

Fig. 49 : Speed estimation magnitude as a function of frequency for speed observer

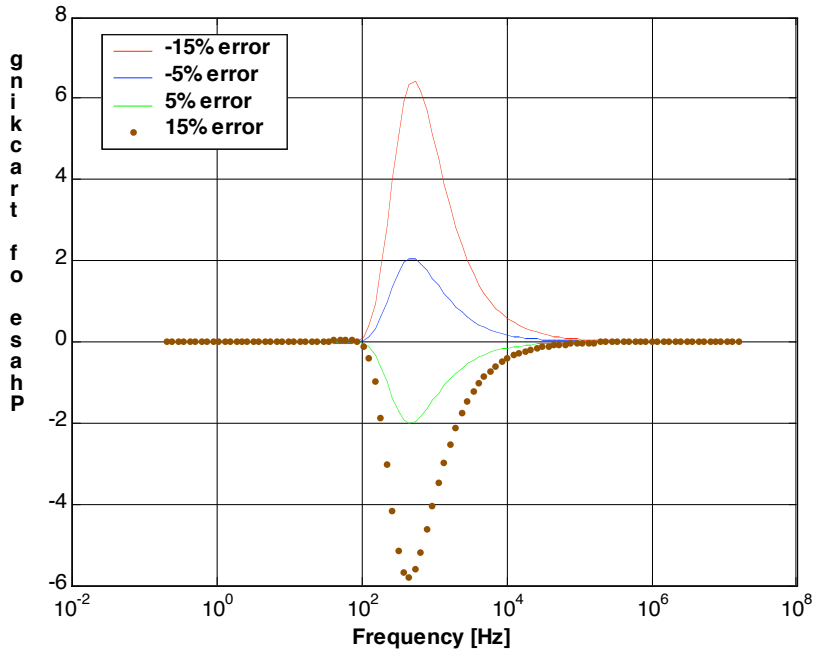

Fig. 50: Speed estimation phase as a function of frequency for speed observer

The design of the observer ensures that we have no estimation error below the desired bandwidth. The gains Kp, Ki and bo are chosen such that the eigenvalues for the transfer function are located at 200Hz. The observer output is the rotor position and the estimated speed.

6.3.2 Synchronous machine electrical states observer

In the woudn field machine the field voltage provides us with the handle to control the output voltage. The change in field voltage changes the 'd' axis mutual flux voltage which changes the 'q' axis terminal voltage. Hence the observer must estimate the value of the mutual flux linkage which can be passed on to the voltage controller. The transfer function between the field voltage E_f and the 'd' axis mutual flux voltage ('m(s)') can be derived from the machine state equations and is given below:

$$\frac{\psi_{md}(s)}{E_f(s)} = \frac{\frac{x_{lfd}}{x_{md}}}{\left[\left(1+s\frac{x_{lfd}}{r_{fd}\omega_b}\right)\left(1-\frac{1}{x_{lkd}\chi_d\left(1+s\frac{x_{lkd}}{r_{kd}\omega_b}\right)}\right)-x_{lfd}\chi_d\right]} \quad (43)$$

The field voltage is the output of the brushless exciter which is controlled by the current flowing through its stator terminals. The transfer function between the field voltage and the voltage input to the brushless exciter is:

$$E_f(s) = \frac{V_c(s)}{1+s\tau_e} \quad (44)$$

The transfer function between the ‘d’ axis mutual flux voltage and the brushless exciter input can be obtained from equations and is denoted as m(s).

Now that we have the relationship between the brushless exciter input voltage and the ‘d’ axis mutual flux voltage we can design a closed loop observer (Fig. 51) using the estimated and measured ‘q’ axis stator voltage.

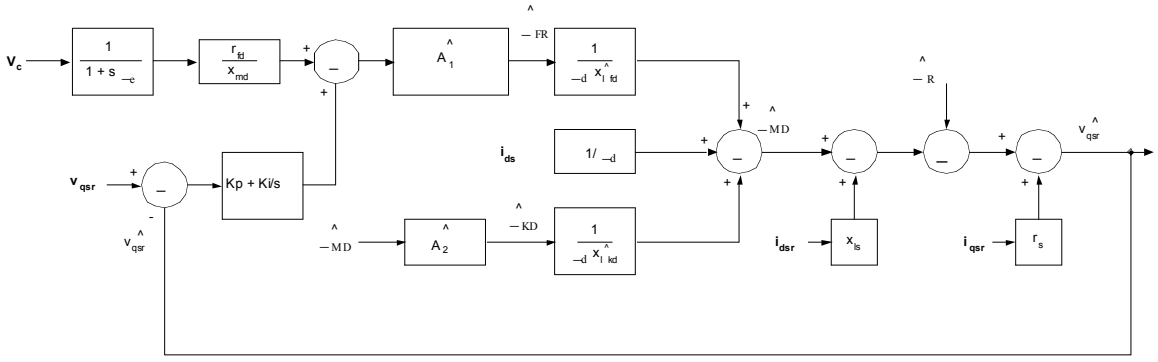

Fig. 51: Schematic of closed loop observer for ‘d’ axis mutual flux voltage

The transfer function between the estimated and actual‘d’ axis flux voltage is given below

$$\frac{\hat{\psi}_{md}(s)}{\psi_{md}(s)} = \frac{\omega_r\left(K_i/s + K_p\right) + \frac{\hat{m}(s)}{m(s)}}{\hat{\omega}_r\left(K_i/s + K_p\right) + 1} \tag{45}$$

From the discussion on the rotor angle observer we know that we can accurately track the speed of the rotor within the bandwidth of the observer. Hence we will be able to track the 'd' axis mutual flux voltage as long as we have an accurate estimate of speed. Even in the presence of uncertain parameter values we will still be able to accurately predict the flux voltage magnitude. The magnitude and phase of the flux voltage tracking function is shown in Fig. 52 and Fig. 53 respectively for errors in 'd' axis mutual reactance, field reactance, field resistance, and leakage reactances.

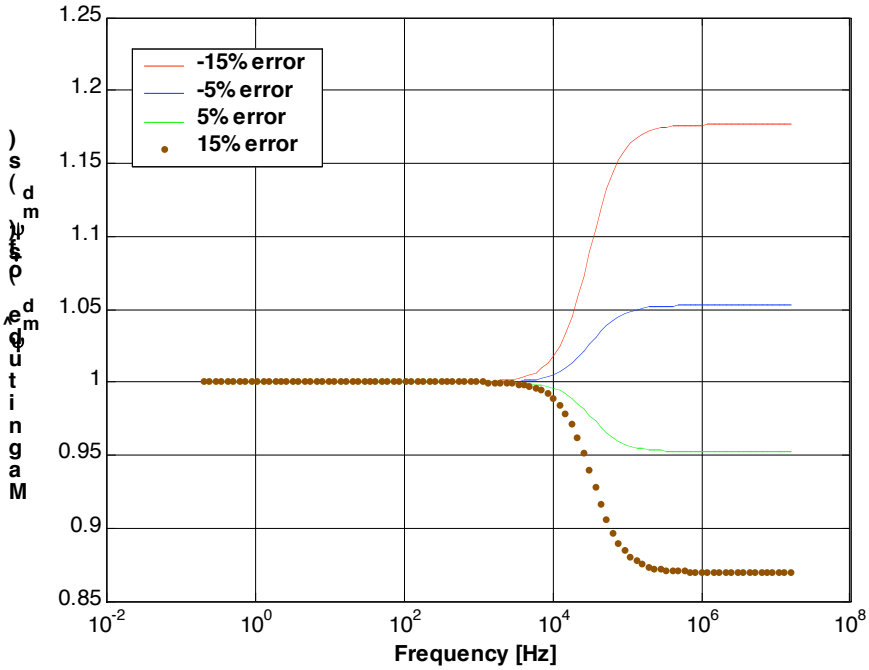

Fig. 52: Magnitude of $\frac{\hat{\psi}_{md}(s)}{\psi_{md}(s)}$ as a function of frequency

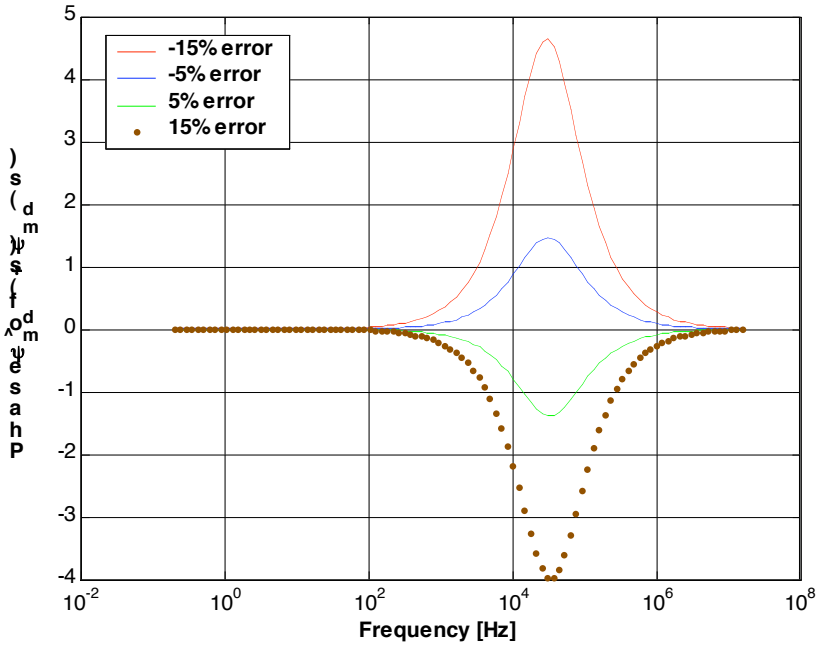

Fig. 53: Phase of $\frac{\hat{\psi}_{md}(s)}{\psi_{md}(s)}$ as a function of frequency

6.4 Controller design and analysis

Using the outputs of the observer we can now design a state variable controller for the exciter field and fuel solenoid. In the case of the exciter field input the disturbance inputs are the stator 'd' and 'q' axis currents. These currents are measured and hence we are able to reject these disturbances in our controller. The terminal voltage command is set using the reactive power droop curves. Once we have the desired terminal voltage command we can use the measured vds, ids, iqs and estimated speed to generate the desired field axis voltage. We integrate this command with the state variable PI controller on the q-axis field voltage to generate the field voltage command. The block diagram for the voltage controller is shown in Fig. 54.

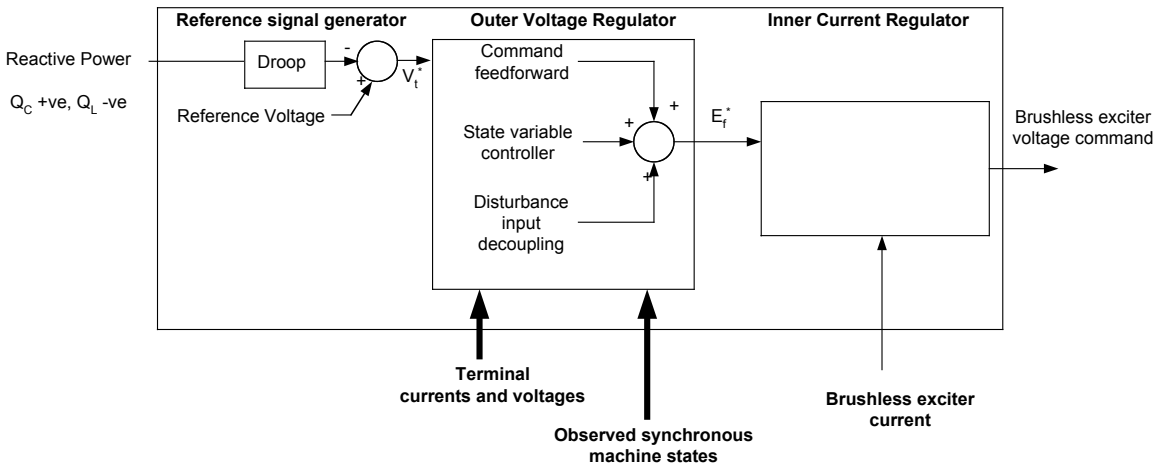

Fig. 54: Overall block diagram of proposed voltage regulator

The magnitude of the tracking between actual voltage and commanded voltage is shown in Fig. 55 for a system that has errors in parameter estimation. The voltage controller bandwidth depends on the estimation of speed to accurately determine the necessary 'd' axis mutual flux voltage. The speed observer bandwidth was designed with eigenvalues at 200Hz and the voltage controller eigenvalues are designed at 20Hz.

The overall block diagram for the engine fuel controller is shown in Fig. 56. For the fuel controller the disturbance input is the friction torque and electrical torque estimate. The reference speed is set using the real power droop curve. This speed reference is used to generate the reference torque command. This command is summed with the disturbance magnitude and the output of a state variable controller on the speed. Using the desired torque command the desired fuel command is generated which is given to the fuel solenoid controller. This controller implements a current regulator to convert the fuel command to the desired solenoid current value.

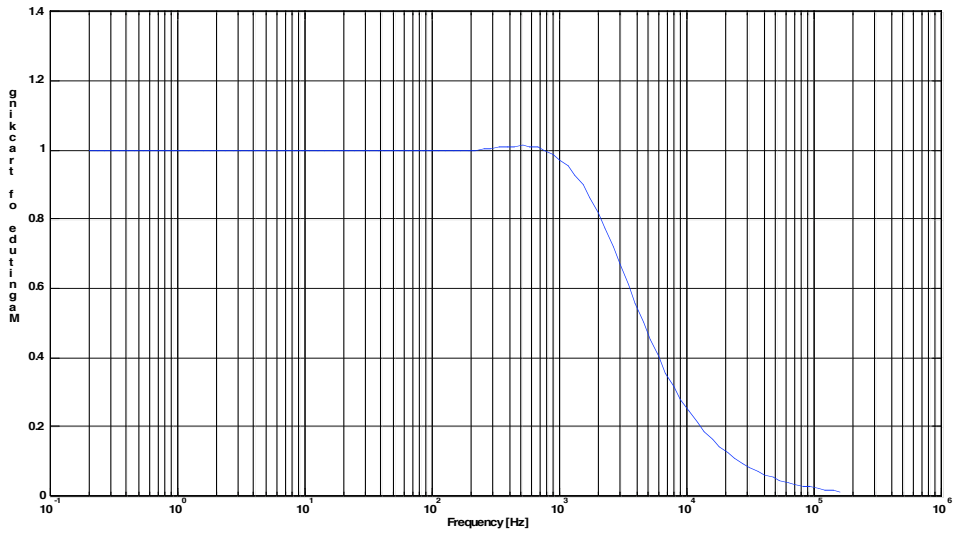

Fig. 55: Magnitude of $\frac{v_{qsr}}{v_{qsr}^{*}}$ as a function of frequency

The magnitude of the speed controller tracking transfer function is shown in Fig. 57. The bandwidth of the controller is set to 20Hz to achieve fast control of the genset speed. One of the key aspects of the engine model is the presence of a pure time delay that represents the time for a power stroke. This time delay ensures that the shaft mechanical torque does not change instantaneously after a fuel command change. Hence during this time interval the speed will vary and the difference in power would need to be supplied from the other sources in the system and the mechanical inertia in the genset.

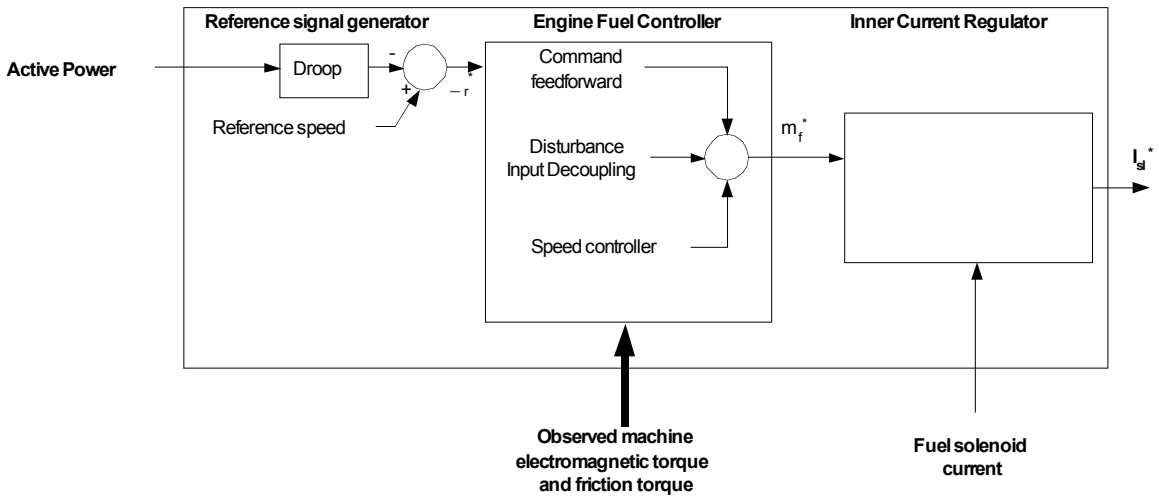

Fig. 56: Overall block diagram of proposed electronic governor

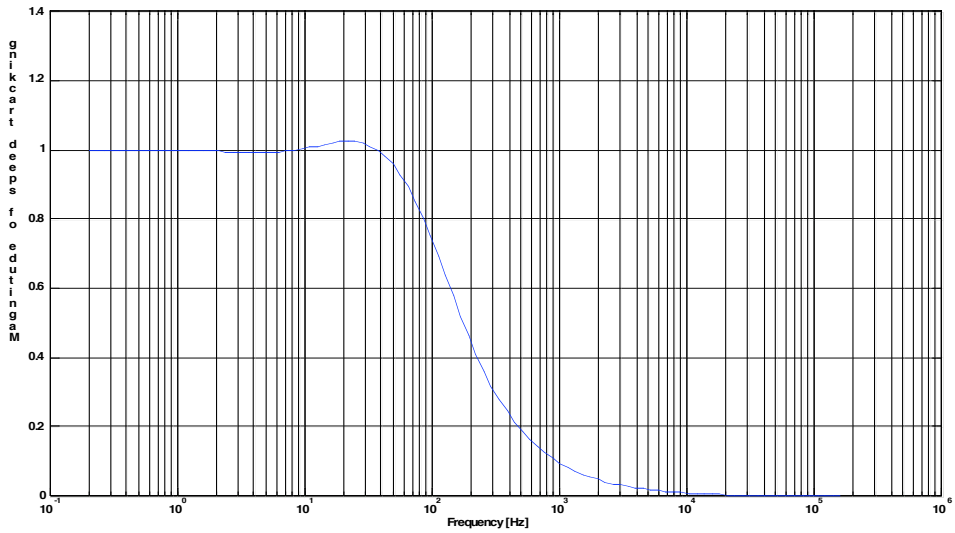

Fig. 57: Magnitude of $\frac{\omega_r}{\omega_r^*}$ as a function of frequency

6.5 Experimental setup for genset controller

The proposed controller was experimentally verified using the UW-Microgrid setup shown in Fig. 58. The chapter explains the various modifications carried out on the genset controller and documents the experimental results obtained. Several challenges were encountered during the experimental work and this section attempts to document the difficulties faced and the steps taken to solve the issues.

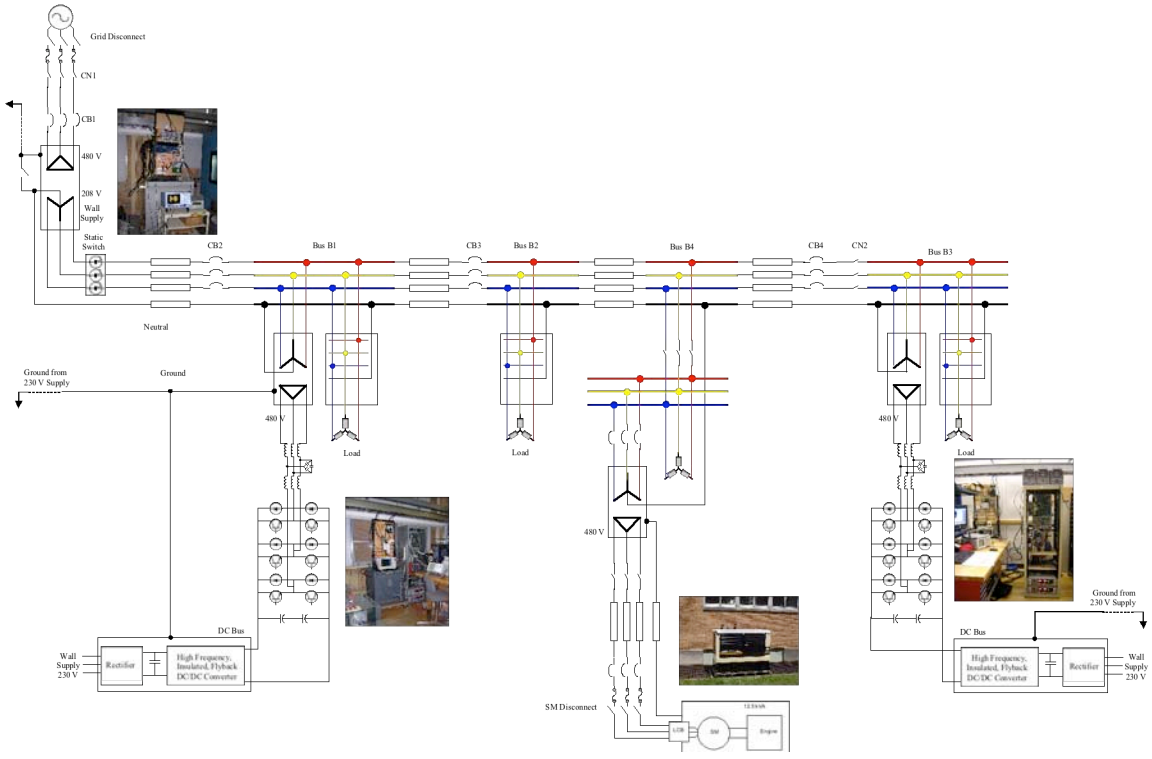

Fig. 58: Microgrid setup at University of Wisconsin Madison

The main changes made to the genset controller were to replace the existing mechanical governor with an electronic governor and to design a new voltage regulator for the brushless exciter. To incorporate an electronic governor the existing fuel shut off solenoid was replaced by a linear solenoid and the mechanical governor throttle was changed to its full open position. The linear solenoid was characterized to determine its resistance and inductance. Fig. 59 shows the test setup for characterizing the linear

solenoid. The solenoid was connected to a fixed DC supply at a preset voltage and the plunger was clamped to prevent it from moving. The supply was disconnected and the solenoid voltage and current was measured. Fig. 60 shows the experimental waveforms for current and voltage for various voltage preset values.

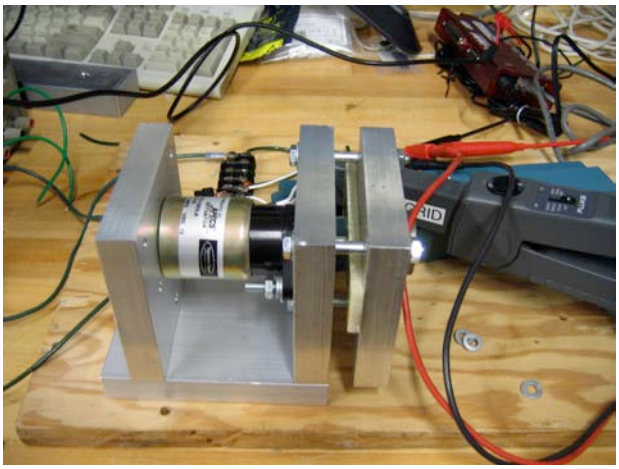

Fig. 59: Test setup for characterizing solenoid for diesel genset electronic governor

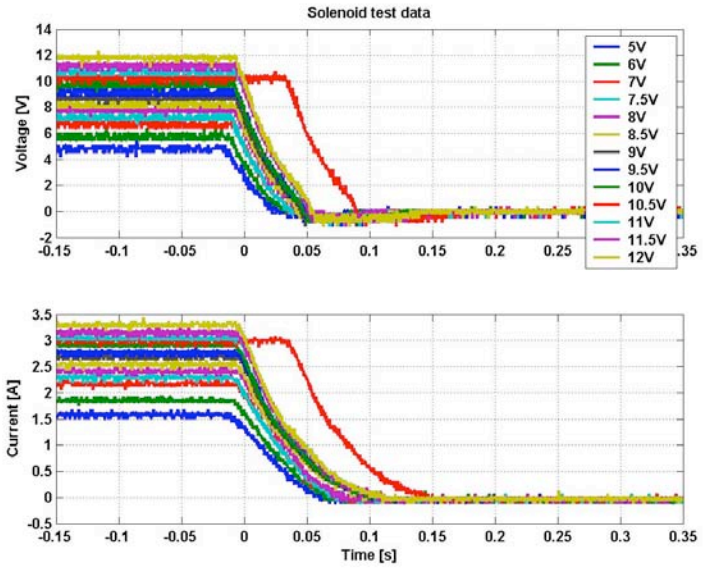

Fig. 60: Solenoid voltage and current waveforms for test involving sudden removal of supply voltage at fixed solenoid position

Using the voltage and current measurements the change in flux linkage as a function of current during the test was calculated and this shown in Fig. 61. The slope of the flux linkage curve gives the inductance of the solenoid as a function of position and current. We can see from the curves that the solenoid has an unsaturated and a saturated inductance value. While running the genset it was observed that the solenoid typically operated at a current greater than 2A and hence for the controller the saturated value of inductance was used.

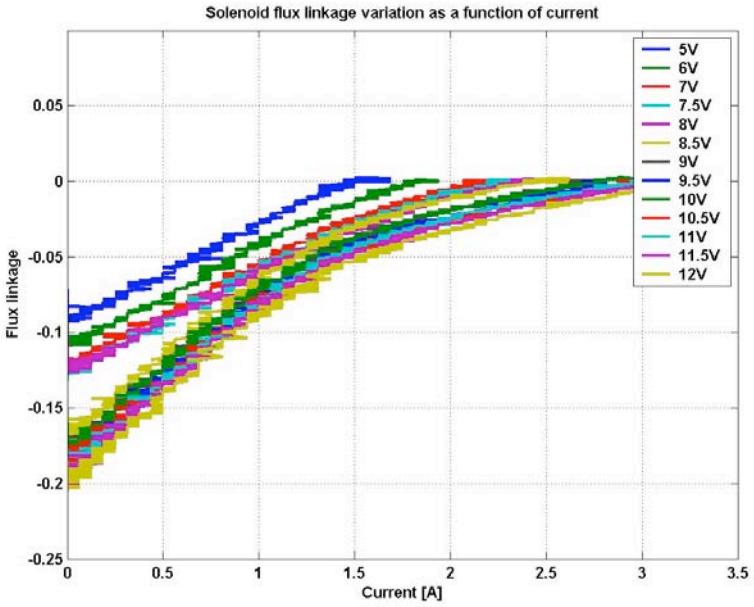

Fig. 61: Solenoid flux linkage variation as a function of solenoid current

To drive the solenoid a power board was designed. The solenoid is driven using the 12V battery present on the genset. A two quadrant drive board was designed to drive the solenoid as well as the brushless exciter. Fig. 62 shows the schematic for the power stage board. The presence of the freewheeling diodes ensures that in event of a loss of gate signals the current through the solenoid or the brushless exciter automatically starts

decaying and the genset turns off. This backup protection ensures that in the event the controller loses communication the genset is still safe. To measure the genset currents and voltages a separate signal conditioning board was designed and this was installed inside the lab. The power stage board for the brushless exciter and solenoid were mounted in a weather proof box and installed inside the genset enclosure. As the weather in Wisconsin can fall below -30F all the components used in the power drive board were carefully selected and the box was carefully located to ensure that the electronics are not damaged by dust, snow and rain.

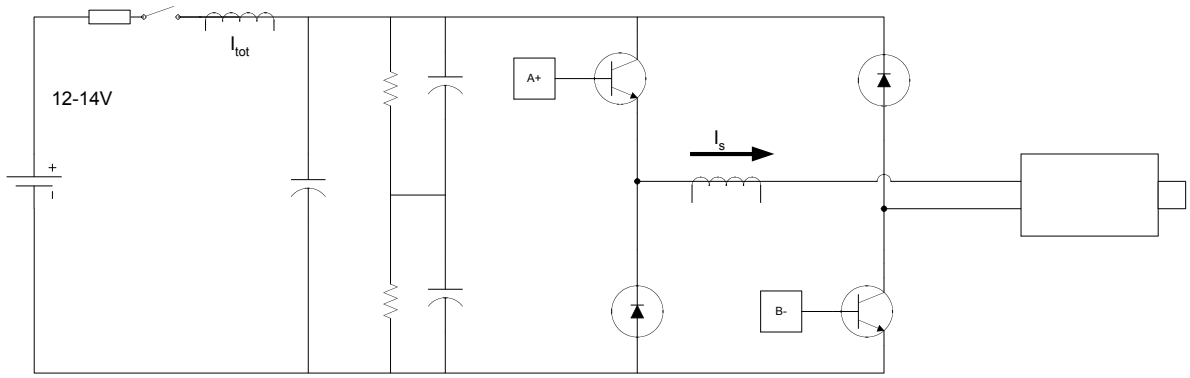

Fig. 62: Schematic of power stage board used to drive exciter and governor solenoid

The final modification to the genset was to install an incremental encoder on the shaft to obtain the position of the rotor. The vibrations of the genset during starting, running and stopping operations caused this to be a very challenging exercise. In its current form the encoder is cantilevered off the end and is connected to the genset shaft using a flexible metal coupling. The encoder itself is mounted on a plate fixed to the genset chassis to minimize vibrations. The best option would be to have the manufacturer incorporate the encoder into the genset during the design phase.

The electronic governor and voltage regulator control are implemented on Motorola 56F805 DSP. The measured genset voltages, current, exciter current, solenoid current and rotor position are fed into the DSP as inputs. The signals from the genset are fed to the DSP using shielded twisted pair cables to decrease noise and cross-talk. The DSP implements the control algorithm proposed in Section and outputs a duty ratio signal to the power devices that control the brushless exciter and fuel solenoid.

The DSP used for the control is a 16 bit controller and is capable of a limited number of 32 bit operations. To improve the resolution of the controller most of the critical operations are performed using 32 bit math. No significant disadvantages were observed in implementing the controller digitally as the fundamental frequency of the system is nominally 60Hz and the controller was set to run at 1.25 kHz .

6.6 Test results for operation of modified genset controller in a microgrid

The section presents the simulation and experimental results for the operation of the genset with the modified controller. The first subsection discusses the variation of the genset reference while connected to the grid, which enables the user to change the dispatch within the microgrid. The second subsection presents simulation and experimental results for an islanding event of the genset similar to the one discussed in section 5.4. Finally the third subsection looks at the performance of the modified genset for an islanding event with inverter based sources present, similar to the discussed in section 5.5.

6.6.1 Test results for genset power reference variation while connected to grid

The EMTP model for the diesel genset in a microgrid environment with grid is shown in Fig. 63. The ability of the genset to vary its output power while grid connected was tested extensively. The various events taking place during the experiment are:

1. Increase in power reference from 0.2pu to 0.325pu
2. Decrease in power reference from 0.325pu to 0.2pu

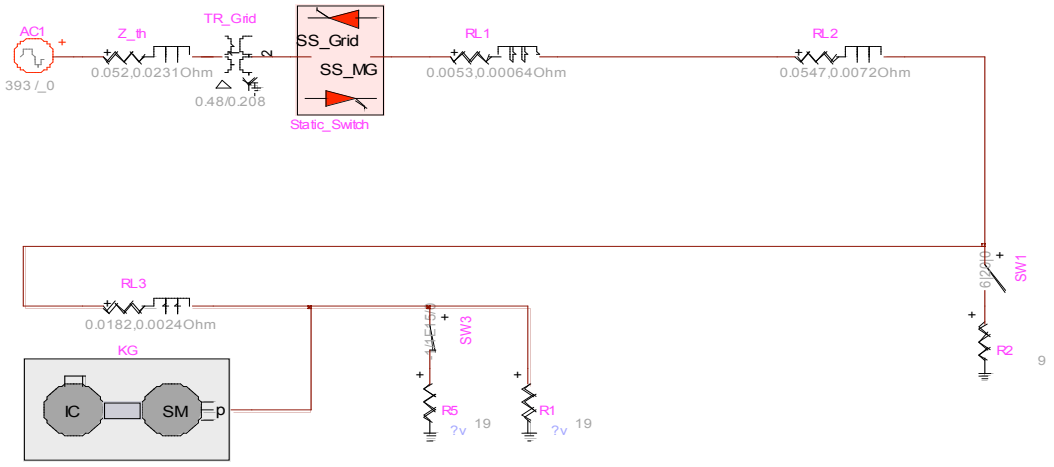

Fig. 63 : EMTP model of diesel genset connected to grid through static switch

Fig. 64 shows the real and reactive power variation of the grid and genset during step changes in the genset power reference and Fig. 65 shows the system frequency and genset terminal voltage during the same set of events. We can see that the genset is able to respond to the reference change in roughly 1-2s, the gradual change in power is due to the slight variation in grid frequency (Fig. 65) that affects the output of the genset .

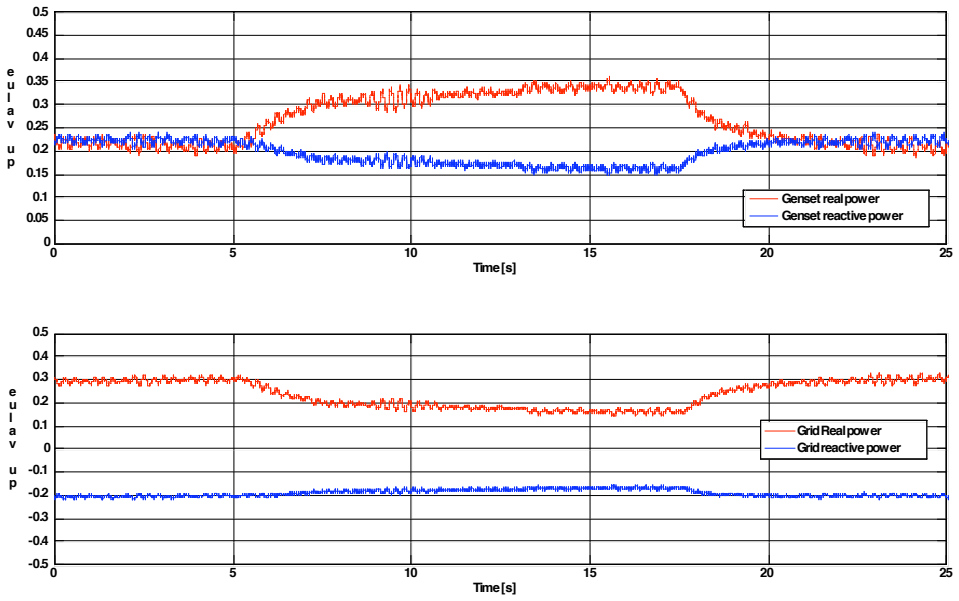

Fig. 64: Experimental waveforms for genset real , reactive power and grid real, reactive power during power reference variation of genset with modified controller

During the reference change the flow of reactive power changes and the Q-V droop ensures that the reactive power is kept under check. With the conventional controls the genset was constrained to output a fixed power while connected to the grid. The modified controls enable us to change the power and/or the voltage reference on the fly to vary the dispatch based on the users requirements.

One of the problems with the conventional genset controls was the inability to change power reference on the fly of the mechanical governor. With the electronic governor and the ability to change the power reference using software the user now has the ability to layer on a dispatch schedule either based on reducing emissions, cost or any other objective. This is a key step in utilizing the microgrid to not only maintain reliability and power quality but also to utilize the various distributed resources optimally.

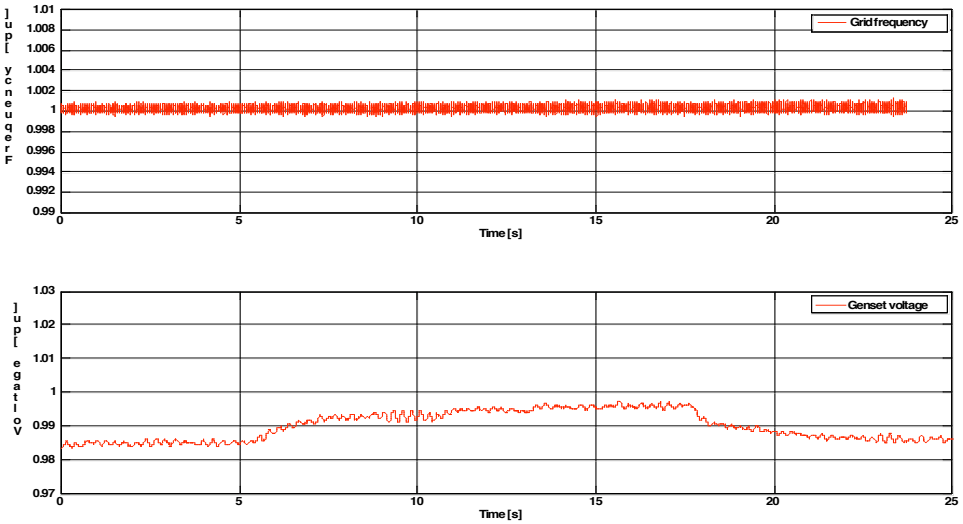

Fig. 65: Experimental waveforms for system frequency and genset voltage during power reference variation of genset with modified controller

6.6.2 Test results for operation of modified diesel genset in a Microgrid

In this section the response of the genset with the modified control to an islanding event is studied. The various events taking place in the test are:

1. Initially the genset is connected to the grid
2. The load in the system is increased at 5s simulation and 0.75s experiment
3. The grid is disconnected at 12s simulation and 7.5s experiment

Fig. 66 and Fig. 67 show the simulation results obtained from EMTP for the test and Fig. 68 and Fig. 69 show the experimental results obtained. Prior to the increase in load event we can see that the circulating VAR's have been decreased to a very minimal amount

using the new controller (Fig. 66 and Fig. 68) due to the presence of the reactive power droop curves which changes terminal voltage. We can see that when the genset is connected to the grid and the load is increased the genset does not pickup the load (Fig. 69). This is to be expected as the genset operates at a fixed output reference power due to the fixed frequency maintained by the grid. At 7.5s when the grid disconnects the genset picks up the excess load. At the instant of islanding the genset frequency falls and this cannot be changes due to the fixed time-delay inherent to the operation of the genset.

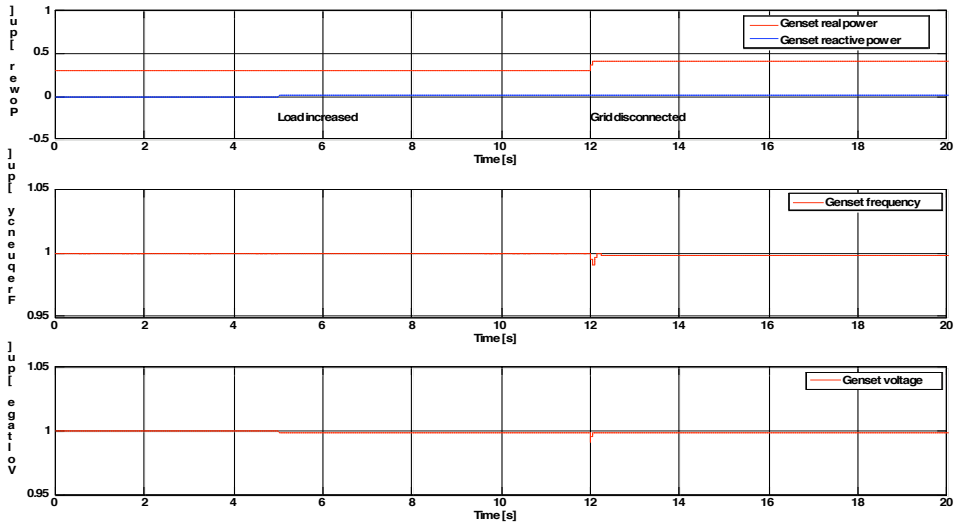

Fig. 66: Simulated genset output real power, reactive power, frequency and voltage waveforms with modified controller for load increase and islanding test

The speed of the genset (Fig. 68) is restored to its steady state value within two seconds with very good dynamics in comparison to the 3-5s response seen with the mechanical governor. In the simulation results the speed is restored much quicker as it does not account for all the filter delays used in the experimental setup. The effect of the islanding

and change in load shows negligible effect on load terminal voltage shown in Fig. 67 which is desired.

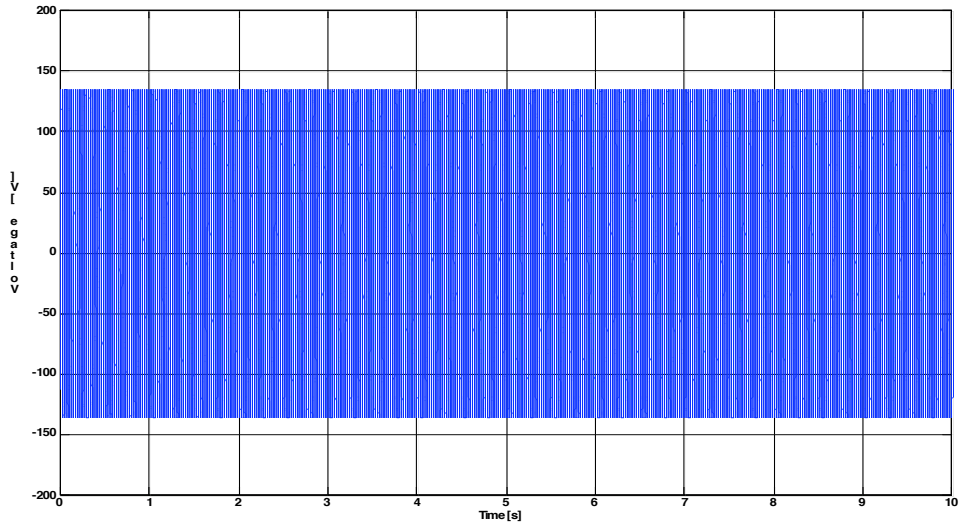

Fig. 67: Simulated load voltage waveform with modified controller for islanding and load decrease scenario

The decoupling of the electrical torque in the electronic governor is one of the critical elements of the speed controller. The presence of this disturbance input decoupling helps the control to respond quickly to load changes and enhances the performance of the genset.

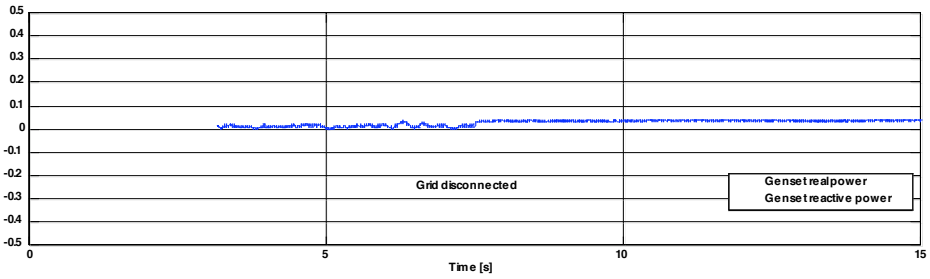

Fig. 68: Experimental waveforms for genset real power, reactive power and frequency with modified controller for load increase and islanding test

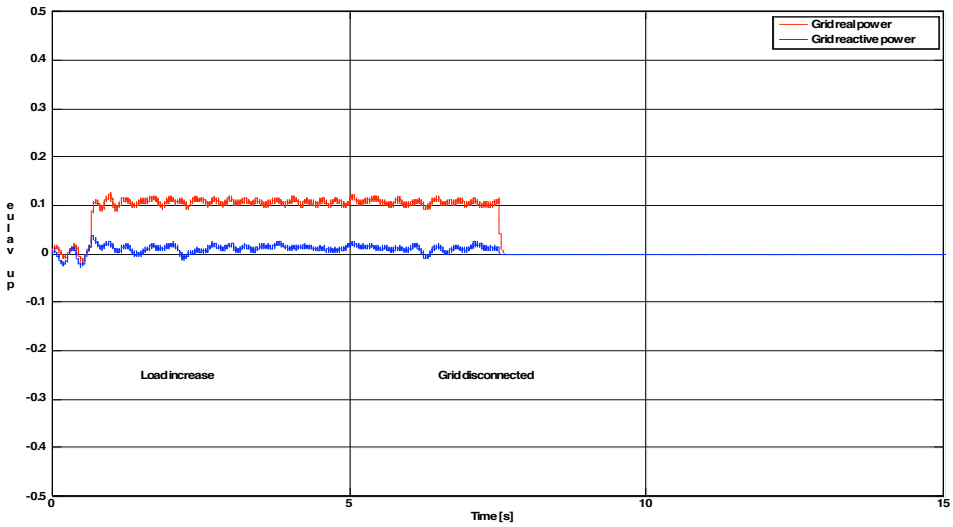

Fig. 69: Experimental waveforms for grid real and reactive power during islanding operation of modified genset in a microgrid

6.6.3 Test results for modified genset controller in microgrid environment with inverter based microsource

Fig. 70 shows the EMTP model of the system being tested and Fig. 71 shows the steady state points in the power frequency plane; the various events taking place are:

1. Initially the grid, genset and inverter based source are all connected together
2. The load in the system is increased at 2s (simulation), 2s(Experiment)
3. The grid is disconnected at 6s (simulation) and 9.2s experiment

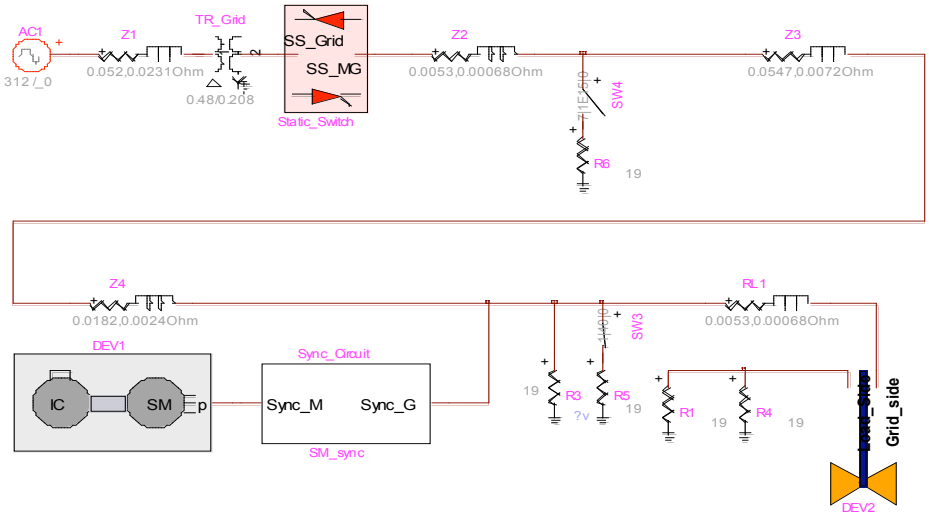

Fig. 70: EMTP model of diesel genset with modified controller in UW-microgrid system

Fig. 72 to Fig. 74 gives the various results obtained from the simulation and Fig. 75 to Fig. 77. Fig. 72 shows the simulation results for the genset output during the test and Fig. 75 the experimental results. Fig. 74 and Fig. 76 present the simulation and experimental waveforms for the inverter output respectively during the test. Fig. 77 presents the real and reactive power delivered by the grid during the experimental test.

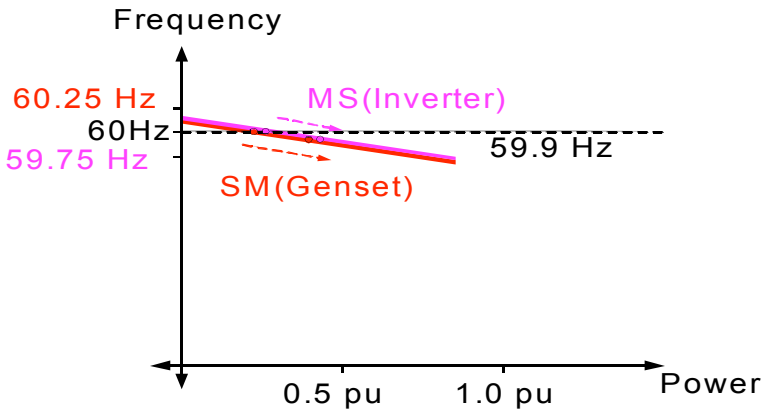

Fig. 71: Power frequency droop curves for microsource and genset with modified controller

One of the chief problems with the existing genset voltage regulator was the large circulating VAR's due to the absence of a reactive power droop. From Fig. 72 and Fig. 75 we can see that the circulating VAR's have been significantly brought down.

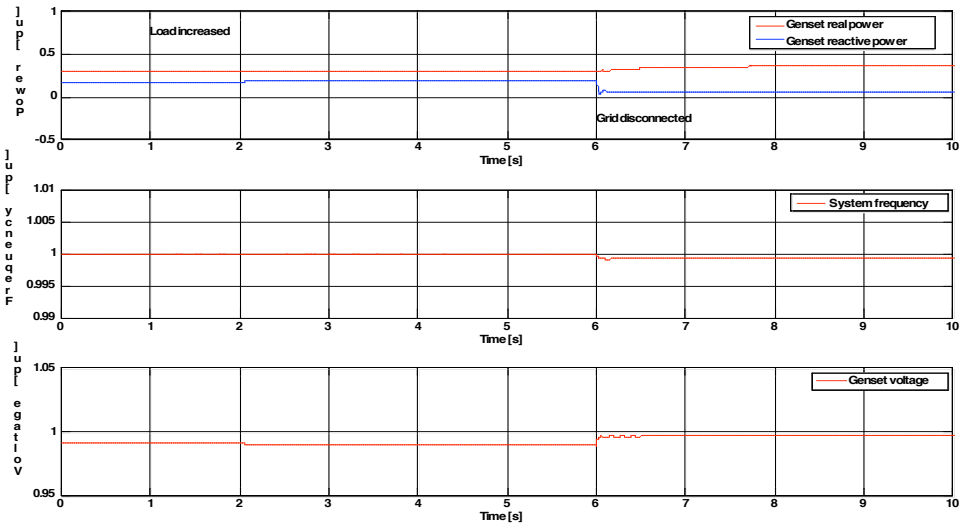

Fig. 72: Simulated genset real power, reactive power, voltage and frequency waveformd in a microgrid system with modified genset and inverter based source

After the islanding and subsequent load change events the system is stable and the frequency and voltage are within prescribed (IEEE 1547) limits. During the load increase the genset and the inverter do not pick up the load as shown in Fig. 75 and Fig. 76. The sources put out their reference power and the grid picks up the increased load as shown in Fig. 77. The circulating reactive power between the various sources is kept under control due to the QV droop and is much lesser than the value with the original controller .

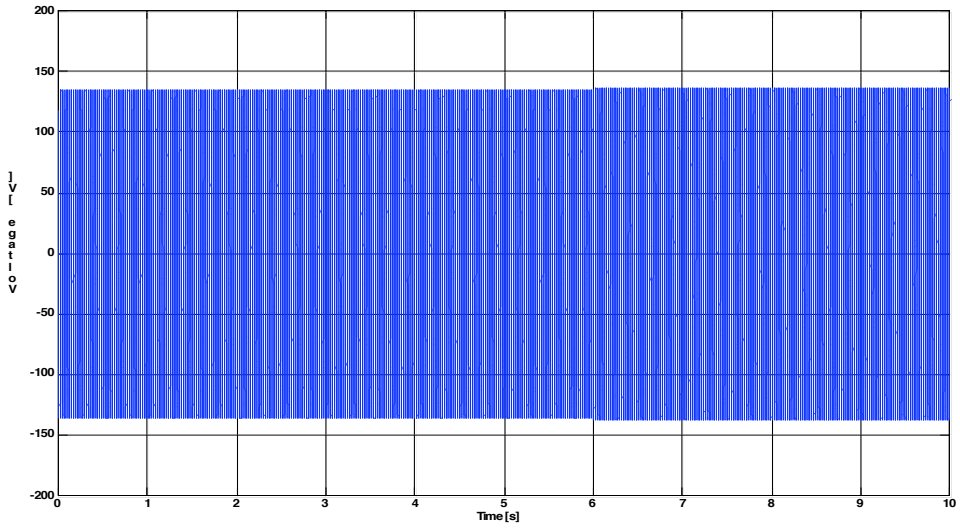

Fig. 73: Simulated load voltage waveform in a microgrid system with modified genset controller and inverter based source

At 9.2s when the grid is disconnected the inverter picks up the load increase initially (Fig.), the genset picks up it share in roughly 1-2s. This is to be expected as the inverter can respond much faster than the IC engine. The frequency variation after the islanding operation is minimal as the two sources pick up the load. The load is shared more evenly between the genset and inverter as the droop of the genset has been reduced. Due to the

electronic governor the speed of the genset reaches its steady state value (Fig. 75) within two seconds. The overall effect of the set of events on the load voltage waveform is negligible and this is a desirable feature..

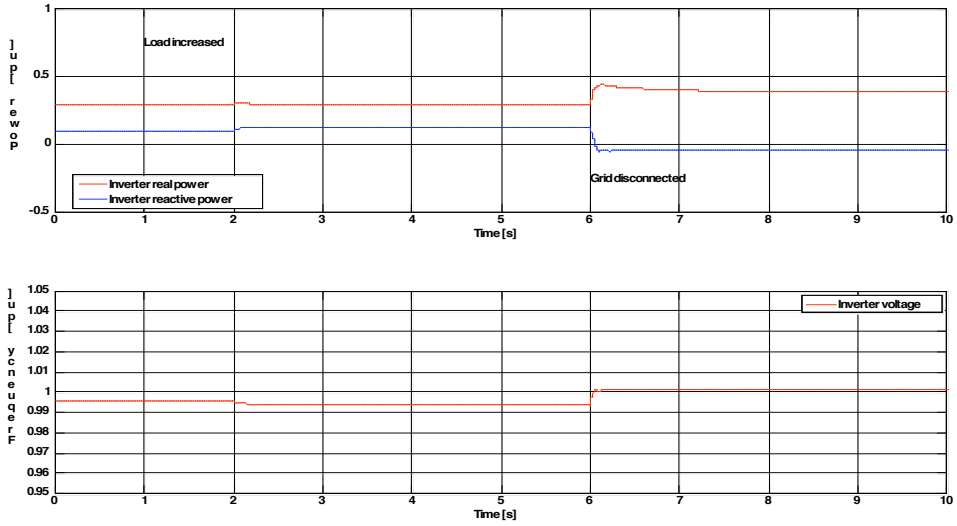

Fig. 74: Simulated real power, reactive power and voltage waveforms for inverter based source in a microgrid system with modified genset controller

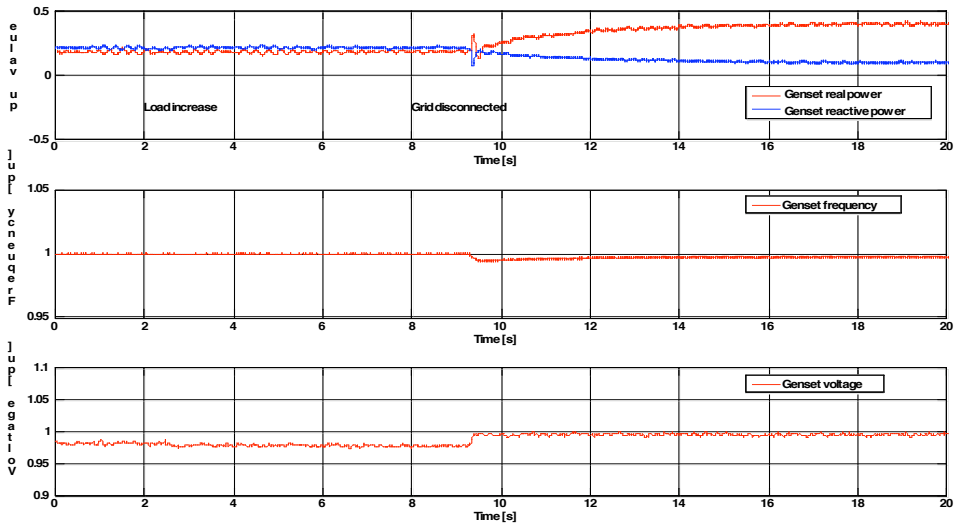

Fig. 75: Experimental waveforms for genset real power, reactive power, frequency and voltage during islanding operation of modified genset in a microgrid with inverter based sources

The results show the improvement in genset performance for microgrid operation. The presence of the QV droop decreases the circulating VAr's between the sources. The observer based genset controller improves the dynamics of the genset response and the electronic governor enables the engine to respond much quicker to load changes. Furthermore the modified controller enables the genset to share load more evenly with the inverter based source. This demonstrates that gensets and inverter based sources can coexist in a microgrid environment and maintain system reliability and power quality. The simulation results match closely with the results obtained from the experimental setup and validate the model for the genset proposed in the previous chapter.

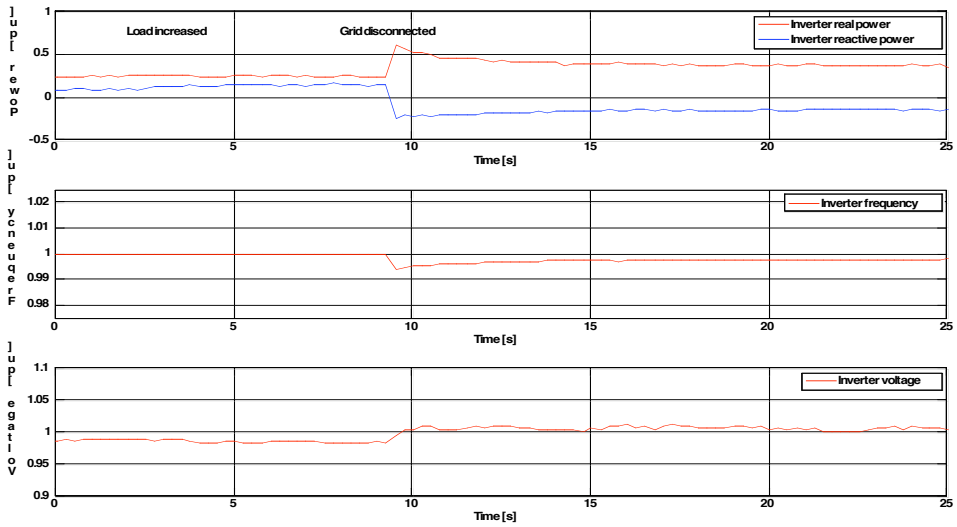

Fig. 76: Experimental waveforms for inverter real power, reactive power, frequency and voltage during islanding operation of modified genset in a microgrid with inverter based source

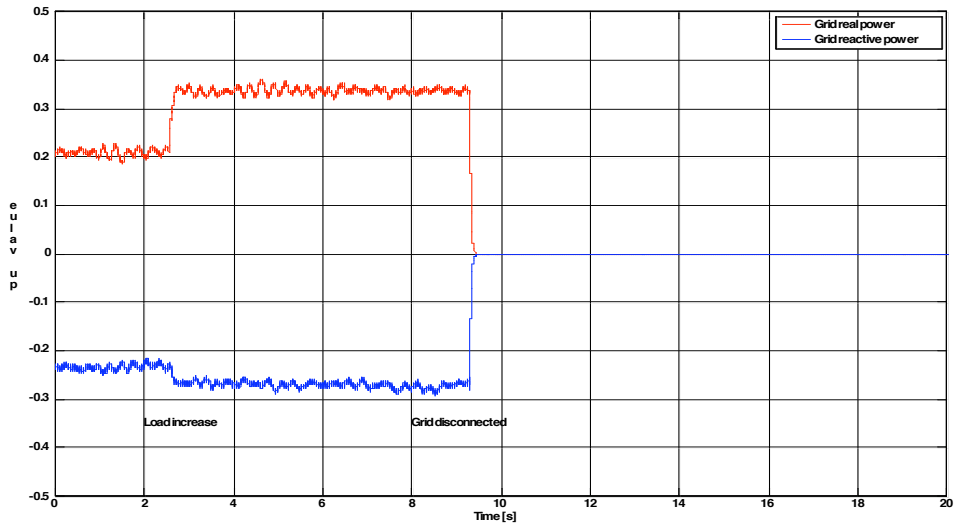

Fig. 77: Experimental waveforms for grid real and reactive power during islanding operation of modified genset in a microgrid

6.6.4 Test results for operation of multiple gensets in microgrid environment

In this section the operation of multiple gensets in a microgrid environment will be studied using a simulation study. Fig. 78 shows the EMTP model of the UW microgrid setup with two diesel gensets each equipped with the proposed controller. Both the gensets in the system are modeled on the 10kW kohler genset , only simulation results are presented due to the absence of a second genset to carry out experimental results.

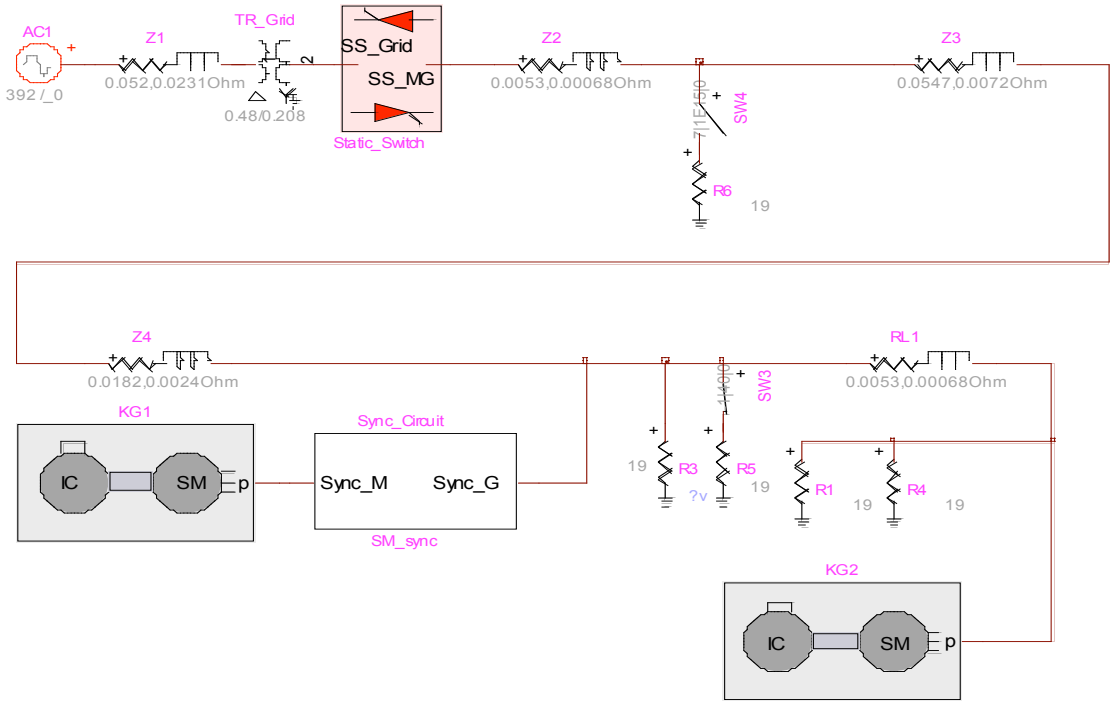

Fig. 78: EMTP model of UW-Microgrid containing multiple gensets each equipped with modified controller

In this simulation case both gensets have the same power reference point (0.5pu) and are initially connected to the grid. The initial load in the system is close to 9kW and is provided by the two gensets and the grid.

The various events occurring in the simulation are:

1. Initially grid and two gensets are connected and are supplying 9kW load
2. Load increases by 2kW at time 2s
3. Grid is disconnected at 6s

Simulation results for the test are presented in Fig. 79 and Fig. 80. Fig. 79 shows the real power, reactive power, frequency and voltage for Genset 1 and Fig. 80 depicts the same results for Genset 2. From the simulation results we can see that during grid connected operation the circulating VAR's are kept under check and both the sources are operating at their reference powers.

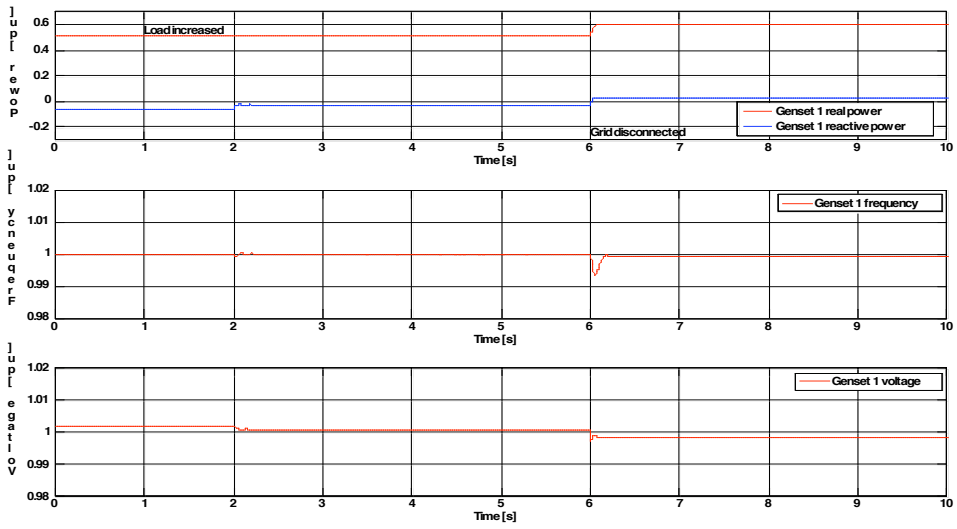

Fig. 79: Simulation waveforms for Genset 1 real power, reactive power, frequency and voltage for operation in a microgrid system with two gensets operating with modified controller

The increase in load at 2s is picked up by the grid and hence the output real power of the sources does not change. There is a change in the reactive power produced by each genset due to change in system node voltages after the load pickup by the grid. After the grid disconnects at 6s the two gensets pick up the load in the system and there is a slight drop in frequency at the instant of islanding. Due to the presence of the stroke delay the gensets are not able to respond instantaneously and this results in the drop of frequency which is absent if an inverter based source is present (Fig. 76).

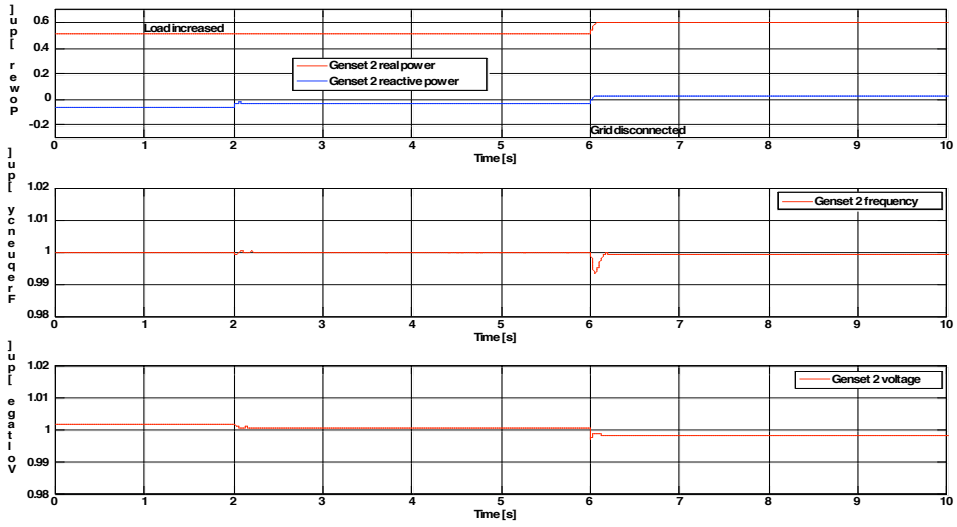

Fig. 80: Simulation waveforms for Genset 2 real power, reactive power, frequency and voltage for operation in a microgrid system with two gensets operating with modified controller

Overall the system is stable during the entire simulation run and shows that the system can operate even in the absence of inverter based sources.

6.7 Summary

The chapter presents the design and analysis and experimental validation of the observer and controller for the IC engine genset. An enhanced luenberger topology is chosen for the observer that accurately estimates the rotor speed and genset 'd' axis mutual flux voltage. The observer guarantees zero steady state error within its bandwidth even in the presence of parameter errors. Using the output of the observer an electronic governor and a voltage regulator has been designed. The electronic governor incorporates command feed forward, state variable controller and a disturbance input decoupler. Due to the presence of the engine delay the governor cannot instantaneously correct for sudden load changes. This time delay ensures that the shaft mechanical torque does not change instantaneously after a fuel command change. Hence during this time interval the speed will vary and the difference in power would need to be supplied from the other sources in the system and the mechanical inertia in the genset. However the incorporation of the electronic governor significantly decreases the time during which the other sources have to contribute the excess power. Simulation and experimental results confirm that the incorporation of the reactive power droop characteristic decreases the amount of circulating VAR's in the system. The decoupling of the electrical torque in the electronic governor is one of the critical elements of the speed controller. The presence of this disturbance input decoupling helps the control to respond quickly to load changes and enhances the performance of the genset. Furthermore the proposed controller also enables it to share load more evenly with other sources in the system.

The proposed controller demonstrates the ability of the IC engine based source to work in conjunction with inverter based sources in a microgrid environment and share load

evenly, maintain system voltage and improve the genset dynamics during various events. Simulation tests demonstrate the performance of multiple gensets operating in a microgrid environment in the absence of any inverter based sources. Due to the time delay inherent to the operation of IC engines there is a drop in frequency during load changes occurring in an islanded operation. This drop in frequency is absent if an inverter based source is present due to the much faster response of such sources, however the absence of an inverter based source does not cause any system instability.

CHAPTER 7. Induction machine starting in a microgrid environment

Induction machines are commonly used in distribution systems to drive fan loads, pump loads etc. These machines are typically line-started and draw significant reactive power from the utility supply during the starting phase. Typically with a stiff supply the starting of an induction machine causes a negligible effect on the supply voltage. However in areas with a weak connection to the grid the starting of induction machine causes significant voltage sag which effects power quality. In the analysis of microgrid power systems the loads that have been considered were typically passive loads [20, 21]. In this chapter we study the effect of line starting induction machine in a microgrid environment by performing EMTP simulations.

7.1 Starting kVA requirements for line start induction machines

The induction machine is a very nonlinear device and draws significant reactive power when it is line started. To reduce the inrush current, starters are used which decrease the line voltage during start for a certain period of time and then restore full voltage to the machine. Reducing the line voltage decreases the starting torque and increases the time it takes to reach steady state speed. In the EMTP simulation studies performed we do not employ a reduce voltage starter and essentially look at the voltages in the system during the machine starting phase. The maximum size of induction machine that can be used in

the microgrid if its line started can be determined by looking at its starting kVA requirement. We assume that the kVA required by machine being started is less than the kVA rating of the distributed generators in the system. This is a fairly conservative requirement (expand this here). To estimate the kVA required by the machine during start we will use the scaling laws developed for NEMA class B machines in [76].

The parameters for the NEMA class B induction machine can be obtained by using the scaling laws specified in [76] and are mentioned below. The scaling laws are based on the pole pitch of the machine that can be deduced using the power of the machine P in horsepower and the number of pole pairs N_p. Using the pole pitch (τ_p)the other parameters of the machine can be calculated.

$$\tau_p = 0.084\left[\frac{P}{N_p^2}\right]^{6/23} \tag{46}$$

$$x_1 + x_2 = 0.2 \tag{47}$$

$$x_m = 10\left(\frac{\tau_p}{N_p}\right)^{1/2} \tag{48}$$

$$r_1 = 0.0033\left(\tau_p\right)^{-1} \tag{49}$$

$$r_2 = 0.004\left(\tau_p\right)^{-1} \tag{50}$$

Impedance of induction machine at start is (neglecting magnetizing reactance)

$$Z_{start} = 0.0073\left(\tau_p\right)^{-1} + i0.2 \tag{51}$$

Using the impedance of the machine at start the initial kVA required by the machine for a line start at rated voltage can be estimated. The starting kVA in per unit required by the machine for different ratings is plotted in Fig. 81. We can see that the starting kVA required is roughly a maximum of 5pu. The split between starting kW and staring kVAr is plotted in Fig. 82 and we can see that for larger machines the starting kVAr dominates the kVA requirement.

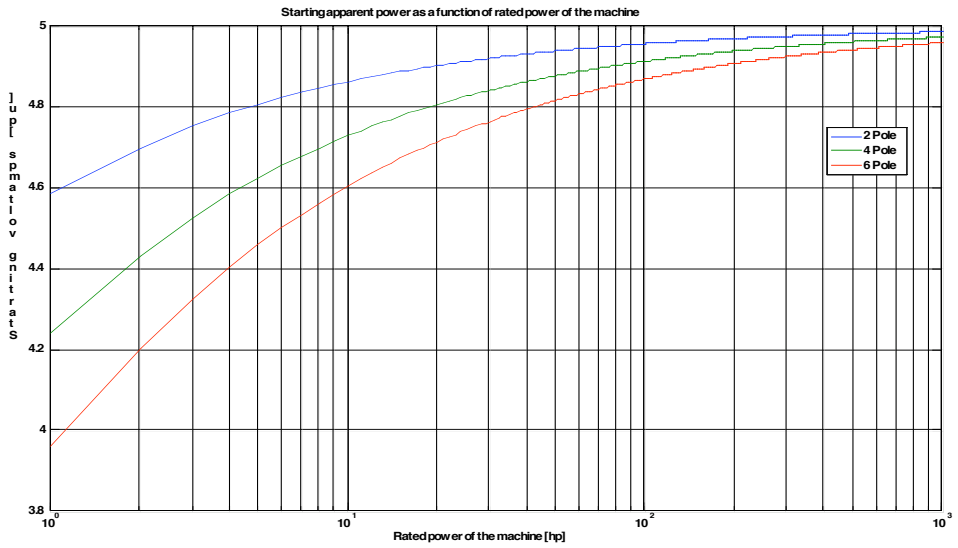

Fig. 81: Starting kVA required by induction machine for line start at rated voltage

It has been shown [77] that during large signal changes such as online starting the saturation of the reactances needs to be accounted to correctly predict the transient of the machine. To correctly predict the saturated reactance of a machine the approach utilizes finite element analysis to calculate the flux linkages in various parts of the magnetic circuit. This method provides for an accurate estimate of the saturation factors for various inductances but results in a significant computational burden on the user. The scaling

laws provide a good estimate of the various inductances in the machine and even though they do not incorporate the saturation phenomenon they still provide a very good initial estimate of the starting kVA requirement for a large range of induction machines.

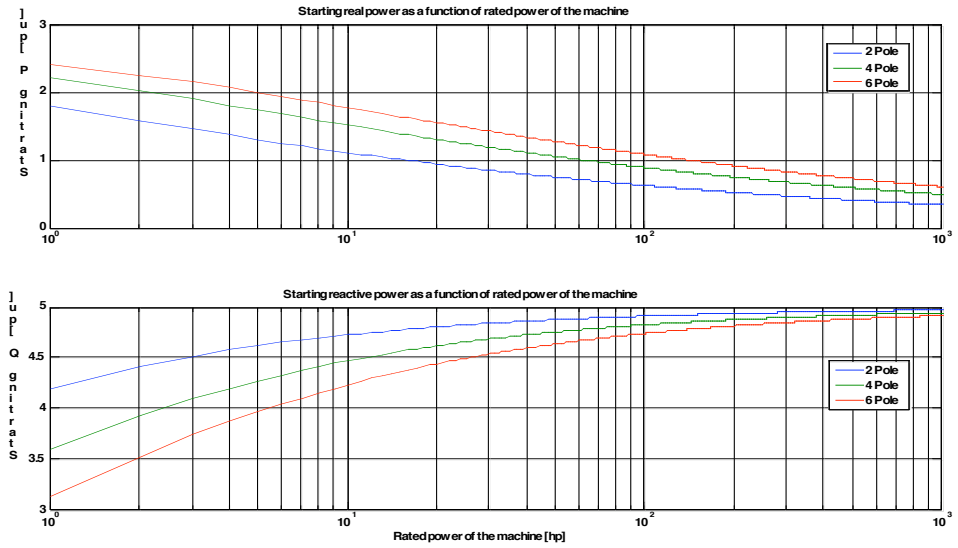

Fig. 82: Starting kW and kVAr required by induction machine for line start at rated voltage

With the decreasing cost of power electronics it is possible that induction machines would utilize an inverter drive at the front end to improve efficiency. Induction machine inverter drives are typically programmed for a soft-start using a V/Hz ramp which allows the motor to run upto speed without drawing excessive currents from the supply. In this case the starting kVA requirement is much lesser and will typically not be an issue for isolated systems.

In the event that a line-start induction machine is to be connected to a microgrid the sizing of the motor becomes a critical issue. From the previous discussion we can see that the starting kVA required by a line started induction machine is roughly 5 times the

rating of the machine. Hence we can argue that the rating of the machine to be started should be roughly 1/5th of the available generation. Most backup gensets are able to start motors that have very similar ratings to the gensets itself. They are able to achieve this by reducing the voltage to start to reduce the kVA requirement. In a microgrid we aim to keep the voltage and frequency under very tight bounds and hence we really cannot start such large motors. Instead we can conservatively limit the size of the motor to 1/5th of the available generation. In a given microgrid the system planner would have to account for the various loads and sources to size the motor that can be connected. This guideline gives an estimate based on starting requirements; the other important issue to consider is the stability of the system under such a transient. The models developed for the genset and microgrid enable us to test such transients using simulation studies, which are explained in the next section.

7.2 EMTP based simulation results for induction machine starting

The induction machine line start phenomenon is studied by performing EMTP simulation tests. The system under test is the UW-Microgrid environment and an induction machine of 2kW rating was connected to the system and line started. The rating of the genset is 10kW and based on the 1/5th sizing a 2kW induction machine was chosen. The system was simulated with different sources connected in the system and the stability of the system was studied. The tests were conducted in 5 steps:

1. Induction machine start in Microgrid with conventional genset
2. Induction machine start in Microgrid with inverter based microsource
3. Induction machine start in Microgrid with modified genset controller

4. Induction machine start in Microgrid with conventional genset and inverter based microsource
5. Induction machine start in Microgrid with modified genset and inverter based microsource

Detailed simulation results for each test are presented in the subsequent sections.

7.2.1 Induction machine starting in microgrid system with conventional genset

Fig. 83 shows the EMTP setup for testing the start of an induction machine in a microgrid system with a genset with a conventional controller. The simulation is carried out with the microgrid disconnected from the utility supply. The genset is initially supplying resistive loads in the network and the induction machine is started at t = 3s. Fig. 84 shows the per unit real and reactive power output of the genset during the entire simulation test. We can see that at 3s when the machine starts there is an increase in reactive and real power output. There is no load torque on the machine shaft and hence at the end of the start the output real power falls back to the value before start. There is a slight change in reactive power at the end of the start as the genset is now providing magnetizing VAr's to the induction machine.

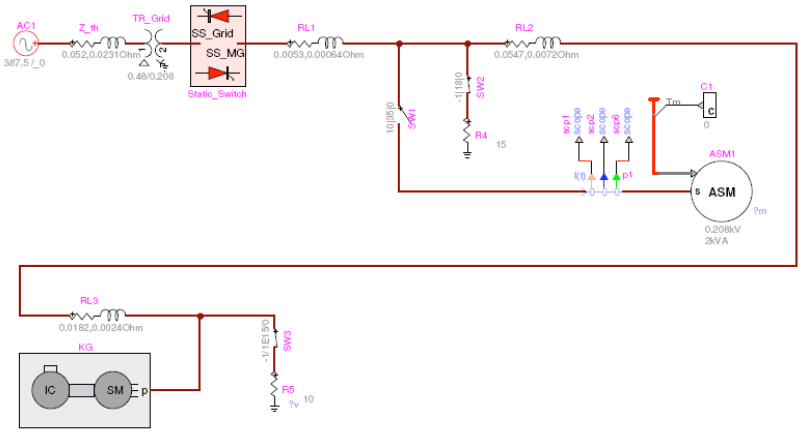

Fig. 83: EMTP model for testing line start of induction machine in Microgrid with conventional genset

Fig. 85 shows the genset terminal voltage and the genset speed during the entire simulation run. We can see that the motor speed reaches steady state in less than 2 seconds and during the staring phase the voltage sags which reduces the kVA required by the machine.

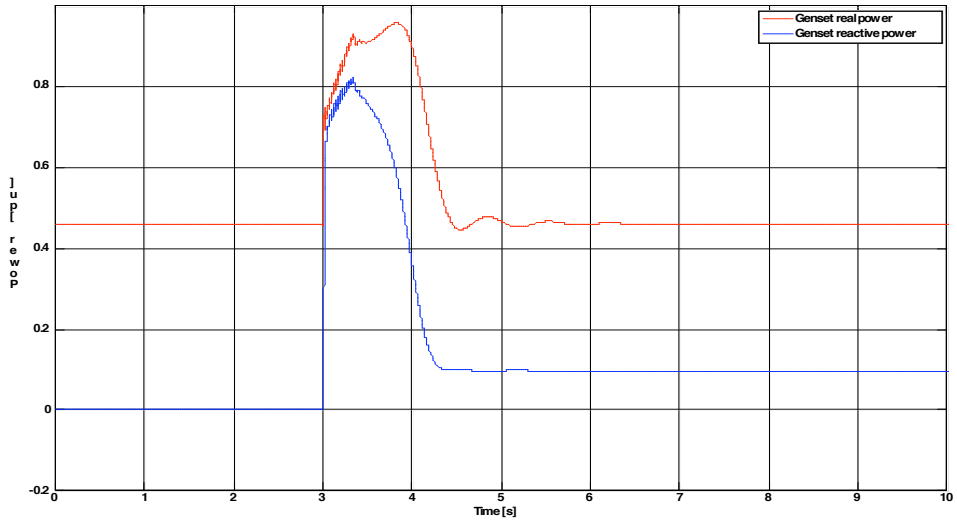

Fig. 84: Simulated genset output real and reactive power waveforms for induction machine line start with conventional controller

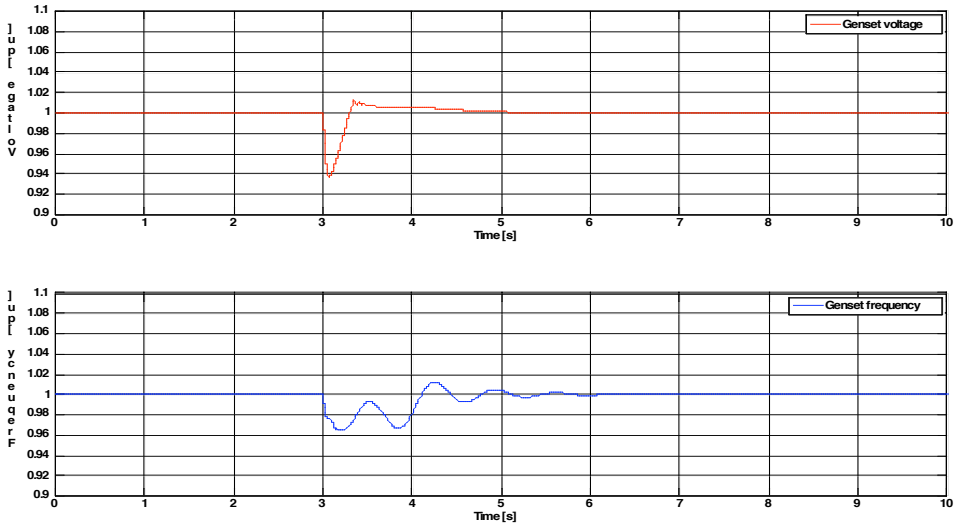

Fig. 85: Simulated genset output voltage and genset per unit speed waveforms for line start with conventional controller

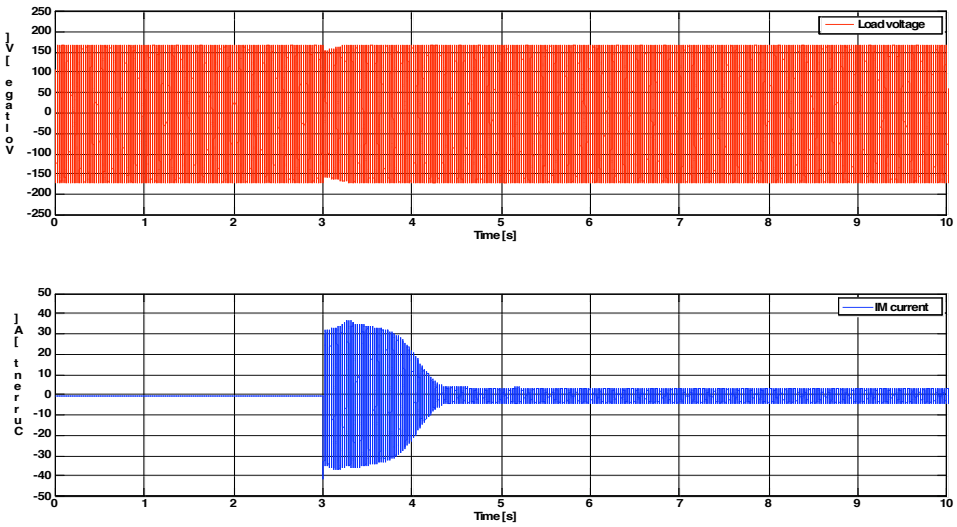

Fig. 86: Simulated load voltage and induction machine phase current waveforms for induction machine line start with conventional controller

The genset speed is governed by the mechanical governor and it takes around 5s for it to settle down. The drop in voltage is observed in the load voltage waveform shown in Fig. 86. Fig. 86 also shows the phase current of the induction machine during the entire simulation result. We can see that there is no instability during the transient and the machine ramps up to speed and the genset survives the transient.

7.2.2 Induction machine starting in a microgrid system with inverter

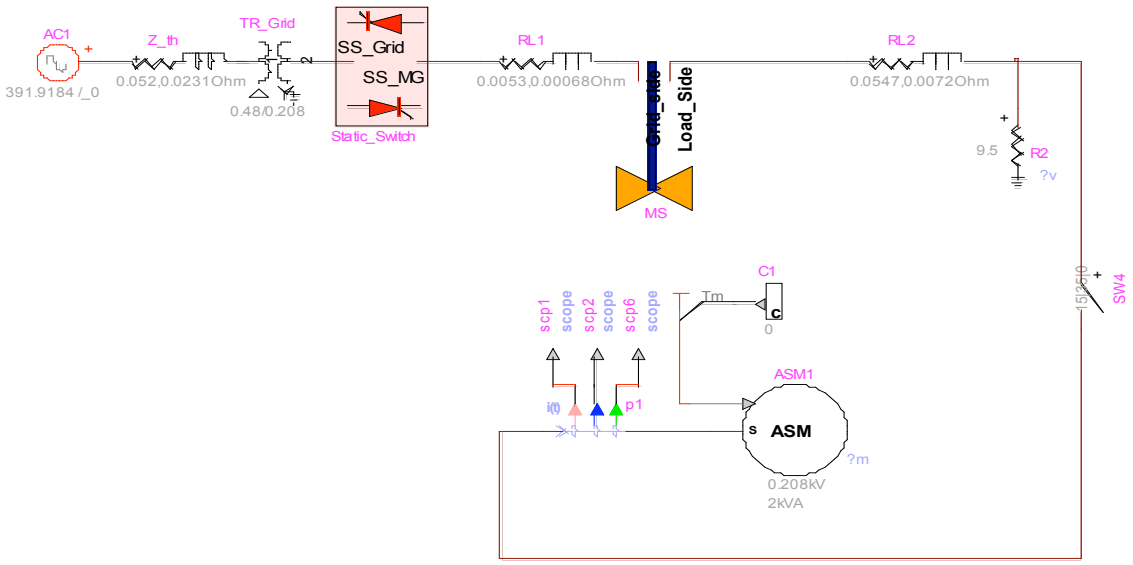

Fig. 87: EMTP model for testing line start of induction machine in Microgrid with inverter

The inverter is initially supplying resistive loads in the network and the induction machine is started at t = 5s. Fig. 88 shows the per unit real and reactive power output of the inverter during the entire simulation test. We can see that at 5s when the machine starts there is an increase in reactive and real power output. There is no load torque on the machine shaft and hence at the end of the start the output real power falls back to the

value before start. There is a slight change in reactive power at the end of the start as the inverter is now providing magnetizing VAr's to the induction machine.

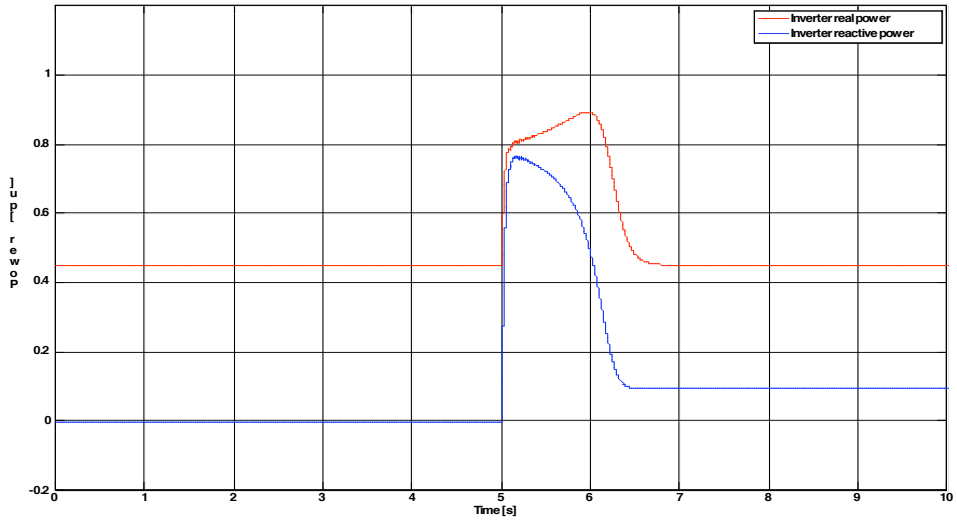

Fig. 88: Simulated inverter output real and reactive power waveforms for induction machine line start.

In comparison with the start using the genset (Fig. 85) we can see from Fig. 89 and Fig. 90 that the inverter terminal voltage drops during the starting phase. The drop in voltage is due to the fact that the inverter employs a QV droop and decreases the voltage as the induction machine demands reactive power during start. Once the machine starts up the reactive power required is just the magnetizing current and the terminal voltage of the inverter is restored to a value close to its initial setting. In comparison to the genset start the only difference is that the voltage in the system does not drop as much during the initial part of the starting phase and the frequency transient is much better.

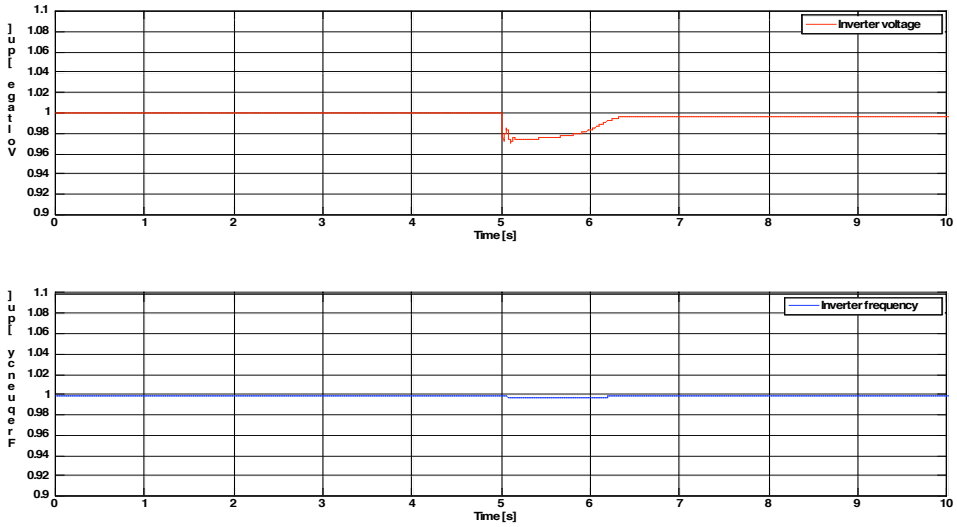

Fig. 89: Simulated inverter output voltage and inverter frequency waveforms for line start of induction machine

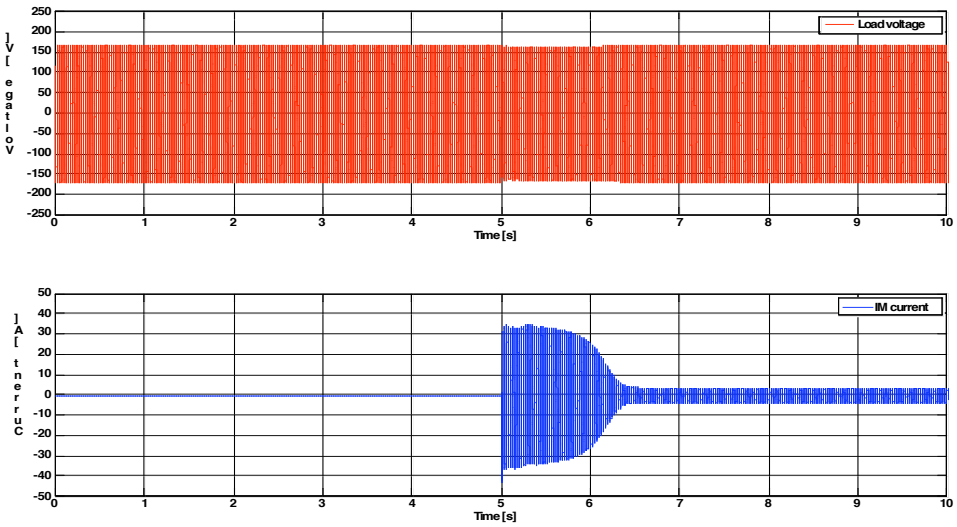

Fig. 90: Simulated load voltage and induction machine phase current waveforms for induction machine line start with inverter based source

7.2.3 Induction machine starting in microgrid system with modified genset controller

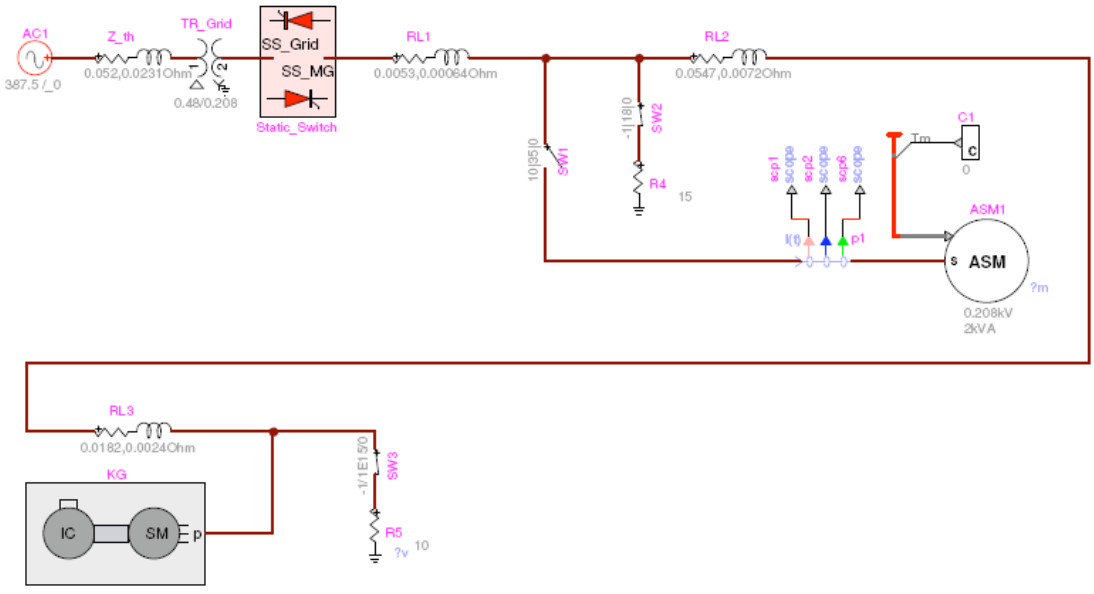

Fig. 91: EMTP model for testing line start of induction machine in Microgrid with genset with modified controller

Fig. 91 shows the EMTP setup for testing the start of an induction machine in a microgrid system with a genset with a modified controller. The simulation is carried out with the microgrid disconnected from the utility supply. As before the genset is initially supplying resistive loads in the network and the induction machine is started at t = 3s. Fig. 92 shows the per unit real and reactive power output of the genset and Fig. 93 shows the genset voltage and speed during the entire simulation test. We can see that in comparison to the conventional controller the terminal voltage is held to a lower value due to QV droop and hence the starting kVA requirement is slightly lower.

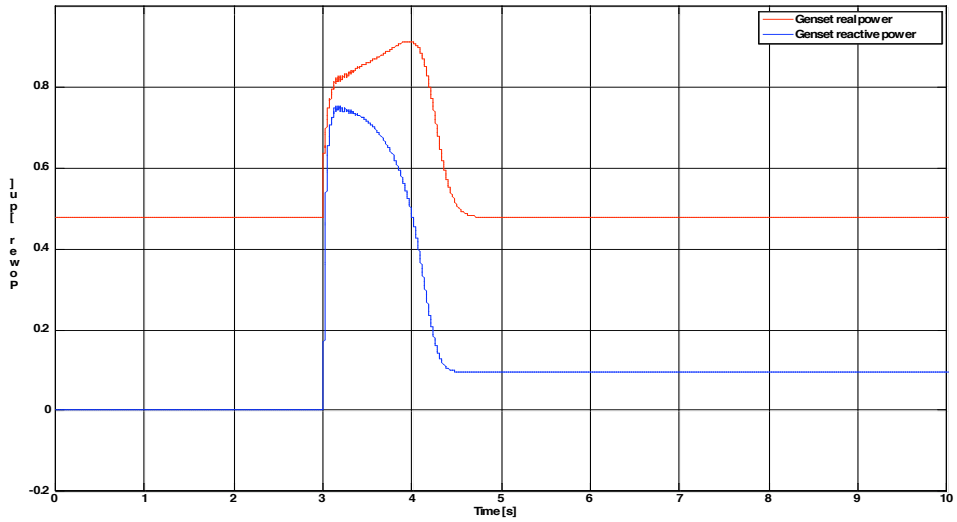

Fig. 92: Simulated genset output real and reactive power waveforms for induction machine line start with modified controller

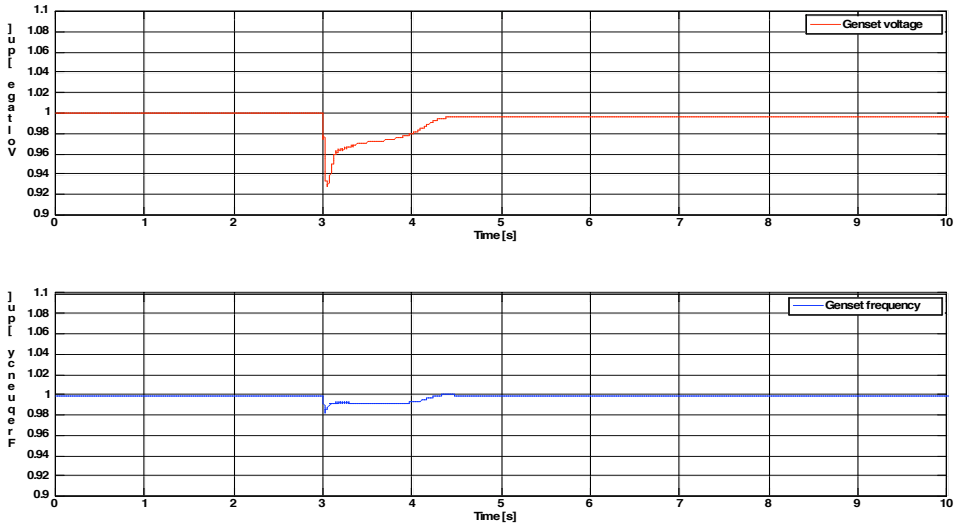

Fig. 93: Simulated genset output voltage and genset per unit speed waveforms for line start with modified controller

There is no appreciable difference in the startup time of the motor as seen in Fig. 94 in comparison to that seen in Fig. 86 with the conventional controller. In both cases the system is stable and is able to survive the start of the motor with no significant over voltages in the system. As expected the genset speed is much better during the transient due to the presence of the electronic governor.

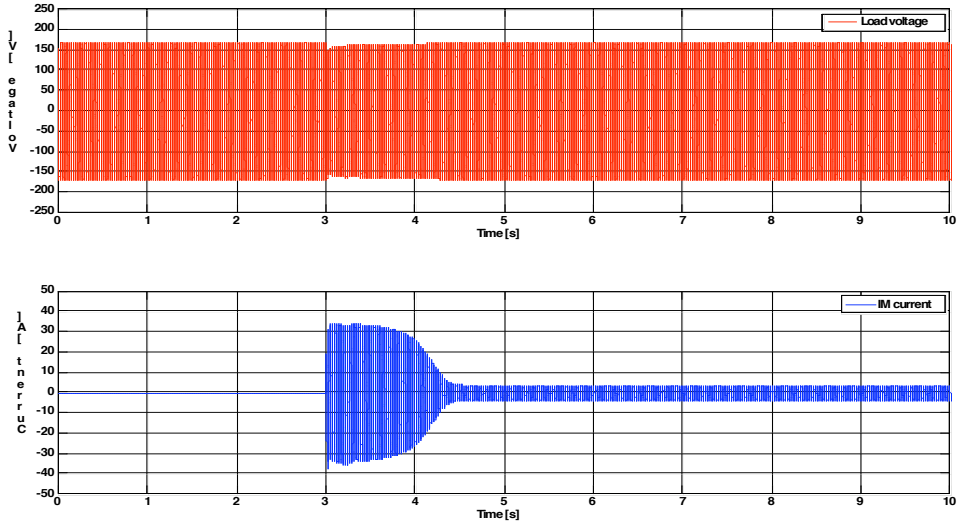

Fig. 94: Simulated load voltage and induction machine phase current waveforms for induction machine line start with modified controller

7.2.4 Induction machine starting in microgrid system with conventional gensets and inverter

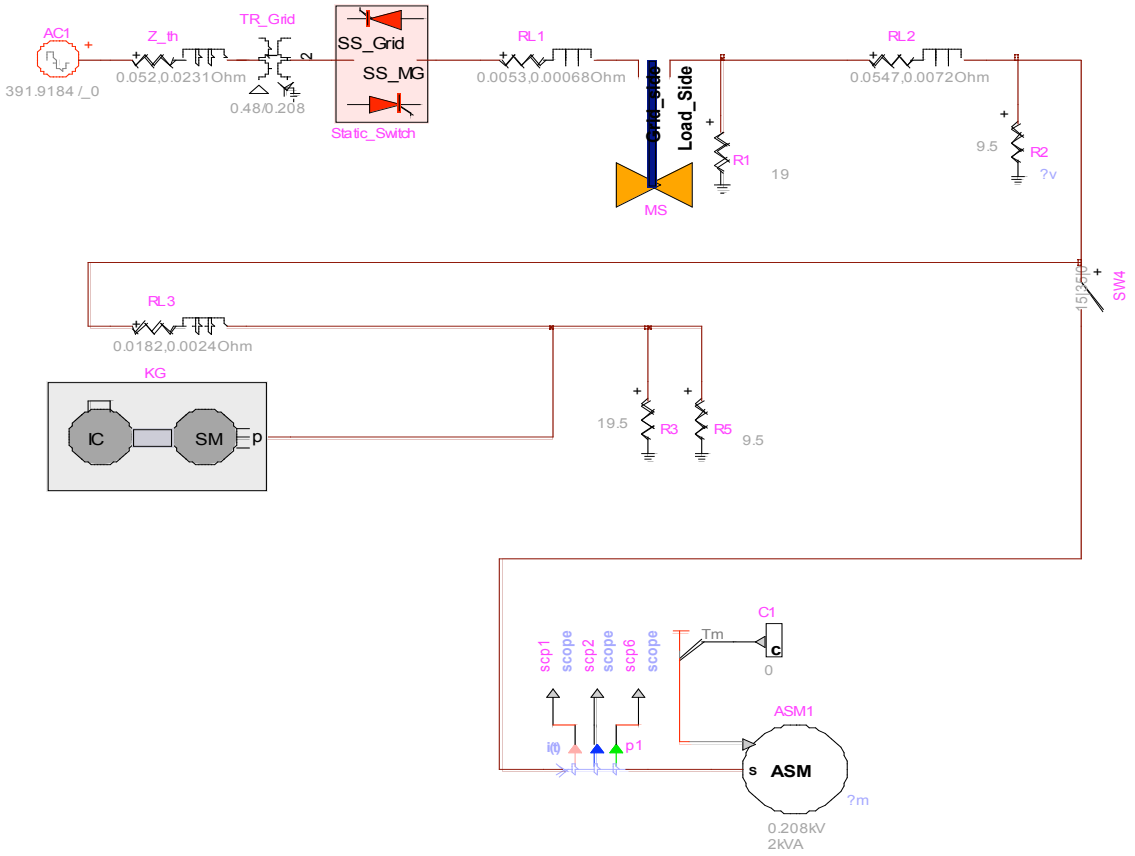

Fig. 95: EMTP model for testing line start of induction machine in Microgrid with inverter and genset with conventional controller

Fig. 95 shows the EMTP setup for testing the start of an induction machine in a microgrid system with an inverter based source and a genset with conventional controller. The simulation is carried out with the microgrid disconnected from the utility supply.

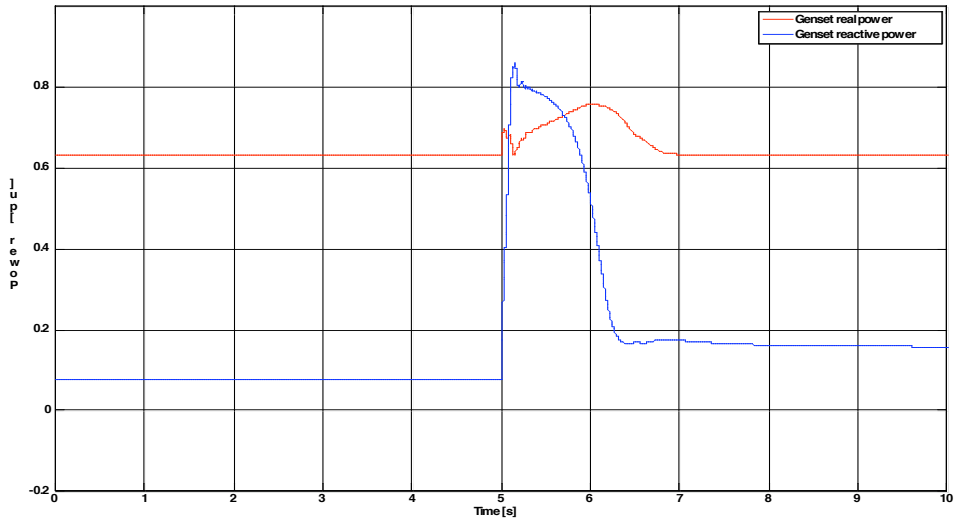

Fig. 96: Simulated genset output real and reactive power waveforms for induction machine line start with inverter based source and genset with conventional controller

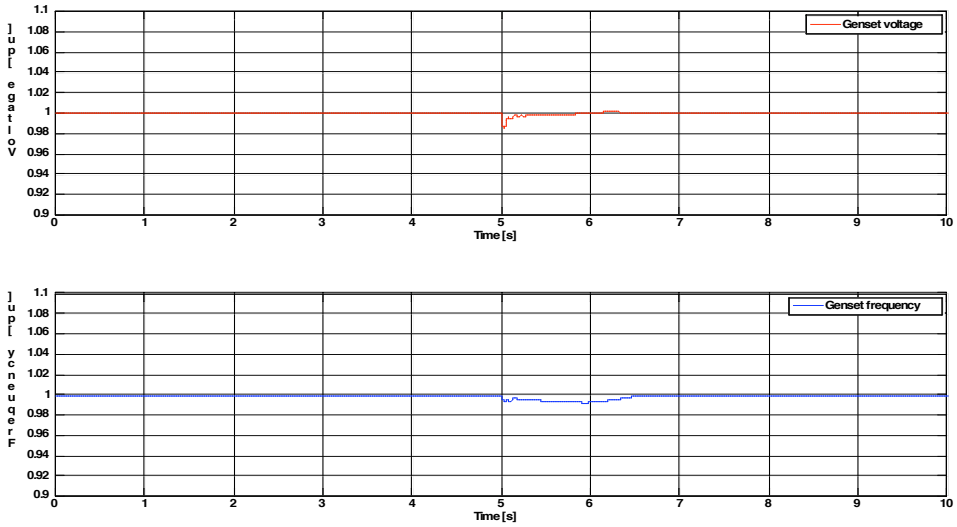

Fig. 97: Simulated genset output voltage and genset per unit speed waveforms for line start with inverter based source and genset with conventional controller

As before the sources is initially supplying resistive loads in the network and the induction machine is started at t = 5s. Fig. 96 and Fig. 98 show the output real and reactive power of the genset and inverter based source. In this simulation the inverter is operated close to its real power limit. The genset terminal voltage shown in Fig. 97 does not fall as much as in Fig. 85 as we now have two sources to provide the needed reactive power during the line start.

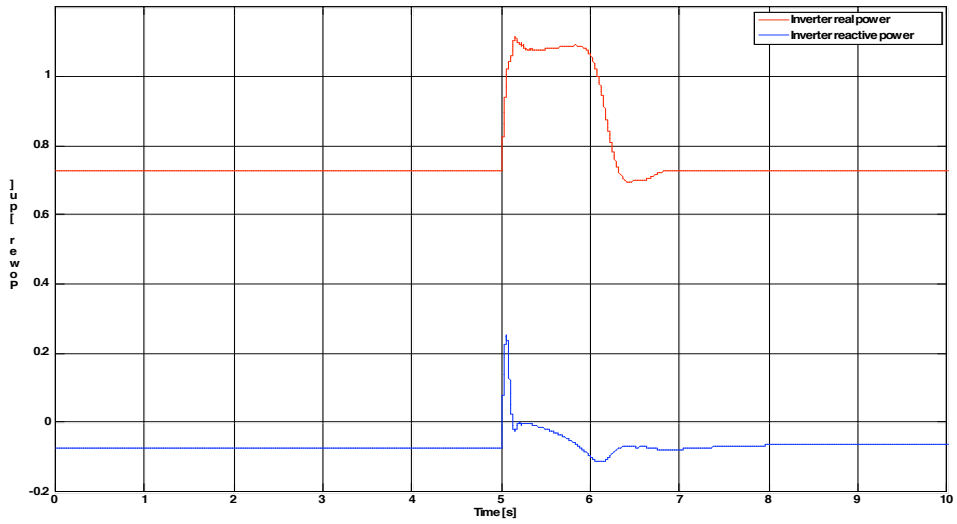

Fig. 98: Simulated inverter output real and reactive power waveforms for induction machine line start with inverter based source and genset with conventional controller

Fig. 99 shows the load voltage and the induction machine phase current during the machine start. We can see from the simulation results that the system is stable during the event and that the induction machine takes less than 2 seconds to startup. The inverter operates above its power limit for almost a second and this could be detrimental to its operation depending on the design.

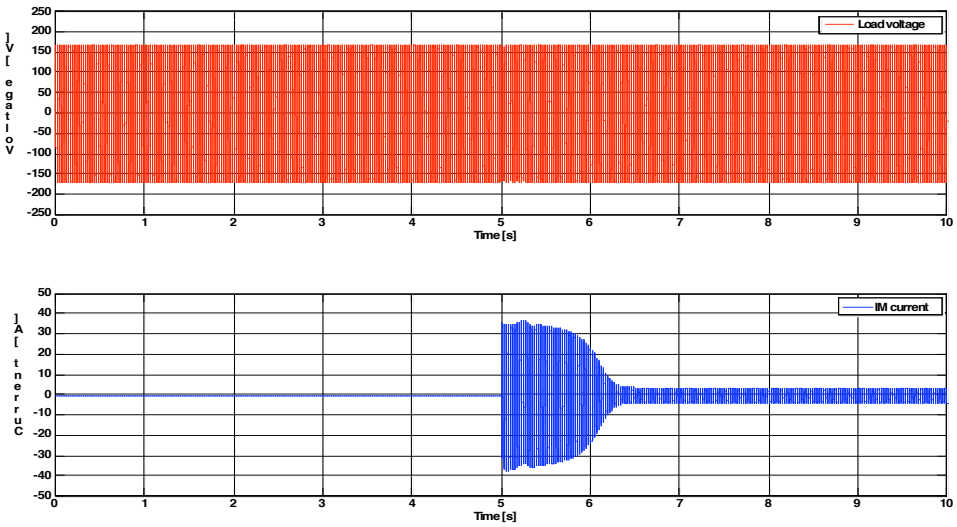

Fig. 99: Simulated load voltage and induction machine phase current waveforms for induction machine line start with inverter based source and genset with conventional controller

7.2.5 Induction machine starting in microgrid system with modified gensets and inverters

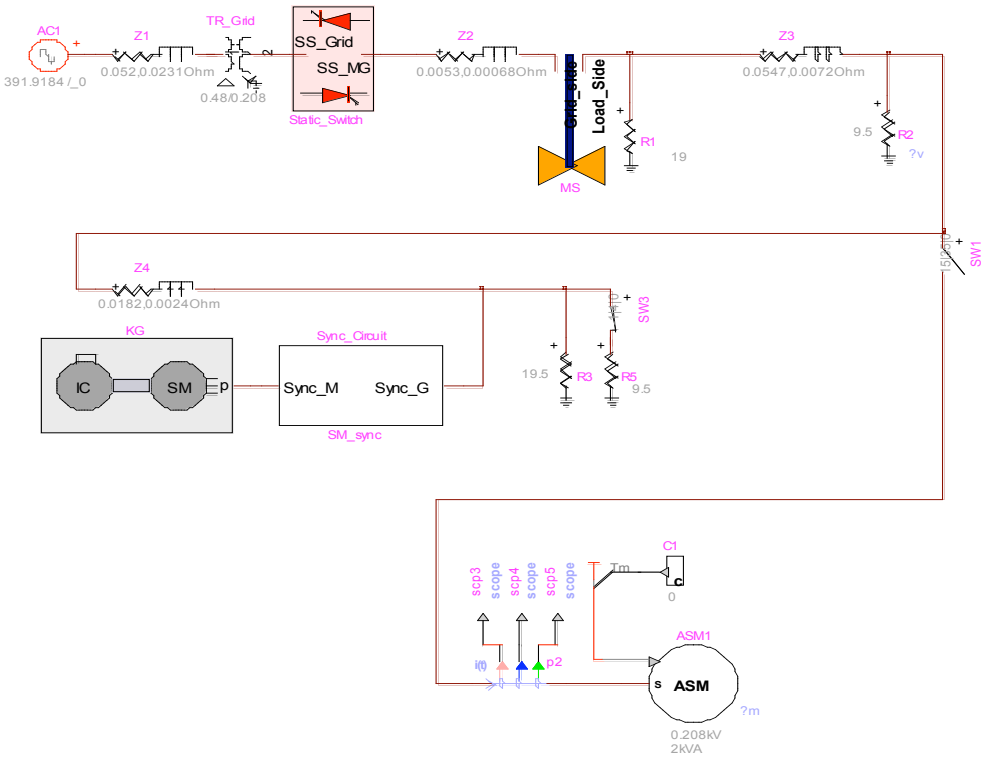

Fig. 100: : EMTP model for testing line start of induction machine in Microgrid with inverter and genset with modified controller

Fig. 100 shows the EMTP setup for testing the start of an induction machine in a microgrid system with an inverter based source and a genset with conventional controller. The simulation is carried out with the microgrid disconnected from the utility supply. As before the sources is initially supplying resistive loads in the network and the induction machine is started at t = 5s. Fig. 101 and Fig. 103 show the output real and reactive power of the genset and inverter based source. The inverter is again operated close to its power limit.

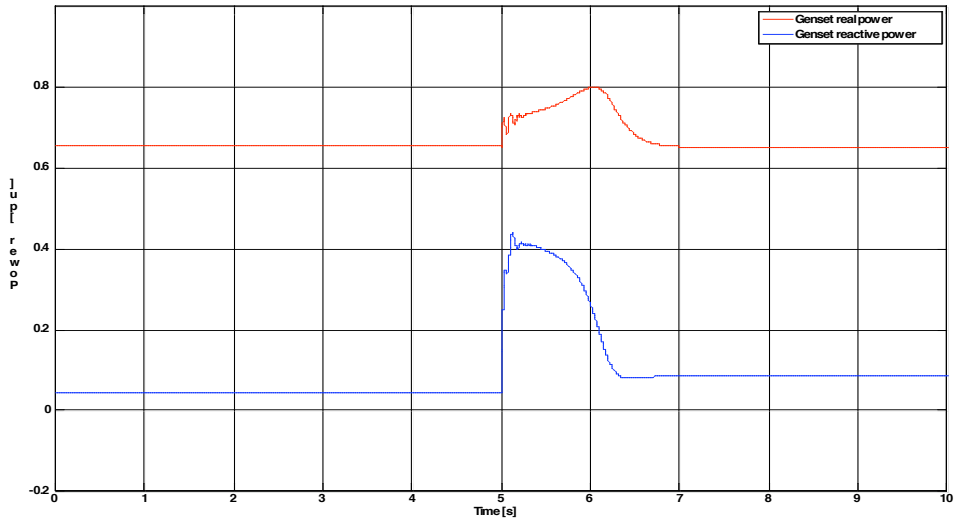

Fig. 101: Simulated genset output real and reactive power waveforms for induction machine line start with inverter based source and genset with modified controller

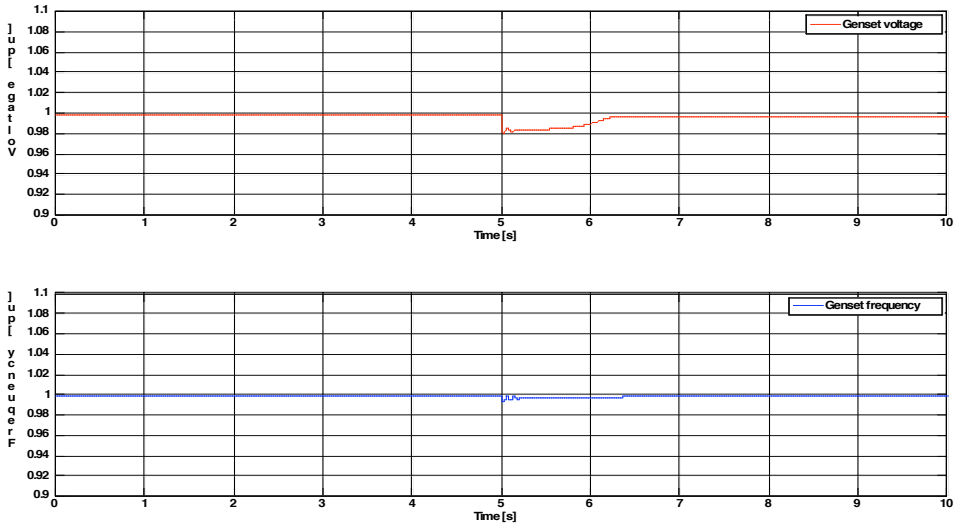

Fig. 102: Simulated genset output voltage and genset per unit speed waveforms for line start with inverter based source and genset with modified controller

The genset terminal voltage remains fairly constant throughout the whole start as seen in Fig. 102 and the load terminal voltage also remains fairly constant.

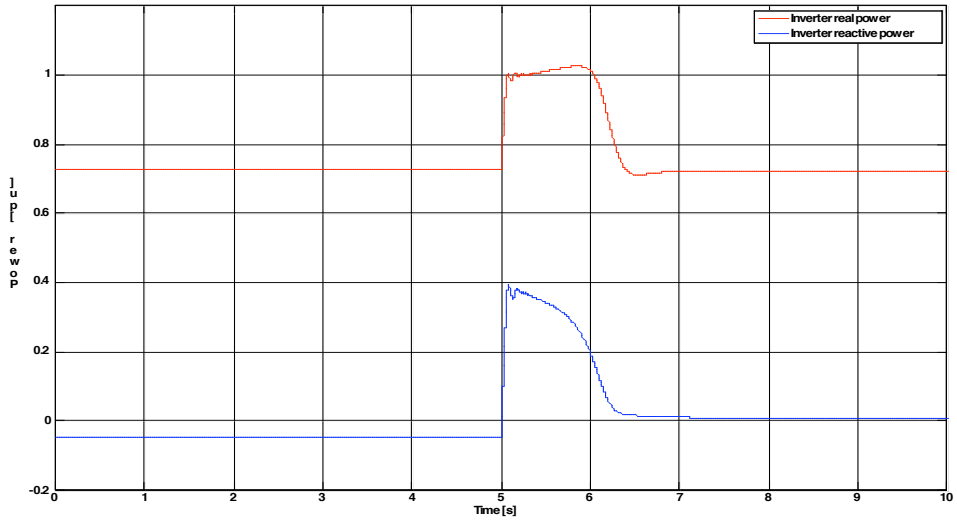

Fig. 103: Simulated inverter output real and reactive power waveforms for induction machine line start with inverter based source and genset with modified controller

From the simulation we can see that the system is stable during the starting of the motor even in the presence of multiple types of sources. The droop control on both the genset as well as the inverter reduces the terminal voltage when the induction machine starts up in response to the kVA required at start. This is similar to employing a reduced voltage or soft starter and hence the machine should have no stability issues during startup. In comparison to the simulation results using the conventional genset controller (Fig. 98) we can see from Fig. 103 that the inverter overshoot in power is much lesser. This is due to the fact that the genset is able to pick up the load much quicker.

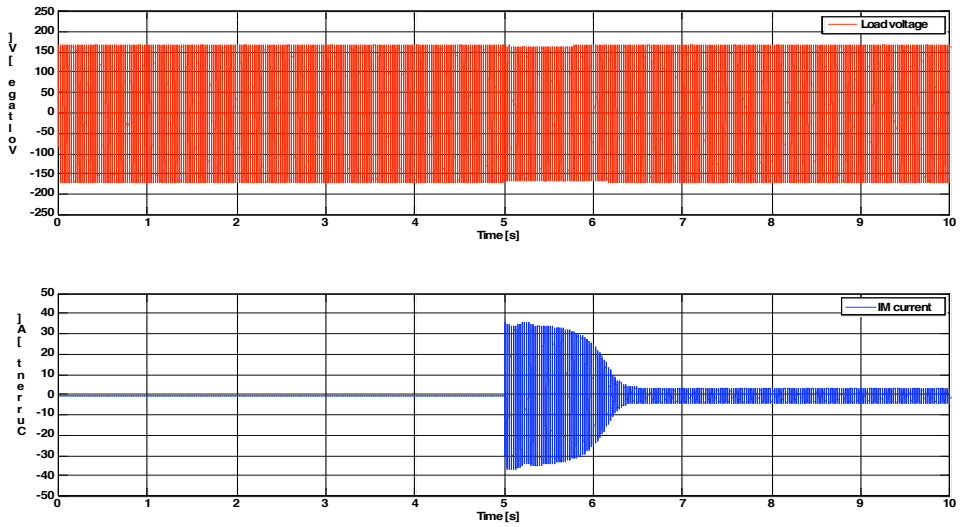

Fig. 104: Simulated load voltage and induction machine phase current waveforms for induction machine line start with inverter based source and genset with modified controller

7.3 Summary

In this chapter the line starting starting of induction machines in a microgrid environment is studied. Based on the scaling laws for NEMA class B induction machines we can estimate the required starting kVA for machines with different ratings. This enables us to size the induction machine that can be started in a given microgrid system with different types of sources. Typically the starting kVA requirement of the motor is 5 times its rating. In the event a soft starter or drive is not used for the induction machine the kVA required by the machine would put a significant burden onto the distributed generators present in the microgrid. To ensure that the sources can provide the necessary kVA the size of the induction motor used in the system is limited to $1/5^{th}$ of the available generation. This study assumes that the starting kVA required by the induction machine

can be provided by any one of the sources in the system. The stability of the microgrid system for the induction machine line start operation is studied by performing EMTP simulations. Simulation tests show that the system is stable and the sources are able to provide the necessary starting kVA. The droop control on both the genset as well as the inverter reduces the terminal voltage when the induction machine starts up in response to the kVA required at start, which is similar to employing a reduced voltage or soft starter.

CHAPTER 8. Stability analysis of UW-Microgrid system using Lyapunov's first method

8.1 Introduction

This chapter looks at the stability analysis of the UW-Microgrid system with genset and inverter based sources. The stability of the system is studied by looking at its eigenvalues at a steady state operating point. The movement of the eigenvalues with varying load at different real and reactive droop values is also studied. The microgrid system and in general a power distribution system with multiple interconnected sources is a highly nonlinear system. Traditionally the method to study the stability of nonlinear systems is to use an appropriate lyapnuov function. However in the case of a power system with non trivial conductances it has been claimed that there does not exist an appropriate lyapunov function [78]. New developments in interconnection and damping assignment based passivity control (IDA-PBC) [79] however raise the possibility of developing a globally stable control law for lossy power systems.

The approach used is to look at small signal stability of the system at various operating points when the microgrid system is connected to the grid and as an islanded system. Even though this method does not cover large signal changes it still provides us valuable information regarding the contribution of the real and reactive power droops of the individual generators to the system eigenvalues.

8.2 Modeling of system components

The first step in the formulation of the problem is to derive the model of the system. The various components include the inverter based sources, the genset and its controller as well as the various lines and load in the system. The model for the genset and its controller has already been presented in Chapter 6 and this section discusses the modeling of the inverter based source and passive impedances in the network. A key thing to note is that in the approach presented in this section the lines connecting the various sources are modeled using dynamic equations instead of algebraic equations.

8.2.1 Modeling of inverter based source

The design of the droop controllers for an inverter based source has been presented in [20] and [21]. The relevant equations that describe the control of the inverter are presented below:

$$P_i = v_{qi}\, i_{qi} + v_{di}\, i_{di} \tag{52}$$

$$Q_i = v_{qi}\, i_{di} - v_{di}\, i_{qi} \tag{53}$$

$$v_i^* = v_i^{ref} + m_q\left(Q_i^{ref} - Q_i\right) \tag{54}$$

$$v_i^c = \left(v_i^* - v_i\right)\left[K_p + \frac{K_i}{s}\right] \tag{55}$$

$$\omega_i^* = \omega_i^{ref} + m_p\left(P_i^{ref} - P_i\right) \tag{56}$$

$$\theta_i = \omega_b\left(\frac{\omega_i^*}{s}\right) \tag{57}$$

$$v_{qi} = v_i^c \cos \theta_i \quad (58)$$

$$v_{di} = -v_i^c \sin \theta_i \quad (59)$$

The LC filter for the inverter is integrated with the network impedances and is used in the calculation of the equivalent Ybus of the system. In the system model the values of the real and reactive power droops are set as variables and the movement of the eigenvalues with respect to these droops can be plotted.

8.2.2 Modeling of network

The microgrid system consists of several generators connected to each other via lines and feed various loads in the system. Each of the lines in the system can be modeled in the dq-frame rotating synchronously with the system frequency. In steady state this would result in constant DC values for the line dq currents. The state equations describing the dynamics of a line and similarly for a load are presented below.

$$v_{di} - v_{ds} = R_{1d} + L_{1d}\frac{dI_{1d}}{dt} - \omega I_q \quad (60)$$

$$v_{qi} - v_{qs} = R_{1q} + L_{1q}\frac{dI_{1q}}{dt} + \omega I_d \quad (61)$$

The next step in the process is to derive the equations for all the passive impedances in the system. The schematic for the microgrid system with two inverter based sources and a genset based source is shown in Fig. 105.

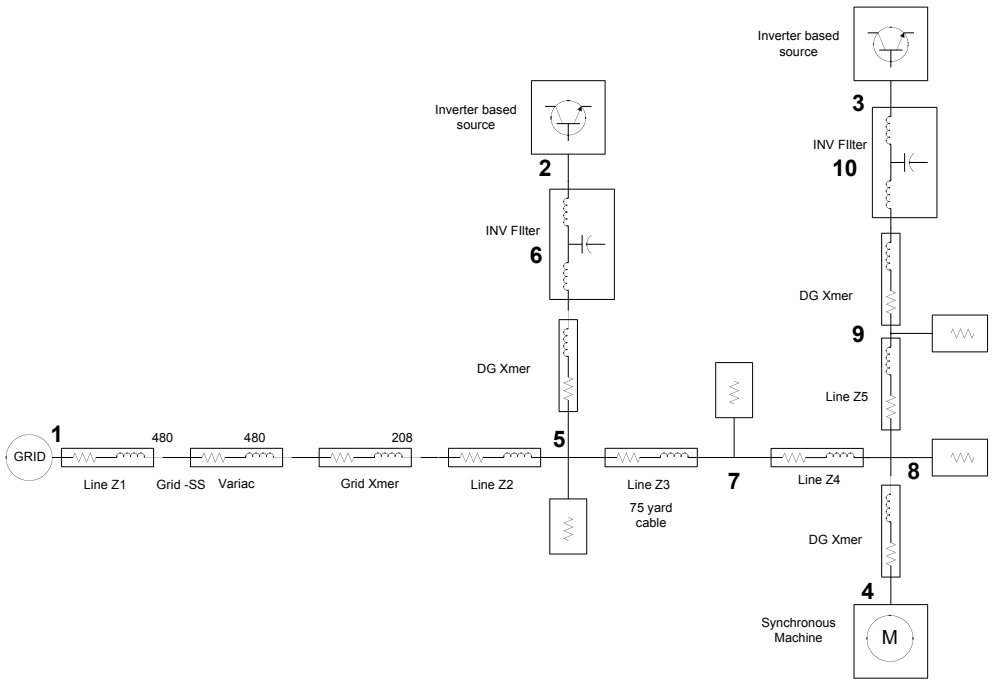

Fig. 105: UW-Microgrid schematic with two inverter based sources and a diesel genset source

To reduce the complexity of the network, Kron's reduction was used to eliminate all nodes except for the generator internal nodes. To achieve this we first calculate the system Ybus. The system Ybus for a given network provides a relationship between the voltages and currents.

$$[\,I] = [\text{Ybus}] \times [V] \tag{62}$$

Here the current vector I is given by the injected currents at each bus. Now we know that current injections occur at nodes that have generators and hence the equation can be rearranged to have the following form:

$$\begin{bmatrix} I_g \\ 0 \end{bmatrix} = \begin{bmatrix} Y_{aa} & Y_{ab} \\ Y_{ba} & Y_{bb} \end{bmatrix} \times \begin{bmatrix} E_g \\ V_n \end{bmatrix} \tag{63}$$

Solving for Ig we get :

$$I_g = [\text{Yaa} - \text{Yab}(\text{Ybb}^{-1})\text{Yba}]\, E_g \tag{64}$$

This implies that the Ybus of the reduced system is :

$$Ybus\_reduced = Yaa - Yab(Ybb^{-1})Yba \quad (65)$$

This process reduces the network complexity and allows us to focus on the dynamics of the equivalent lines connecting the various sources together; the resulting network is shown in Fig. 106.

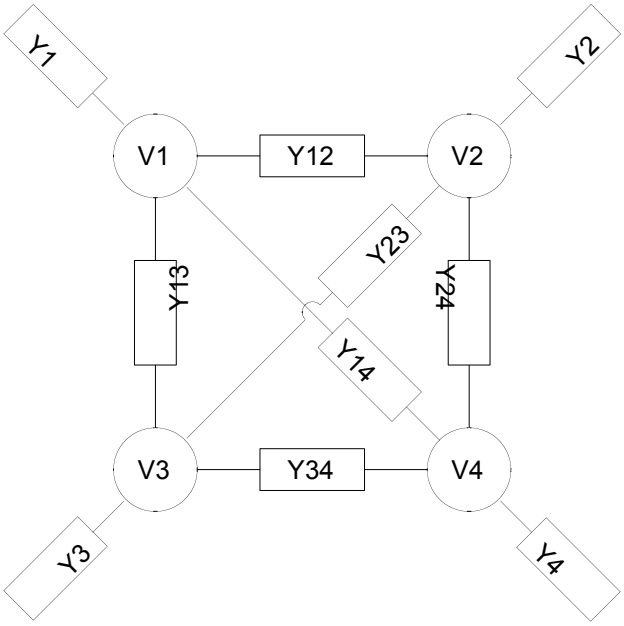

Fig. 106: UW-Microgrid schematic with two inverter based sources and a diesel genset source

8.3 Eigenvalues of microgrid system

The microgrid system consists of multiple sources connected by lines that feed passive loads. Even though the network impedances are passive the nature of the power frequency and voltage-reactive power droop curve based control makes the resulting set of dynamic equations for the system highly non-linear. We will utilize lyapunov's first method to determine the eigenvalues of the microgrid system. The non-linear equations of the system are solved at an operating point using numerical methods; at this operating point the jacobian is calculated which is then utilized to calculate the eigenvalues of the

system. Due to the large number of states in the system we will attempt to study the movement of the eigenvalues with changing parameters such as power reference, droop value etc to gain an insight into the stability of the system. The focus of the analysis is to evaluate the system stability as a function of the genset parameters. Previous work (20, 21) has shown the stability of inverter based sources and here we will focus on the impact of the genset on the system. We will look at the stability of the system for grid connected as well as islanded operation. The transient from grid connected to islanded operation cannot be studied using this method as it's a large signal change.

8.3.1 Eigenvalues of grid connected microgrid system

In a grid connected microgrid environment the grid provides a reference voltage and frequency to the analysis of the system. The grid is assumed to be a stiff source and causes the other units to operate at its frequency. The presence of the grid simplifies the modeling of the system as it provides us with a convenient synchronously rotating reference frame. As mentioned before the network with the grid and the three sources is reduced to the form shown in Fig. 106 using Kron's reduction. The resulting system with the dynamic equations for the sources is modeled in Simulink; a numeric solver is used to calculate the operating point for a specified droop and power reference value for each of the sources. Once the operating point is reached the 'A' matrix of the system is obtained using the 'linmod' command in Matlab whoch is subsequently processed to obtain the eigenvalues. Fig. 107 shows the eigenvalues of the system for a given operating condition with power frequency droop (m_p) value of 1% and reactive power droop value (m_q) of 5%. The power setpoints for each of the sources was set at 0.1pu. The number of states in the system is 44 and the figure charts out the location of each of the eigenvalues. Due to

the complexity of the system looking at the individual eigenvalues does not provide us with a lot of information. The key thing to note however is that all the eigenvalues are in the left half plane and hence the resulting system is stable for small perturbations around the operating point. The scale of the 'x' and 'y' axis in Fig. 107 is different and it must be noted that most of the eigenvalues are highly damped.

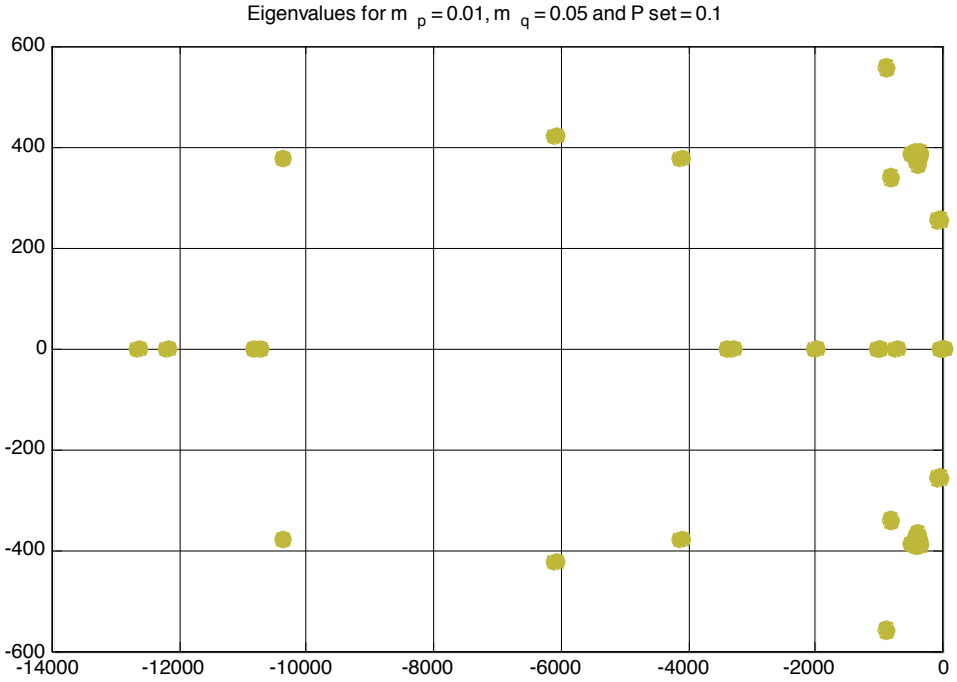

Fig. 107: Eigenvalues for microgrid system with two inverter based sources and a IC engine based source with mp of 1% and mq of 5%

Using this process the eigenvalues for the system for variations in reference power of the genset from 10% to 100% was calculated and the results are plotted in Fig. 108 and Fig. 109. Fig. 108 shows all 44 eigenvalues for each of the 9 power reference points of the genset. Again all the eigenvalues are in the left half plane and the system is stable for small perturbations. If we look into a zoomed in version of the figure shown in Fig. 109 we can see the motion of the critical eigenvalues closest to '0' with the change in reference is towards the left of the imaginary axis.

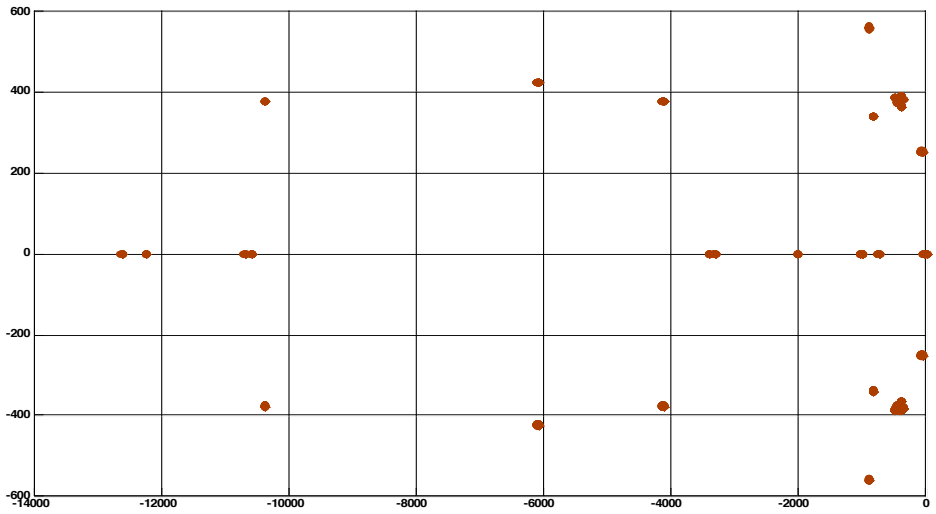

Fig. 108: Eigenvalues for microgrid system with grid, two inverter based sources and a IC engine based source with mp of 1% and mq of 5%

The direction of the arrow indicates the direction of migration of the eigenvalues with power reference.

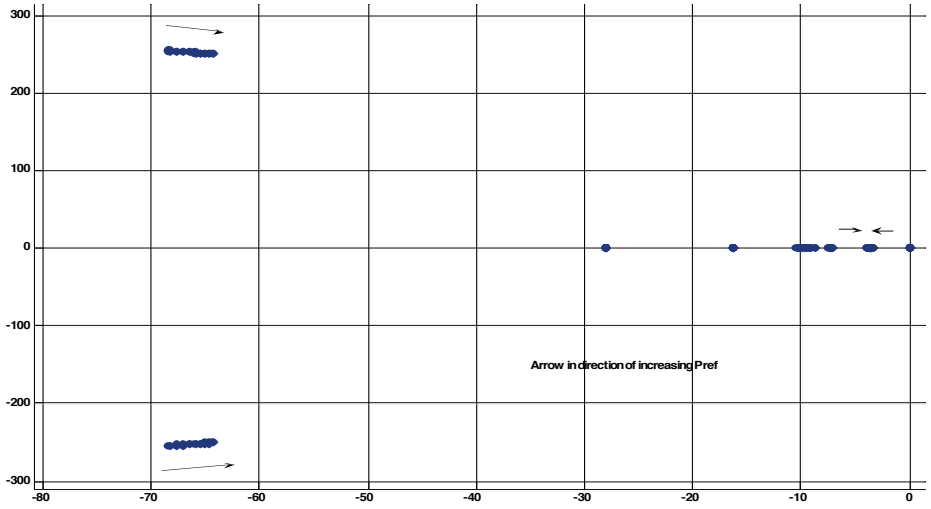

Fig. 109: Critical eigenvalue migration for genset Pref variation from 0.1pu to 1.0 pu for microgrid system with grid, two inverter based sources and a IC engine based source

We can see that the real eigenvalues closest to the real axis move towards each other but do not become complex and hence the small signal response is not oscillatory. The imaginary eigenvalues move closer to the positive real axis but their damping is large enough to not cause any significant oscillations for small changes.

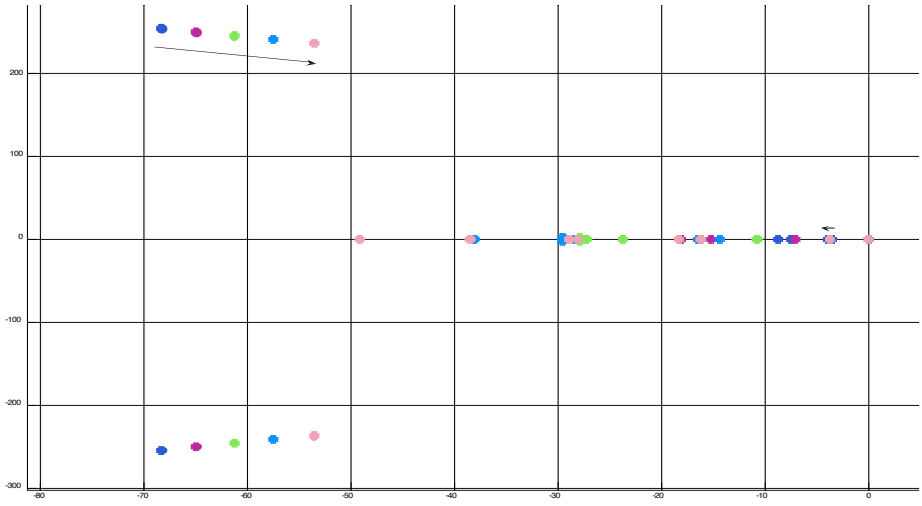

Fig. 110: Critical eigenvalue migration for genset mp variation from 1% to 5% for microgrid system with grid, two inverter based sources and a IC engine based source

In Fig. 110 we see the variation of the critical eigenvalues for variation of the genset power frequency droop from 1% to 5% for a fixed power reference of 0.1 pu. We can see that all the eigenvalues are in the left half of the real plane and they move with the change in droop value. The arrows indicate the direction of movement and we can see that the eigenvalues closest to the real axis don't move much and they do move left and away from the real axis. It must be noted there are other real eigenvalues that are actually moving towards the right. For droop percentages less than 1% the real part of the eigenvalues closest to the imaginary axis is smaller and hence the system is closer to

instability. The analysis for zero power frequency droop fails as the system is unstable and the simulation does not converge.

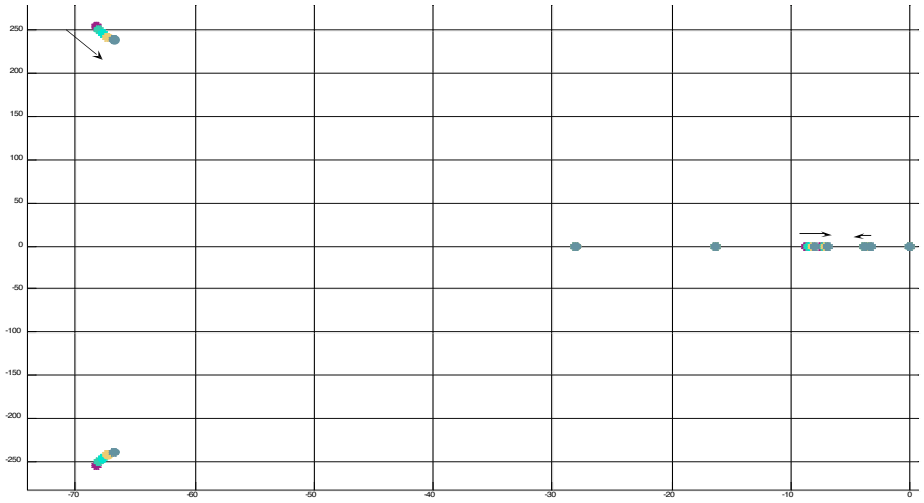

Fig. 111: Critical eigenvalue migration for genset mq variation from 1% to 5% for microgrid system with grid, two inverter based sources and a IC engine based source

Fig. 111 shows the variation of the critical eigenvalues for variation in reactive power droop value from 5% to 1%. Again the system is stable for the change and most of the eigenvalues close to '0' are moving towards the left. There are certain eigenvalues that are moving towards the right but do not cross over to the right half side and hence do not cause any instability.

8.3.2 Eigenvalues of islanded microgrid system

In a islanded microgrid system the system frequency is set by the combination of the load in the network, power reference and droop values for the individual sources. Using the power reference and droop curves for each of the sources it is possible to compute a 'system power versus frequency droop curve'. This curve can then be used in a

simulation to calculate the system frequency at any point in time. The procedure used to calculate the eigenvalues is almost the same as the method used in the previous sub-section. In the islanded system the number of generating nodes is three and hence we would have to recalculate the Ybus of the reduced network using Kron's reduction. Once we have the reduced network parameters we can combine them with the source models to develop the dynamic equations for the whole system. The key thing to note is that the transformation to the synchronous reference frame uses the system frequency calculated using the 'system power versus frequency droop curve'. At any point in time the total load seen by each of the sources is summed, filtered and then the appropriate frequency is read of the curve using a lookup table. The filtering is necessary to prevent an algebraic loop from forming and results in an additional eigenvalues.

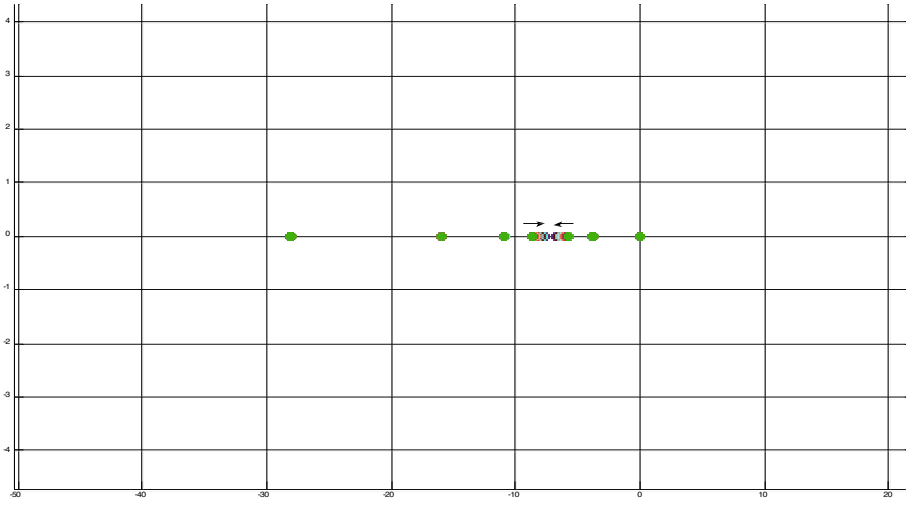

Fig. 112: Critical eigenvalue migration for genset mp variation from 1% to 5% for microgrid system with two inverter based sources and a IC engine based source

Fig. 112 and Fig. 113 show the migration of the eigenvalues for variation in genset power reference from 10% to 100% and variation of mp from 1% to 5% respectively. We can see that the critical eigenvalues are all real due to the presence of the electronic governor. Hence the dynamic response for small disturbances will be damped. Again if we see the migration of eigenvalues in Fig. 112 the movement is away from the real axis to the left and overall the system is stable. There are eigenvalues that are moving towards the right but they are further away from the real axis.

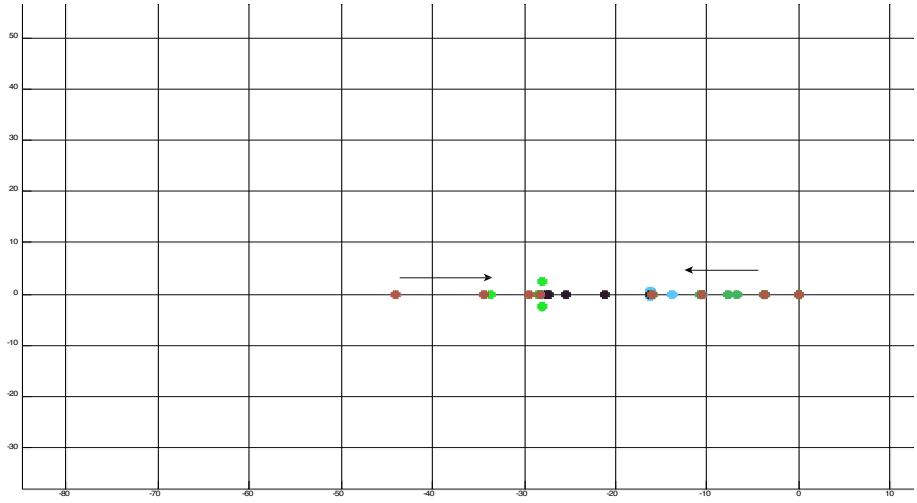

Fig. 113: Critical eigenvalue migration for genset mq variation from 1% to 5% for microgrid system with two inverter based sources and a IC engine based source

8.4 Summary

The chapter discusses the stability of the microgrid system using eigenvalues analysis. The model of the system includes detailed models for the genset, inverter based source as well as dynamic models for the passive impedances. Kron's reduction is used to simplify

the network equations and numerical techniques are used to determine the operating points of the non linear equations. At the operating point the eigenvalues are calculate and these are used to study the small signal stability of the system.

It was observed that for the grid connected and islanded system all the eigenvalues were located in the left half plane for a variety of operating conditions and hence the system is small signal stable. The migration of the eigenvalues for variations in power frequency droop and power reference was plotted and most of the critical eigenvalues were observed to be moving away from the real axis. Some of the eigenvalues on the real plane were moving towards the real axis but their effect is small as they are highly damped.

CHAPTER 9. Scaling of controller scheme

This report has presented a controller scheme that improves the performance of the IC enegine based genset and enables it to work in a microgrid environment with inverter based sources. The effectiveness of the controller scheme has been demonstrated using simulation studies as well as experimental tests for a given test system. The scale of microgrid systems has been increasing and its use at the sub-transmission system is being investigated. At higher power and voltage levels, power electronic front ends are typically used to interface energy storage systems with the power distribution system. The storage systems are controlled similar to the inverter based sources with an additional state of charge estimate that determines the minimum and maximum power limits. The algorithms for the control of energy storage systems in microgrid systems has are currently been researched at UW-Madison. The scaling of the engine model and the controller scheme for IC engine based gensets of higher power rating upto 2MVA will be discussed in this chapter. The scaling of various elements of the IC engine model presented in Chapter 4 include the pure engine delay, engine inertia, engine friction loss as well as voltage regulator with power rating will be investigated in this chapter.

9.1 Time delay associated with power stroke for larger machines

The power stroke delay represents the maximum amount of time before which the engine can respond to a change in fuel command. If the change occurs before the fuel is injected into the cylinder the delay would be much smaller. Hence on an average the time delay

would be less than one power stroke. However if we include the fuel actuator time constant and the intake manifold dynamics the net time delay can be modeled as one full power stroke. For a four stroke three cylinder engine operating at 1800 rpm the time delay can be calculated to be Td = $\frac{240}{360}\frac{1}{30}$ = 22ms. The pure engine delay is very critical in the analysis of the operation of the engine system in a microgrid environment. During this time frame the stored energy in the shaft of the system is depleted and the speed of the engine decreases causing the output frequency of the generator to fall. In comparison for an inverter based source the frequency drop is set artificially using the power frequency droop curve and is maintained to within a half a hertz of the nominal frequency. In a system with engine based sources and inverter based sources the drop in frequency of the engine drive generator can cause significant over current and power oscillations. From the simulation results presented in Chapter 4,5 we can see that after a load change there is no significant over current for smaller engines and the power oscillations are controlled effectively. The drop in frequency due to a load change for larger engine based gensets will be quantified in this chapter.

As the power rating of the genset increase the IC engine typically has multiple cylinders to produce the higher torque needed. However the increased number of cylinders does not decrease the power stroke delay as multiple cylinders are fired at the same time. For example a V12 engine may have upto three cylinders fire at the same time to result in 4 distinct firing instants during one complete cycle. The range for the engine delay for engines upto HP is from 0.02 to 0.04 s [84]. The higher engine delays occur in machines that run at a lower rated speed such as 1200rpm to decrease friction losses. Hence even as

we the size of the engine increases the value of the pure engine delay still is less than three electrical cycles. During this period the stored energy in the shaft will be depleted and the governor cannot restore the frequency at which the genset operates. The drop in frequency of the genset during this time is quantified in the next section.

9.2 Inertia and friction losses for large machines

In an IC engine genset the generator, engine and exciter contribute to the total inertia of the system. In the 10kW Kohler genset installed at UW-Madison that has an inertia constant of 0.19s the inertia of the individual machines is:

1. Engine: 0.3275 kg-m^2
2. Generator: 0.116 kg-m^2

From the inertias of the various components we can see that the inertia of the engine is much larger than the inertia of the generator. The brushless exciter has negligible inertia and does not contribute significantly to the total inertia of the system. Table 3 presents the inertia of selected machines available from publicly available literature and Fig. 114 plots the inertia for alternators manufactured by Uljanik Inc [85].

	A [80]	B[80]	C[80]	D[80]	E[81]	F[82]	G[83]
Rating [kVA]	69	156	781	1044	1000	3125	4510
H [s]	0.329	0.205	0.5	0.535	1	1.07	1.05

Table 4: Inertia constant in seconds for various generators

We can see that as the rating of the generator increases the inertia of the machine also increases significantly. In a genset where the engine dominates the inertia of the system we can conclude that the total inertia will significantly increase with the rating.

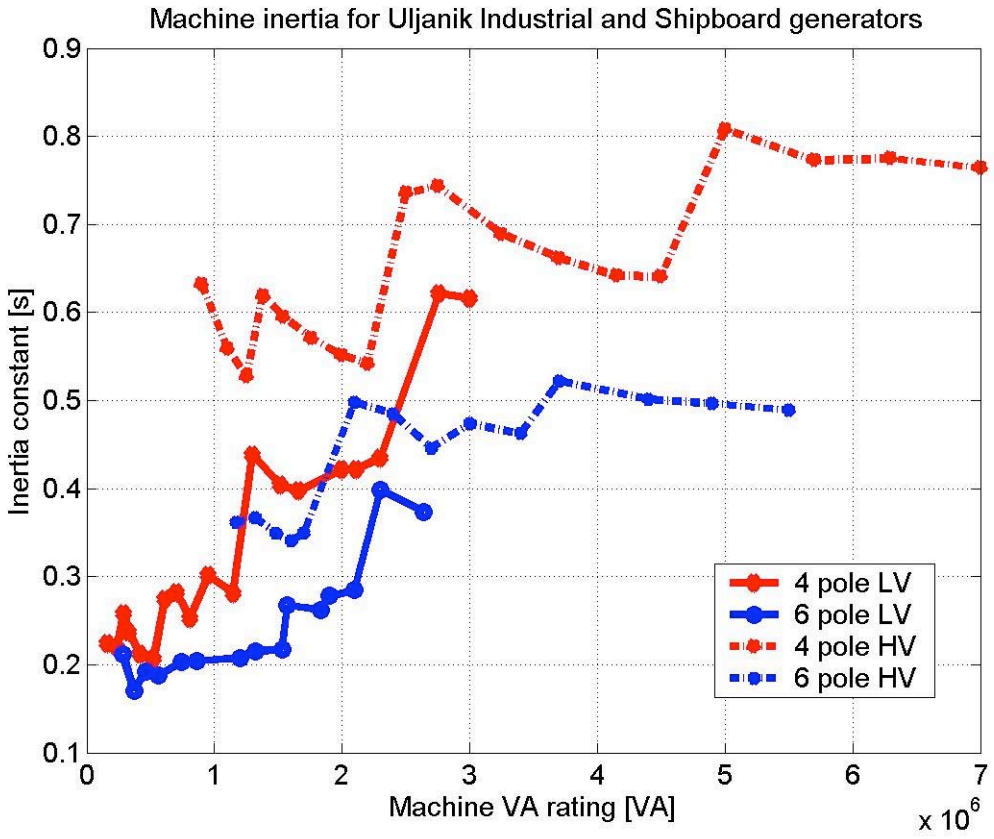

Fig. 114: Inertia of 480V (LV) and 6.3kV (HV) synchronous generators manufactured by Uljanik Inc [85].

With higher inertia the per-unit drop in speed for a load change decreases and hence the frequency variation is lesser in comparison to machines that have smaller inertia. During the pure engine time delay we can assume that the mechanical input to the shaft remains constant. Neglecting the friction coefficient the change in speed of the shaft for a step load is:

$$\Delta\omega(t) = \omega_0 - \left[\frac{\Delta P_e}{2H}\right] T_d \qquad [66]$$

Incorporating the friction coefficient K the speed of the engine at the end of the pure engine time delay is:

$$\omega(T_d) = \omega_0 \, e^{-\left(\frac{K}{2H}\right) T_d} - \left(\frac{2P_e}{K}\right) \sinh\left(\frac{K\,T_d}{4H}\right) \qquad (67)$$

Fig. 115 shows a diesel engine model for engines rated from 100HP to 1000HP from [84]. The range of values for α (1/2H) is 0.1 to 2, θ upto 0.04 and friction loss ζ is from 0.01 to 0.1. Hence for larger genset systems the maximum drop in frequency during the pure engine time delay Td can be calculated using and is plotted in Fig. 116 as a function of the inertia for starting from an initial frequency of 60Hz

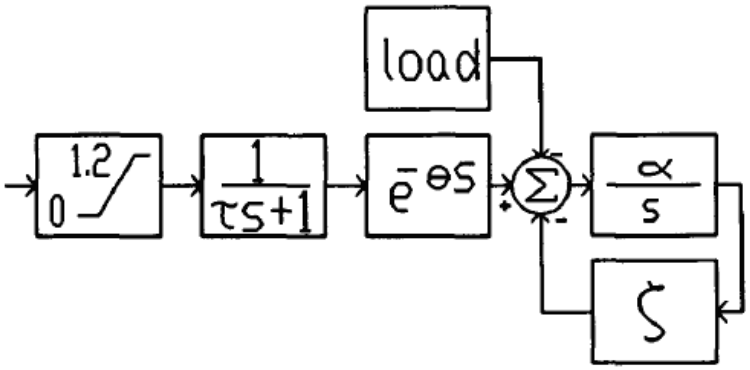

Fig. 115: Model for 100HP to 1000HP Diesel Genset [84]

.

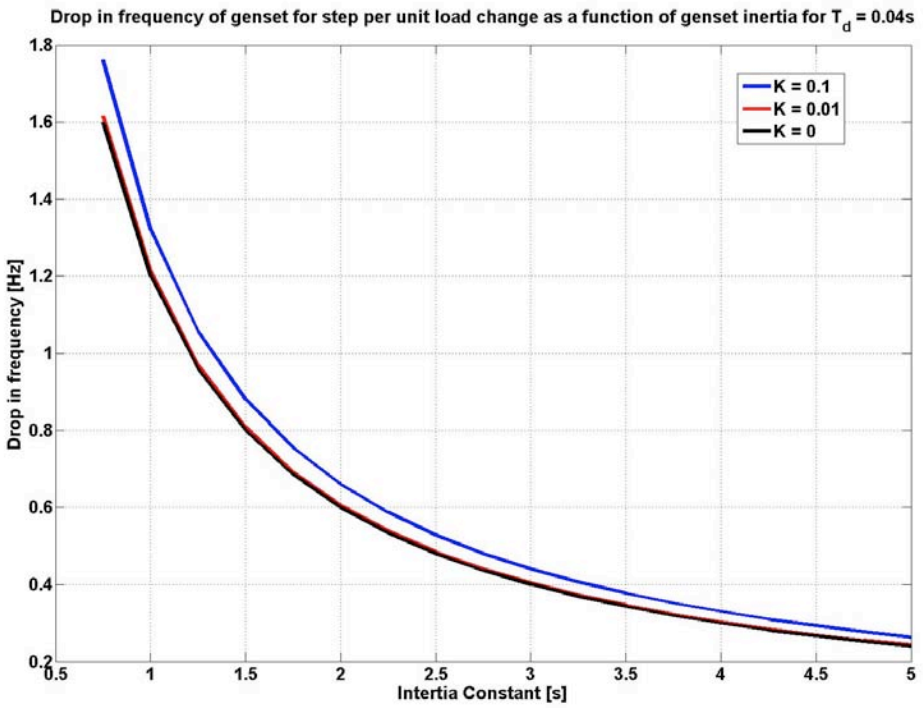

Fig. 116: Model for 100HP to 1000HP Diesel Genset [84]

In larger machines that have higher inertia the drop in frequency is smaller and this prevents the phase difference between the genset voltage and inverter based voltage source from increasing beyond limits. In fact the worst case scenario is for smaller machines that typically have much lower inertia and higher friction losses, resulting in a larger percentage change in speed during a load transient. From the simulation and experimental results presented in Chapter 6 for load changes for a 10kW genset we can see that the sudden drop in frequency does not cause the system to go unstable. Hence the response for larger gensets if the controller is designed using the principle presented in this work would be better and the resulting system would be able to survive large step load changes. The effect of the electronic speed governor to restore the frequency following the engine delay is studied in the next section.

9.3 Electronic governors for large engines

The final aspect of the control of the engine is the action of the electronic governor. Typically large gensets have PID controllers that track the commanded speed reference. The governors work by sensing a change in shaft speed measured by a magnetic pickup-toothed gear arrangement to either increase decrease the fuel command. Hence the governor has to wait for the speed to change before it can implement its restoring actuation. However in the controller scheme presented the change in electrical power is directly fed to the electronic governor as feedforward and hence it can respond much quicker to a change in load. The transfer function for the system between electrical output and speed incorporating actuator time constant and governor is given below.

$$\frac{\omega_r(s)}{P_e(s)} = -\left[\frac{1 + s\tau - e^{-sTd}\left(1-m_p(K_p+K_i/s)\right)}{(1 + s\tau)\left(2Hs + K + e^{-sTd}\left(K_p - \hat{K} + K_i/s\right)\right)}\right] \tag{68}$$

The speed command tracking function based on the controller designed in Chapter 6 is given below:

$$\frac{\omega_r^*(s)}{\omega_r(s)} = -\left[\frac{K_p+K_i/s}{\left((2Hs + K)e^{sTd}(1 + s\tau) + \omega_{obs}(s)\left(K_p - \hat{K} + K_i/s\right)\right)}\right] \tag{69}$$

The stiffness transfer function and the speed command tracking transfer function can be used to design the gains Kp and Ki needed to achieve the desired response and dynamic stiffness. The main advantage of this form of governor is the incorporation of the electrical output power and friction loss as additional signals to the controller. Traditionally in a genset the voltage regulator and the electronic governor are individual controllers that do not communicate amongst each other. This report presents a unified

controller with a system observer that enables the genset to respond much better to change in load and commands.

9.4 Voltage regulator and exciter machines for large generators

The voltage regulator and exciter machine work together to control the main field winding voltage and hence the terminal voltage of the machine. As the size of the generator increases the various schemes used for exciting the field winding also increase. The IEEE standard [86] covers most of the popular schemes used for regulating large synchronous machines (in the MVA range). Smaller machines with ratings in the 100's of kVA typically use a brushless exciter that is powered by an auxiliary winding or from a permanent magnet pilot exciter. The brushless exciter is an inside-out synchronous machine with field windings on the stator and ac windings on the rotor. Smaller gensets (ratings less than 100kW) use a single phase brushless exciter to reduce costs whereas larger gensets use a three phase brushless exciter machine. The three phase machine provides lesser ripple at the output of the flying rectifier module and hence lowers heating losses in the rotor. Typically voltage regulators are PI or PID controllers that regulate the terminal voltage to a commanded value by varying the field excitation. As mentioned in chapter 6.4 the voltage regulator typically does not incorporate the speed signal in its control. The terminal voltage of a machine depends on the product of the flux linkage and the rotor speed and hence the speed signal can be used to decouple the effects of the governor and help better regulate the terminal voltage of the machine to the desired value. The controller presented in chapter 6.4 utilizes the speed command as well as

command feedforward to generate the desired field voltage command enabling it to regulate the voltage to the commanded value in a much better fashion. The design of the controller for the field voltage presented in chapter 6.4 can be utilized directly for machines of larger ratings. The choice of the controller gains would need to be made by plotting the command tracking transfer function and deciding the gain values based on the desired bandwidth. The design of the observer would have to be modified based on the type of excitation system used but the principles remain the same irrespective of the rating of the machine. Hence from a scaling perspective there are no issues with respect to the control of the output voltage of the generator using the proposed voltage regulator structure.

9.5 Summary

The chapter discusses the various issues related to the scaling of the controller presented for gensets of larger rating. The main issue related to scaling is the variation in frequency of the genset during a sudden load change. Due to the presence of an ideal time delay in the engine the governor cannot control the output frequency for a brief period of time during a load change. In a system with engine based sources and inverter based sources the change in frequency of the engine driven generator can cause significant over current and power oscillations. This chapter quantifies the change in frequency during the engine delay for a step load change for machines with higher power ratings and shows that larger rating machines have a much smaller drop in frequency. Due to the smaller drop in frequency there is less of a phase shift between various sources in the system and the power oscillation during a load change decreases. In fact the worst case scenario is for smaller machines that typically have much lower inertia and higher friction losses,

resulting in a larger percentage change in speed during a load transient. This report has presented simulation and experimental test results for a step load change for a small genset (10kW rating) which show that the drop in frequency does not cause the microgrid system to go unstable. The presence of the reactive power droop and power frequency droop in conjunction with the proposed controller enables the system to recover and operate at the new steady state point.

References

1 U.S. Department of Energy, "National transmission grid study", May 2002

2 U.S. Department of Energy, "Strategic plan for distributed energy resources", September 2000

3 C.L. Smallwood, "Distributed generation in autonomous and non-autonomous micro-grids", Rural Electric Power Conference 2002, pp D1-D1_6

4 P. Plahn, "How will fuel cells, micro-turbines and the evolution of current engine genset technologies stack up in the evolving market place.", Proc. INTELEC 2002, pp-338-341

5 US-Canada power system outage task force, "Final Report on the August 14th 2003 Blackout in the United States and Canada, Causes and Recommendations", April 2004

6 Capstone Microturbine, website address : **http://www.capstoneturbine.com/**

7 Caterpillar generator set pocket rating guide, website address: **http://www.cat.com/cda/components/securedFile/displaySecuredFileServletJSP?fileId=190491&languageId=7**"

8 N. Al-Khayat, J. Al-Tayie and R. Seliga, "Stand alone adjustable speed power generating set", Proc. Intl conf. on harmonics and power quality 2002, Vol. 2, pp- 639 – 643

9 N. Al-Khayat and W. Koczara, "Variable speed integrated generator VSIG as a modern controlled and decoupled generation system of electrical power", Proc. European conf. on power electronics and applications 2005.

10 TecoGen Inc., website address : **http://www.tecogen.com**

11 MagnaSmart variable speed generator, website address: http://www.marathonelectric.com/generators/BROCHURE/GPN031.pdf

12 U.S. Department of Energy, "Energy Policy Act of 2005".

13 J. Baba, S. Suzuki, S. Numata, T. Yonezu, S. Kusagawa, A. Denda, T. Nitta, E. Masada, "Combined power supply method for micro-grid by use of several types of distributed power generation systems", 2005 European Conference on Power Electronics and Application, pp P.1-P.10

14 K. Temma, Y. Kono, M. Shimomura, M. Kataoka, T. Goda and S. Uesaka, "Proposal and development of power quality improvement method under islanding operation in a micro-grid", IEEJ Transactions on Power and Energy, Vol 126(2006), No 10, pp. 1032-1038.

15 J. Cardell, M. Ilic, "Maintaining stability with distributed generation in a restructured industry", Power Engineering Society General Meeting 2004, Vol-2, pp. 2142-2149.

16 IEEE Std 1547-2003, "IEEE Guide for Interconnecting Distributed Resources with Electric Power Systems"

17 Directorate-General for research, Sustainable Energy Systems, "European Smart Grids technology platform – Vision and strategy for Europe's electricity network of the future".

18 R. H. Lasseter, "Microgrid," Power Engineering Society Winter Meeting, vol. 1, pp. 146–149, 2001.

19 CERTS, "Integration of distributed energy resources – The CERTS microgrid concept" Submitted to the U.S Department of Energy April 2002.

20 P. Piagi, "Microgrid Control", PhD Dissertation 2005, University of Wisconsin-Madison

21 M. Illindala, "Vector control of PWM VSI based distributed resources in a Microgrid", PhD Dissertation 2005, University of Wisconsin-Madison

22 M.Illindala and G. Venkataramanan, “Control of distributed generation systems to mitigate load and line imbalances”, Conference proceedings PESC 2002, pp 2013-2018

23 G. Venkataramanan, M. S. Illindala, C. Houle, R. H. Lasseter, “Hardware development of a laboratory-scale microgrid Phase 1 – Single Inverter in Island Mode Operation,” NREL/SR-560-32527 Report, National Renewable Energy Laboratory, Nov. 2002.

24 Y. Zhou, “ Analysis and control of distributed energy resources”, PhD Dissertation, Washington State University 2002

25 IEEE Std 1110-2002, “IEEE Guide for Synchronous Generator Modeling Practices and Applications in Power System Stability Analysis”

26 I.M. Canay, "Causes of discrepancies on calculation of rotor quantities and exact equivalent diagrams of the synchronous machine", IEEE Trans. Power App. Syst., July 1969, Vol. PAS-88, pp. 1114-1120.

27 I.M. Canay, “Modeling of alternating current machines having multiple rotor circuits”, IEEE Transactions on Energy Conversion, Vol. 8, No. 2, June 1993, pp 280-296

28 I.M. Canay, “Physical significance of sub sub-transient quantities in dynamic behavior of synchronous machines” IEE Proceedings, Vol. 135, Part B, No. 6, November 1988

29 R.I. Davis, “A nonlinear observer for instantaneous internal combustion engine crankshaft torque and active torque smoothing control using a crankshaft mounted electric motor” PhD Dissertation 1999, University of Wisconsin-Madison

30 J.A. Putman, “Rule-based control of an I.C. engine driven electric generator system”, M.S. Thesis 1997, University of Wisconsin-Madison

31 K. Jaeger, “Digital multivariable controller for engine generator systems” M.S. Thesis 1998, University of Wisconsin-Madison

32 T.R. Tesch, "Dynamic torque estimation in a sensor limited environment", PhD Dissertation 2005, University of Wisconsin-Madison

33 Y.H. Zweiri, J.F. Whidborne, L.D. Seneviratne and K. Althoefer, "A Comparison of Dynamic Models of Various Complexity for Diesel Engines", Mathematical and Computer Modelling of Dynamical Systems 2002, Vol. 8, No. 3, pp. 273–289

34 S-C Kong, Y Ra, and R D Reitz, "Performance of multi-dimensional models for simulating diesel premixed charge compression ignition engine combustion using low- and high-pressure injectors", International journal of engine research , 2005, Vol. 6, Issue 5, pp 475 -86

35 Y.H. Zweiri, J.F. Whidborne and L.D. Seneviratne, "Dynamic simulation of a single-cylinder diesel engine including dynamometer modelling and friction", Proc Instn Mech Engrs 1999, Vol 213 Part D, pp 391-402.

36 J.J. Moskwa, "Automotive engine modeling for real-time control", PhD Dissertation 1988, Massachusetts Institute of Technology

37 A.Makartchouk, "Diesel Engine Engineering-Thermodynamics, Dynamics, Design and Control." Marcel Dekker. New York, 2003 (seventh edition).

38 M.J. Ryan and R.D. Lorenz, "A power mapping variable speed control technique for a constant frequency conversion system powered by an I.C. engine and PM generator", Conf. Record IAS 2000, Vol. 4, pp 2376-2382.

39 R.I. Davis and R.D. Lorenz, "Engine Torque Ripple Cancellation with an Integrated Starter Alternator in a Hybrid Electric Vehicle: Implementation and Control", IEEE Transactions on Industry Applications, Nov.-Dec. 2003 vol. 39, no. 6, pp 1765-1774

40 S. Roy, O.P. Malik, G.S. Hope, "A low order computer model for adaptive control of diesel driven power plants", Conf. Record IAS 1991, Vol. 2, pp 1636-1642.

41 Y. Hu, M. Cristea, M. McCormick and L. Haydock, "Modeling and simulation of a variable speed stand alone generator system", Proc. Power Electronics and Variable Speed Drives 2000, pp 372-377.

42 G.S. Stavrakakis and G.N. Kariniotakis, " A general simulation algorithm for the accurate assessment of isolated diesel-wind turbine systems interaction - Part 1 : A general multimachine power system model", IEEE Transactions on Energy Conversion 1995, Vol. 10, No. 3, pp 577-583.

43 J. Jiang, "Optimal gain scheduling controller for a diesel engine" IEEE Control Systems Magazine, Vol. 14, Issue 4, August 1994, pp 42-48

44 J.D. Powell and J.A. Cook, "Modeling of an internal combustion engine for control analysis", IEEE Control Systems Magazine, Vol. 8, Issue 4, August 1994, pp 20-26

45 J.D. Powell, N.P. Fekete and C.F. Chang, "Observer based air-fuel ratio control", IEEE Control Systems Magazine, Vol. 18, Issue 5, October 1998, pp 72-83

46 M. Jankovic, "Control design for a diesel engine model with time delay", Proc. IEEE Conf. on Design and Control, Dec 2001, pp 117-122

47 P. Falcone, M. Gennaro, G. Fiengo, L. Glielmo, S. Santini, P. Langthaler, "Torque generation model for diesel engine" Proc. IEEE Conf. on Design and Control, Dec 2003, pp 1771-1776

48 B. Kuang, Y. Wang, Y. Tan, " An H_∞ Controller design for diesel engine systems" Proc. PowerCon 2000, Vol. 1, pp 61-66.

49 Y. Li, G. Liu and X. Zhou, "Fuel injection control system design and experiments of a diesel engine", IEEE Transactions on Control System Technology, Vol. 11, No. 4, July 2003, pp 565-570

50 Working group on prime mover and energy supply modes for system dynamic performance studies, " Dynamic models for combined cycle plants for power system simulation studies", IEEE Transactions on Power Systems , Vol. 9, No. 3, August 1994, pp 1698-1708.

51 C. Rakopoulos and E. Giakoumis, "A computer program for simulating the steady-state and transient behavior of direct-acting engine governors," Advances in Engineering Software, vol. 30, pp. 281–289, 1999.

52 A. Tomilson, J. Quaicoe, R. Gosine, M. Hinchey, N. Bose, "Modeling an autonomous wind-diesels system using simulink", Canadian conference on electrical and computer engineering, Vol. 1, pp 35-38.

53 R. H. Park, "Two-Reaction Theory of Synchronous Machines Generalized Method of Analysis – Part 1," AIEE Transactions, July 1929, pp. 716-730.

54 M. Tartibi, "Design procedure calculation and analysis of A.C. exciter of a brushless exciter", M.S Thesis, University of Florida 1994.

55 J.M. Vleeshouwers, "Derivation of a model of brushless exciter for a synchronous machine" EUT-Report 92-E-258 submitted to Eindhoven University of Technology June 1992.

56 A. Godhwani and M.J. Basler, "A digital excitation control system for use on brushless excited synchronous generator" IEEE Transactions on Energy Conversion, Vol. 11, No. 3, September 1996, pp 616-620.

57 M.G. Mcardle, D.J. Morrow, P.A.J. Calvert and O. Cadel, "Implementation of a digital AVR for small alternators", Proc. International Conference on Electric Utility Deregulation and Restructuring and Power Technologies 2000, pp 620-625

58 K. Kim, A. Godhwani and M.J. Basler, "Supplemental control in a modern digital excitation system", Panel Session, IEEE PES 2000, pp 603-608

59 M. C. Chandorkar, Distributed Uninterruptible Power Supply Systems, Ph. D. Thesis, Univerity of Wisconsin-Madison, 1995.

60 F. Katiraei and M.R. Iravani, "Power Management Strategies for a Microgrid with multiple distributed generation units", IEEE Transactions on Power Systems , Vol. 21, No. 4, November 2006, pp 1821-1831.

61 F. Katiraei, P.W. Lehn and M.R. Iravani, "Micro-grid autonomous operation during and subsequent to islanding process", IEEE Transactions on Power Delivery , Vol. 20, No. 1, January 2005, pp 248-257.

62 A. Darabiand C.E. Tindall, "Analogue AVR model for use in real-time transient simulation of small salient pole alternators", International Conference on Power Electronics Machines and Drives 2002, pp 451-455.

63 A. Darabi and C.E. Tindall, "Brushless exciter modeling for small salient pole alternators using finite elements", IEEE Transactions on Energy Conversion , Vol. 17, No. 3, September 2002, pp 306-312.

64 S.M.L. Kabir and R. Shuttleworth, "Brushless exciter model", IEE Proc. on Generation, Transmission and Distribution, Vol. 141, Issue 1, Jan. 1994, pp 61 - 67

65 A. J. Wood, B. F. Wollenberg, Power Generation Operation & Control, John Wiley & Sons, Inc., New York, 1984.

66 N. Cohn, Control of Generation and Power Flow on Interconnected Power Systems, John Wiley & Sons, Inc., New York, 1984.

67 F. Saccomanno, Electric Power Systems Analysis and Control, IEEE Press, Piscataway, NJ, 2003.

68 O. Elgerd,, “Electric energy systems theory”, McGraw Hill publication

69 Ong Chee Mun, “ Dynamic simulation of electric machinery using Matlab-Simulink”, Prentice Hall publication

70 T.A. Lipo, “ECE 511 course notes”, WEMPEC, University of Wisconsin-Madison

71 R.D. Lorenz, “ME746 course notes:, WEMPEC, University of Wisconsin-Madison

72 W. G. Heffron and R. A. Phillips, "Effect of modern amplidyne voltage regulators on underexcited operation of large turbine generators," AIEE Trans. (Power Apparatus and Systems). vol. 71, pp. 692-697, August 1952.

73 C. Concordia, "Steady-state stability of synchronous machines as affected by voltage regulator characteristics," AIEE Trans., vol. 63, pp. 215-220, May 1944.

74 F.P. deMello and C. Concordia, “Concepts of Synchronous Machine Stability as Affected by Excitation Control” IEEE Transactions on Power Apparatus and Systems, Vol. 88, Issue 4, April 1969, pp 316 – 329

75 EMTP-RV simulation platform, **www.emtp.com**

76 HCJ deJong, “AC Motor Design with Conventional and Converter Supplies”, Clarendon Press, 1976

77 J. O. Ojo, A. Consoli and T. A. Lipo, "An improved model of saturated induction machines," IEEE Transactions on Industry Applications. vol. 26, pp. 212-221, March/April 1990

78 H.D. Chiang, “Study of the existence of energy functions for power systems with losses”, IEEE Transactions on Circuits and Systems, Vol. 36, pp 1423-1429, November 1989

79 R. Ortega, M. Galaz, A. Astolfi, T. Shen, Y. Sun, "Transient stabilization of multimachine power systems with nontrivial transfer conductances", IEEE Transactions on Automatic Control, Vol. 50, pp 60-75, January 2005

80 W. B. Gish," Small Induction Generator and Synchronous Generator Constants for DSG Isolation Studies", IEEE Transactions on Power Systems, Vol. PWRD-1, No. 2, April 1986.

81 M.Davis, D. Costyk and A. Narang," Distributed and Electric Power System Aggregation Model and Field Configuration Equivalency Validation Testing", July 2003, NREL/SR-560-33909

82 Parameters from Simulink Power System Blockset (3.0) Example "power_machines.mdl"

83 X. Wu, J. Mutale, N. Jenkins and G. Strbacfrom," An investigation of Network Splitting for Fault Level Reduction" Tyndall Centre for Climate Change Research

84 D.W. Augustine, K.S.P. Kumar, "A method for self-tuning a PID controller for control of small to medium sized diesel engines", IEEE International Conference on Systems Engineering , pp 85-88, August 1991.

85 Uljanik Inc, Alternator manufacturers, http://www.tesu.uljanik.hr/alternators.htm

86 IEEE standard 421.5-1992, "IEEE Recommended Practice for Excitation System Models for Power System Stability Studies"